Mapping brain activity *in vivo* during spatial learning in mice

Dissertation zur Erlangung
des Doktorgrades
der Naturwissenschaften
(Dr. rer. nat.)

dem Fachbereich Psychologie
der Philipps-Universität Marburg
vorgelegt von Benedikt T. Bedenk
aus Vorwerk in Niedersachsen

München, Oktober 2013

Vom Fachbereich Psychologie der Philipps-Universität Marburg als Dissertation am 4. November 2013 angenommen.

Erstgutachter:	Dr. Markus Wöhr
Zweitgutachter:	PD Dr. Carsten T. Wotjak
Tag der mündlichen Prüfung:	21. Februar 2014

„Ja, Kalzium, das ist alles!“

(Otto Loewi, 1959)

Contents

List of Figures

List of Tables

Abbreviations

AAV adeno-associated virus

AMPA α-amino-3-hydroxy-5-methyl-4-isoxazolepropionic acid

Amy amygdaloid complex

ANOVA analysis of variance

BLA basolateral amygdala

BNST bed nucleus of the stria terminalis

CA1 cornu ammonis 1

CA3 cornu ammonis 3

COV coefficient of variance

CREB cAMP response element-binding protein

CT computed tomography

Ctrl control

d day

DTI diffusion tensor imaging

EEG electroencephalography

F free training

F$_r$ free retraining

fMRI functional magnetic resonance imaging

GP globus pallidus

HPC hippocampus

IA ibotenic acid

IC inferior culliculus

IEG immediate early gene

KO knockout

L learner

LTCC L-type voltage dependent calcium channel

LTP long-term potentiation

MEMRI manganese-enhanced magnetic resonance imaging

mPFC medial prefrontal cortex

MR magnetic resonance

MRI magnetic resonance imaging

NL non-learner

NMDA *N*-methyl-D-aspartic acid

P place training

$\mathbf{P}_r$ place retraining

PET positron emission tomography

ROI region of interest

R response training

$_r$ retraining

$\mathbf{R}_r$ response retraining

RSC retrosplenial cortex

SD standard deviation

S.E.M. standard error of the mean

T1w T1-weighted

Veh vehicle

WCM water cross maze

WT wild type

Abstract

Deficits in the encoding, retrieval and manipulation of sensory or memory information in the brain contribute to a number of neuro- and psychopathologies in humans. To better understand the underlying principles of memory processes, efforts still have to rely on animal research. The laboratory mouse as a model organism provides many advantages to study the underlying mechanisms as one can directly interfere with brain functions via a number of tools including genetic manipulation. For this reason, it is very important to have memory tasks that match human memory testings and suits the characteristics of mice. One cognitive capability that is highly preserved across species is spatial learning, what enables the daily required relocation of certain positions in space. Mice and men have developed two different strategies to do so, which rely on different types of reference information. During place learning, environmental cues are adopted and incorporated into a cognitive map. In contrast, response learning is based on directed movements along a specific route. Place and response learning can also be dissected in terms of their biological substrate. While place learning requires the hippocampus (HPC), response learning depends on the striatum. Most behavioral tests, that can clearly distinguish between the two strategies were originally designed for rats. Since the behavior of mice and rats can be considerably different, it is necessary to adapt these tasks to the requirements of mice. In order to improve then the translation of structural and functional results from rodents to humans, methods must be applied that match the coarse *in vivo* imaging typically used in humans. Manganese-enhanced magnetic resonance imaging (MEMRI) may therefore be useful, as it provides three-dimensional maps of the living mouse brain. Since manganese increases the brain contrast in magnetic resonance (MR) images, MEMRI is regularly applied to depict the volume of specific brain structures *in vivo*. A second feature of manganese is, that it enters neurons through L-type voltage-dependent calcium channels (LTCCs) and therefore might be an indicator for neuronal action. However, it

has never been shown that LTCCs directly regulate the MEMRI contrast *in vivo*, which would be essential to establish it as a functional tool in order to measure brain activity in the living mouse brain. The application of MEMRI to cognitive tasks might then be helpful to identify underlying brain circuits and in combination with other techniques also essentially involved neurobiological mechanisms. Finally, it may also increase the comparability of human and rodent research.

Therefore, I wanted to establish the water cross maze (WCM) as a suitable tool to study different learning strategies in mice and relate them to HPC functioning. Next, I aimed to dissect the influence of LTCCs on MEMRI contrast (specifically $Ca_v1.2$ and $Ca_v1.3$ as the two major LTCCs in the brain) in order to justify a functional application of MEMRI. At last, MEMRI should be implemented to depict learning processes in the WCM before I wanted to interfere with LTCC functioning to further explore their role in spatial learning.

I had been able to demonstrate that the WCM was particularly suitable for mice because it prevented most unwanted strategies that mice often adopt during the Morris water maze task. Further the test clearly dissected response from place strategies, which were both successfully acquired by C57Bl/6N mice. However, mice failed to relearn under response training independent of the original navigation strategy that was adopted within the week before. These results suggested, that not only place learning but also relearning is predicated on the HPC. Accordingly, HPC-lesioned mice were unable to acquire a place strategy, however, they adopted a response strategy instead. Further, relearning was blocked by the lesion, if less than 40% of the entire HPC remained. The inability to relearn was best reflected in the residual volume of the left ventral HPC. Second, I investigated the contribution of $Ca_v1.2$ and $Ca_v1.3$ on MEMRI contrast with the help of corresponding knockout mice. I was able to demonstrate that the $Ca_v1.2$ knockout affected at least 50% of the manganese-dependent contrast increase seen in MR images, whereas $Ca_v1.3$ knockouts caused no significant alterations. In addition, a locally defined knockout of $Ca_v1.2$ induced contrast differences in a projection region far away from the knockout side suggesting a bias in contrast differences away from the soma towards the axon terminals. Overall, this indicated a voltage-dependent manganese displacement in the brain and

therefore suggested the functional application of MEMRI. For this reason, I combined place training in the WCM with manganese injections to map brain activity *in vivo*. On the one hand, the accuracy score was related to a fear associated network comprising the basolateral amygdala (BLA) and ventral HPC. On the other hand, the latency correlated with the dorsal HPC, specifically the left CA3 and the right CA1 region. First, this was in line with functional magnetic resonance imaging (fMRI) results obtained in humans, where the left HPC indicated response navigation and the right place memory formation. Second, the associations indicate the integration of emotional information into cognitive processing. At last, learning and relearning capabilities of $Ca_v1.2$ knockout mice were explored. Despite reduced MEMRI intensities in learning associated regions, knockout mice successfully acquire place and response memories and were also capable to revert the place memory afterwards. However, animals exhibited a significant retardation during place learning ,which can be attributed to impairments of late long-term potentiation (LTP) in the CA1 region of the HPC.

Overall, the WCM suits the characteristics of mice and allows the distinction of different learning strategies. Further, mice similar to rats require an intact HPC to use place strategies in the WCM and at least 40% of the total HPC volume is necessary to accomplish relearning. Since I could demonstrate for the first time that MEMRI contrast largely depends on $Ca_v1.2$, MEMRI was employed to map brain activity in freely moving mice. I could identify brain regions most in the HPC that correlate with place learning parameters in the WCM for the first time *in vivo*. These results further match findings in humans, where place and response learning occur in parallel during place navigation in the left and right HPC, respectively. In addition, they suggest the integration of emotional information into cognitive precessing. At last, $Ca_v1.2$ is involved but not essential for place learning in the WCM. Future investigations with temporary knockouts might be useful to further elaborate the role of $Ca_v1.2$ in learning and memory functions.

Zusammenfassung

Beeinträchtigungen in der Einspeicherung, dem Abruf und in der Bearbeitung von Sinnes- oder Gedächtnisinhalten im Gehirn tragen zu einer Vielzahl von Neuro- und Psychopathologien des Menschen bei. Labormäuse eignen sich als Modellorganismus zur Erforschung der biologischen Grundlagen dieser Gedächtnisprozesse, da deren Gehirnfunktionen direkt durch genetische Manipulationen und mithilfe verschiedener anderer Methoden beeinflusst werden können. Daher ist es wichtig, Lern- und Gedächtnistests zu entwickeln, die speziell auf die Spezies Maus zugeschnitten sind und die mit denjenigen Tests verglichen werden können, die an Menschen angewandt werden. Eine kognitive Fähigkeit, die über verschiedene Spezies hinweg besteht, ist die räumliche Navigation. Damit verbunden ist das Gedächtnis darüber, wie ein spezifischer Ort erreicht werden kann. Hierbei unterscheidet man zwei grundlegend unterschiedliche Strategien, die räumliche und die sensomotorische Strategie. Die räumliche Strategie oder das räumliche Lernen beschreibt die Integration verschiedener Umgebungsreize in eine kognitive Landkarte, die im Hippokampus (HPC) neuronal kodiert wird. Demgegenüber gehört das sensomotorische Lernen zum Funktionsbereich des Striatums und beschreibt eine serielle Aneinanderkettung von direktionalen Handlungen. Die meisten Verhaltenstests, die diese beiden Strategien klar voneinander abgrenzen, wurden ursprünglich für Ratten konzipiert. Da sich das Verhalten von Mäusen deutlich von Ratten unterscheiden kann, ist es notwendig, diese Tests für Mäuse weiterzuentwickeln. Ein weiteres Problem stellt die Übertragung der strukturellen und funktionellen Forschungsergebnisse vom Tier auf den Menschen dar. Die an Nagetieren häufig angewandten Messungen im Gehirn entsprechen in der Regel nicht den in der Humanforschung angewandten Methoden. Mit der Manganverstärkten Magnetresonanztomographie (MEMRI) wurde eine Methode beschrieben, die die Übertragung von Ergebnissen der Tierforschung auf die Humansituation verbessern könnte. Da das applizierte Mangan den Kontrast auf MR

Bildern erhöht, ermöglicht MEMRI die volumetrische Analyse verschiedener Gerhirnregionen. Desweiteren wird angenommen, dass Mangan durch spannungsabhängige Kalziumkanäle des L-Typs (LTCCs) in Neurone einströmt und damit als Indikator für neuronale Aktivität herangezogen werden kann. Um MEMRI als eine funktionelle Methode zu etablieren, muss zunächst nachgewiesen werden, dass der Bildkontrast von LTCCs abhängt. Anschließend kann die Anwendung von MEMRI nicht nur dazu beitragen, die der Navigation zugrundeliegenden Netzwerke im Gehirn zu identifizieren, sondern unter Einbeziehung anderer Technologien auch kausale Zusammenhänge zu neurobiologischen Mechanismen herzustellen.

Für diese Arbeit ließen sich folgende Ziele ableiten: Zunächst sollte das Water Cross Maze (WCM), ein potentiell geeignetes Verfahren zur Testung räumlicher Navigationsstrategien an Mäusen, etabliert werden. Anschließend sollte die Rolle des HPC für verschiedene Lernprotokolle untersucht werden. Als nächstes sollte der Beitrag der primären LTCCs im Gehirn, das heißt $Ca_v1.2$ und $Ca_v1.3$, zur Bildintensität ermittelt werden. Desweiteren sollte MEMRI angewendet werden, um lernabhängige Gehirnaktivität im WCM abzubilden. Zuletzt sollte der Einfluss der LTCCs auf das räumliche Lernen im WCM näher untersucht werden.

Zunächst konnte ich zeigen, dass das WCM insbesondere deswegen für Mäuse geeignet ist, weil es die meisten alternativen aber unerwünschten Strategien unterbindet, die sich Mäuse häufig im Morris Water Maze zu eigen machen. Ferner unterschied der Test klar räumliche von sensomotorischen Strategien, die von C57Bl/6N Mäusen beide gleichermaßen schnell erlernt wurden. Die Mäuse scheiterten hingegen am Umlernen, wenn sie in der zweiten Trainingswoche das sensomotorische Protokoll zu durchlaufen hatten, unabhängig von der ursprünglich in der ersten Woche erlernten Strategie. Dies legt nahe, dass nicht nur das räumliche Lernen, sondern auch das Umlernen abhängig vom HPC ist. HPC-lädierte Mäuse waren dementsprechend nicht in der Lage, die räumliche Strategie zu erlernen. Die Tiere kompensierten dies vielmehr mit einer inadäquaten sensomotorischen Strategie. Zudem wurde das Umlernen durch die Läsion verhindert, wenn mehr als 60% des gesamten HPC zerstört wurden. Die genauere Analyse der verschiedenen Subregionen des HPC ergab, dass das Restvolumen des linken ventralen

HPC die Unfähigkeit zum Umlernen am besten wiedergespiegelte. Als zweiten Schritt untersuchte ich mithilfe entsprechender Knockoutmäuse den Einfluss von $Ca_v1.2$ und $Ca_v1.3$ auf die Bildintensität der MEMRI Aufnahmen. $Ca_v1.2$ verringerte den manganabhängigen Intensitätsanstieg im gesamten Gehirn um mindestens 50%, während $Ca_v1.3$ keinen Einfluss hatte. Interessant war auch, dass die lokale Beseitigung des $Ca_v1.2$ Kanals zu Kontrastunterschieden in Projektionsarealen, nicht jedoch am Ort der Veränderungen führte. Dies gilt es besonders bei Projektionsneuronen zu berücksichtigen, deren Nervenendigungen weit weg vom eigenen Zellkörper liegen. Zusammenfassend weisen diese Befunde auf eine spannungsabhängige Verschiebung von Mangan im Gehirn hin, was die Anwendung von MEMRI als funktionelle Methode nahelegt. Um daher MEMRI zur Abbildung lernabhängiger Hirnaktivität *in vivo* zu verwenden, kombinierte ich das räumliche Training im WCM mit Manganinjektionen. Die Analyse der MEMRI Intensitäten lieferte einerseits einen Zusammenhang zwischen der Akkuratesse und einem angstassoziierten Netzwerk bestehend aus der basolateralen Amygdala (BLA) und dem ventralen HPC. Andererseits war die Latenz mit dem dorsalen HPC korreliert, und zwar mit der linken CA3 und der rechten CA1 Region. Dies stimmt mit funktionellen Humandaten überein, die eine Beziehung zwischen dem linken HPC und sensomotorischen sowie dem rechten HPC und räumlichen Strategien beschreiben. Insgesamt legen die Zusammenhänge die Integration von emotionalen und kognitiven Inhalten während des räumlichen Lernens nahe. Abschließend untersuchte ich die Lern- und Umlernfähigkeiten von $Ca_v1.2$ Knockoutmäusen. Trotz reduzierter MEMRI Intensitäten in lernassoziierten Gehirnregionen absolvierten die Tiere erfolgreich das räumliche sowie das sensomotorische Training und waren ebenfalls in der Lage umzulernen. Allerdings zeigten die Tiere eine signifikante Verzögerung beim räumlichen Lernen, was möglicherweise auf Beeinträchtigungen der späten Langzeitpotenzierung (LTP) in der CA1 Region zurückzuführen ist.

Das im Rahmen der Dissertation etablierte WCM ist also in höchstem Maße für die Arbeit mit Mäusen geeignet und es ermöglicht eine klare Unterscheidung verschiedener Navigationsstrategien. Weiterhin benötigen Mäuse genauso wie Ratten einen intakten HPC für das räumliche Lernen und mindestens 40% des gesamten Hippokampusvolu-

mens ist notwendig, um erfolgreich umzulernen. Da hier erstmalig gezeigt wurde, dass der Bildkontrast von MEMRI in einem hohen Maßvon $Ca_v1.2$ abhängt, habe ich MEMRI eingesetzt, um die Hirnaktivität in Mäusen wärend des Lernens zu bestimmen. Ich konnte erstmals *in vivo* Hirnregionen u.a. im HPC identifizieren, die mit räumlichen Lernparametern im WCM korrelieren. Die Ergebnisse ähneln zudem humanen MR Daten, die zeigen, dass sensomotorisches und räumliches Lernen parallel in den verschieden Hemisphären des HPC verarbeitet werden. Zuletzt ist $Ca_v1.2$ am räumlichen Lernen beteiligt, jedoch nicht notwendig. Die Beseitigung der $Ca_v1.2$ Kanäle zu einem späteren Entwicklungsstadium der Maus könnte zukünftig helfen, deren Rolle bei Lern-und Gedächtnisfunktionen weiter zu erforschen.

1. Introduction

Impairments of the ability to encode, retrieve or manipulate information significantly contribute to neuro- and psychopathologies. To better understand the biological principles of learning and memory, genetic tools are often required that are only available for mice. However, most behavioral testings that are used to investigate cognitive abilities in rodents were originally developed for rats. Since the behavior of rats and mice is considerably different, it is necessary to design memory tests, which meet the specific demands of a mouse. In addition, there are huge differences in the methods that are applied in human and rodent research to identify neural correlates of memory functions. Because of that, morphological and functional methods are particularly required, which facilitate the translation between the two fields.

1.1. Information encoding, retrieval and manipulation

Learning is the process in which the knowledge is acquired, whereas the memory refers to processes by which that knowledge is encoded, stored and later retrieved (Kandel et al., 2000). Memory can be divided into short-term memory, which is limited in capacity and time (several seconds to minutes), and long-term memory, which comprises larger quantities up to periods of several decades and involves *de novo* protein synthesis (McGaugh, 2000). Endel Tulving distinguished two types of long-term memory, i.e. the explicit memory a declarative and highly flexible memory, and the implicit memory a rather non-declarative and more rigid entity (Tulving, 1972; Squire, 1992; Thompson and Kim, 1996). Explicit memories include either information on events like places and people (episodic memory) or facts independent of the context (semantic memory). Acquisition and retrieval - for a limited period of time - of explicit memories depend on the medial temporal lobe including the HPC. Lesions within this area produce severe anterograde

amnesia similarly in rodents and humans (Scoville and Milner, 1957; Eichenbaum et al., 1990; Spiers et al., 2001). Alzheimer patients develop not only a strong impairment in explicit memory, but show also a HPC atrophy which parallels the memory degradation (Knowlton et al., 1996; Fox et al., 1996). Despite the deficits in explicit memory, the ability to learn or retrieve implicit memories remains intact after hippocampal excisions and in Alzheimer patients (Scoville and Milner, 1957; Morris et al., 1982; Knowlton et al., 1996). Implicit memories are more rigid as they are tightly connected to the stimulus conditions under which the learning occurs. They encompass several kinds of procedural and perceptional memories including skills that can become habits and classical or operant conditioning (Tulving and Schacter, 1990; Squire, 1992). As skill learning and operant conditioning comprise sensory and motor elements, they are mediated by the striatum and the cerebellum in both humans and rodents (Packard and McGaugh, 1992; Knowlton et al., 1996; Thompson and Kim, 1996; Doyon et al., 1997). Due to the decreased dopamine action in the nigrostriatal pathway, Parkinson patients develop implicit memory deficits whereas the explicit memory remains unaffected (Knowlton et al., 1996).

Explicit and perhaps some forms of implicit information are maintained and manipulated in the working memory (Miller, 1956; Baddeley and Hitch, 1974; Baddeley, 2000). While at least two short-term memory systems transiently maintain information in a buffer (e.g. the phonological loop responsible for auditory information or the visuo-spatial sketchpad for visual and spatial content), the central executive is crucial for its manipulation. Factor analysis revealed three largely independent components of the central executive, i.e set shifting, information updating and response inhibition (Miyake et al., 2000; Fisk and Sharp, 2004). All have in common that they share a neurobiological substrate in the prefrontal cortex (Robbins, 1996). While a variety of executive functions are conserved in rodents, the prefrontal cortex is significantly less complex compared to primates. Yet, many studies indicate that rats and maybe mice have neuroanatomical and functional homologous in the orbitofrontal and medial prefrontal cortex comprising the anterior cingulate, the prelimbic and the infralimbic cortex (for review see Ragozzino, 2007; Bissonette et al., 2008).

Abnormalities in prefrontal cortex function and corresponding cognitive deficits are reported for a number of psychopathologies including schizophrenia and depression. Both disorders are associated with the inability to maintain goal information in the working memory what parallels a hypoactivity in the prefrontal cortex (for review see Lesh et al., 2011; Barch and Ceaser, 2012; Kupfer et al., 2012; Snyder, 2012). Patients suffering from obsessive compulsive disorder develop specific deficits in response inhibition what is also reflected in orbitofrontal cortex abnormalities (for review see Chamberlain et al., 2005; Milad and Rauch, 2012).

Overall, it appears that deficits in information encoding, retrieval and manipulation can contribute to a number of neuro- and psychopathologies. Because many invasive approaches that could increase our understanding are impractical or infeasible in primates, rodent models represent an important tool to study the underlying mechanisms in the HPC, the striatum and the prefrontal cortex. The laboratory mouse as a model organism provides a number of advantages to challenge these questions, as one can interfere directly with brain functions via a number of tools including genetic manipulation. Therefore it is from great importance to develop memory tests that meet the specific demands of mice and allow the translation to humans.

1.2. In search of a spatial memory test for mice

Due to the cognitive abnormalities observed in different neuro- and psychopathologies, I am in search of a memory test applicable in mice that clearly distinguishes explicit-like (HPC dependent) from implicit memory and further captures aspects of central executive functions (prefrontal cortex dependent). Spatial navigation is a practically relevant ability that is highly preserved across different species and, therefore, suitable for translational research on cognition (Benhamou and Poucet, 1995; Moffat et al., 1998). Humans and rodents have developed two distinct strategies to reach a specific point in space, i.e. place and response learning (Tolman et al., 1946; Maguire et al., 1998). Place learning depends on environmental cues which are spatially referenced to the target point and therefore integrated into a cognitive map (allocentric reference frame). In contrast, response learning

is the acquisition of directed movements along a route to get to a destination (egocentric reference frame). The strategies can be dissociated regarding the underlying brain circuit. Place learning involves the dorsal HPC while response learning is based on the dorsolateral striatum (Packard et al., 1989; McDonald and White, 1994; Packard and McGaugh, 1996). Electrical recordings revealed different cell types in the HPC and the entorhinal cortex that contribute to spatial mapping. Grid cells in the entorhinal cortex provide a two-dimensional metric space and may contribute to the formation of place cells in the HPC that fire at a particular location (O'Keefe and Dostrovsky, 1971; Hafting et al., 2005). In contrast, the striatal system that subserves response learning activates a cortico-striatal loop, which involves somatosensory and motor cortical areas and the dorsolateral striatum (Barnes et al., 2005).

Changing environments require the flexible adaptation of acquired spatial navigation strategies. This can be done either by the conversion of a previously approached stimulus into a now avoided stimulus (i.e. reversal learning) or by replacing the entire learning strategy by another learning modality (i.e. strategy switching; Ritchie et al., 1950; Hicks, 1964; Ragozzino, 2007). Relearning is a generic term and includes both, reversal learning and strategy switching. Reversal learning depends on the orbitofrontal cortex in primates and rodents whereas strategy switching relies on the medial prefrontal cortex in rodents and the dorsolateral prefrontal cortex as the corresponding structure in primates (Dias et al., 1996; Ragozzino, 2007; Bissonette et al., 2008). Both frontal regions project to the dorsomedial striatum, which is therefore essential for both types of spatial flexibility (Ragozzino et al., 2002; Ragozzino and Choi, 2004). Consequences of lesions in any of the responsible regions are behaviorally reflected in perseverance errors indicating the search for the originally acquired place (Ragozzino, 2007).

Despite the controversial discussion about the existence of explicit memories in non-human species, place learning in rodents parallels the human episodic memory concept in the way that it is based on situational information and shares functional similarities in the HPC (O'Keefe and Dostrovsky, 1971; Morris, 2001; Hassabis et al., 2009). Further, response learning in rodents resembles human implicit motor learning and depends on the striatum in both species (Packard et al., 1989; Maguire et al., 1998). Virtual reality

studies not only confirmed the importance of the HPC and the striatum for place and response learning in humans (Maguire et al., 1998), but also introduced a functional heterogeneity between the right and left HPC, where the right HPC subserves place and the left response learning (Iglói et al., 2010). In addition, central executive processes like behavioral inhibition and attentional shifting can be captured in the spatial context by reversal learning and strategy switching protocols. The relevance of spatial relearning could be demonstrated in older people, who developed deficits in the ability to switch to a place learning strategy in a virtual maze (Harris et al., 2012). In contrast, demented patients have severe problems to acquire a place strategy at all (Nedelska et al., 2012). Further, virtual reality tasks are more and more applied to psychiatric patients having e.g. depression or schizophrenia (Gould et al., 2007; Weniger and Irle, 2008; Spieker et al., 2012).

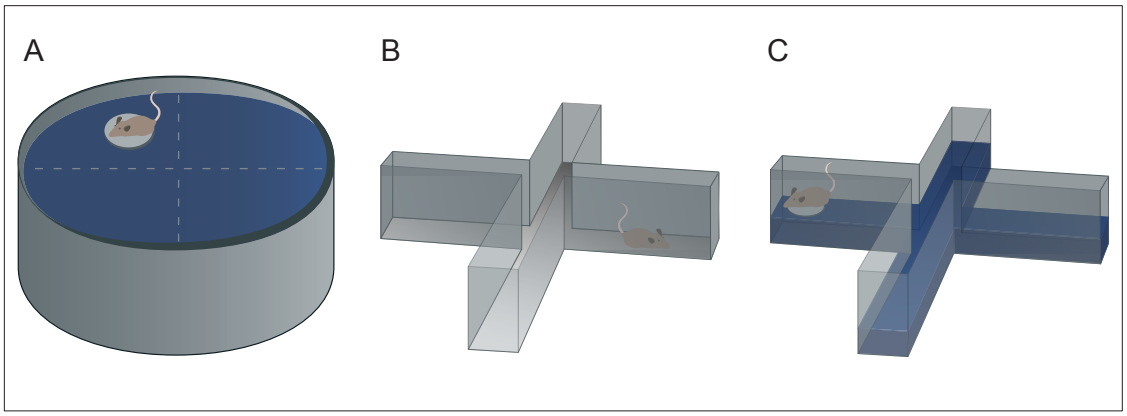

Figure 1.1.: In search of a spatial learning and flexibility test for mice. **(A)** The Morris water maze produces robust performances because water constantly motivates the animals over many trials. **(B)** The dry plus or cross maze circumvents unwanted response based searching strategies, which are preferentially used by mice in open mazes. **(C)** The water cross maze (WCM) combines the advantages of the Morris water maze and the dry cross maze and is therefore well suited for the application in mice.

Typical tasks that are used to study place and response learning as well as relearning are the Morris water maze, the Barnes maze, the radial arm maze and the plus or cross maze to name the most important once. The Morris water maze consists of a circular pool filled with water at ~23°C (figure 1.1 A; Morris, 1984). Naturally, rodents search for a way to escape from the water since it represents an aversive stimulus. Over a number of trials, animals have to locate a hidden or cued platform to get out of the water. One drawback

of the Morris water maze is the considerable stress load induced by the quite long water exposure. The Barnes maze represent a dry alternative to the Morris water maze (Barnes, 1979) and includes an open round and brightly lit platform with holes along the perimeter. Since mice and rats are nocturnal, they try to escape from the bright platform what they can achieve by entering a dark target chamber through one particular hole. The third task, the radial arm maze, is characterized by eight defined arms that are connected by a central platform (Olton and Samuelson, 1976). Here, food restricted animals have to locate baited corridors over several trials. Unlike the Morris water maze, which was originally designed to test explicit-like memories in rats, the radial arm maze was intended as a working memory task. At last, the plus maze as a test of spatial navigation consists of four rectangular arranged arms and also requires food restricted animals to locate a pellet at the end of a target arm (figure 1.1 B; Tolman et al., 1946; Packard, 2009). All four tests were originally evaluated in rats, however, species differences need to be considered before applying a test to the mouse. Because mice tend to response based searching strategies in open mazes, they often develop unwanted strategies like chaining (in this context a concatenation of directed movements) to locate a place in the environment (Schenk, 1987; Wolfer and Lipp, 2000; Branchi and Ricceri, 2004; Ruediger et al., 2012). The radial arm maze and the plus maze circumvent this problem by restricting the movements of the animals on narrow corridors. This is possibly the reason, why dry mazes produce similar results in rats and mice and a reduction in the diameter of the pool increases species similarities (Whishaw and Tomie, 1996; Frick et al., 2000). These arguments rather speak against the Morris water maze, however, water as a motive force produces more robust performances as it keeps the motivation of the animal high over many trials (Ormerod and Beninger, 2002). In addition, water mazes minimize the risk that mice are guided by olfactory cues (e.g. urine) of the predecessor. Overall, a water based plus or radial arm maze would reduce the possibility to adapt unwanted strategies while maintaining the motivation. Further, it could reduce the time an animal spends in the water and therefore avoids hypothermia and, possibly, floating (Iivonen et al., 2003). Essman and Jarvik (1961) developed such a water cross maze (WCM) that clearly distinguishes place from response learning and enables relearning according to the protocols originally applied by Tolman (figure 1.1 C; Tolman et al., 1946). Due to the aforementioned advantages, I first

want to evaluate the WCM as a suitable tool to investigate spatial learning and relearning capabilities in C57Bl/6N mice. In addition, I would like to examine the importance of the HPC for learning and relearning processes in the WCM and therefore relate the different protocols to other learning tasks.

1.3. Structural and functional methods applied in mice and men

The heterogeneity of methods that are applied in humans and rodents to identify structural and functional aspects of the brain makes it difficult to translate between species. Commonly used methods to investigate the neuroanatomy in humans are magnetic resonance imaging (MRI) and computed tomography (CT). Both provide three dimensional reconstructions of the living brain with a resolution in the micrometer range and allow the volumetric analysis of defined brain regions (Meese et al., 1980; Jernigan et al., 1991). In addition, MRI enables morphometric analyses of the brain on a voxel level, which has the advantage that no a priori hypothesis about the exact brain region is necessary (Ashburner and Friston, 2000). New sequences can also depict diffusivity of water molecules and therefore track projection fibers in a three-dimensional image (diffusion tensor imaging (DTI); Basser et al., 1994). This is different to the *ex vivo* histological examination on two dimensional brain slices usually applied in rodents. It presupposes the removal and fixation of the brain, which alters the neuroanatomical characteristics depending on the type of fixation (Lavenex et al., 2009). To differentiate brain structures and visualize even single cells, staining techniques are applied to brain slices that help to identify cell bodies, neurons and astrocytes (e.g. Nissl, Golgi and GFAP staining). Microscopic methods then enable resolutions in the nanometer range and therefore not only allow the estimation of a regional volume (Gundersen and Jensen, 1987), but also a precise morphological analysis of single cells (e.g. Mitra et al., 2005). In addition, anterograde and retrograde tracing techniques allow the detailed assessment of the connectivity of specific neuronal populations (e.g. Ciocchi et al., 2010). Overall, the human brain is depicted *in vivo* on a micrometer range, which allows the precise volumetric analysis of brain regions, whereas the rodent brain is usually imaged *ex vivo* on a nanometer range optimized for a detailed morphological assessment of specific cell assemblies.

A similar mismatch between human and rodent research can be obtained in functional methods. Brain activity in humans is most commonly measured *in vivo* by electroencephalography (EEG), positron emission tomography (PET) or fMRI. The EEG records summed electrical signals on the surface of the head and therefore provides limited spatial resolution concerning the depth of the brain. This is different to fMRI and PET, which depict three dimensional functional images with a spatial resolution up to 2 mm in fMRI and slightly worse in PET studies. Recent data on the number of neurons in the human brain suggest that such a typical fMRI voxel (8 mm^3) would contain around 500.000 neurons on average (Azevedo et al., 2009). Another important aspect is the temporal resolution as brain potentials often occur within 300 ms after a triggering event (Chapman and Bragdon, 1964). The time between two EEG recordings comprises a few milliseconds whereas fMRI acquisition is repeated only every view seconds. PET is normally used to detect long-lasting differences at baseline or after treatment outside the scanner and is therefore based on one single functional image. The most direct measurement of neuronal activity, the electrical signal itself, is only captured by the EEG while the fMRI estimates the oxygen level in the blood. It is controversial but often assumed that oxygen consumption resembles neuronal activity (Logothetis et al., 2001; Peppiatt et al., 2006). Depending on the used radioactive tracer, PET can image energy or protein metabolism as well as receptor occupancies (Lammertsma, 2001). One of the most commonly applied radiotracers is glucose radioactively labeled with flourine (^{18}F-FDG) to image energy metabolism in the brain. On the other hand, frequently used functional methods in basic research on animals are activity related staining methods like immediate early gene (IEG) expression, electrophysiological recordings and calcium imaging. IEGs like c-Fos, Arc or Zif268 are genes that get activated rapidly in response to cellular stimulation (between 1 minute and 2 hours) and allow to measure task-dependent activation within one or two specific time slots (Guzowski et al., 1999, 2005). For that purpose, animals are confronted with a stimulus or task before being killed to remove and fixate the brain at a certain timepoint. Afterwards, proteins or mRNA are then stained *ex vivo* on brain slices, and IEG-activity is quantified in various predefined brain regions often by counting activated cells in a window of interest (e.g. Singewald, 2007). A more sophisticated but less often employed assessment technique is the stereological analysis (Gundersen and Jensen, 1987). It allows

an unbiased and systematic sampling of IEG-reactivity throughout the rostrocaudal axis (thickness) of the slice. While IEGs map neuronal activity at a fairly defined period, other markers like the cytochrome-c oxidase are available that depict rather long-term mitochondrial metabolism (Wong-Riley, 1989; Sakata et al., 2005; Harro et al., 2011). In contrast to IEGs, electrophysiological recordings provide a temporal resolution in the millisecond range. To record the electrical potentials of single neurons or neuronal populations, one or more electrodes are placed into a particular brain region either in a tissue preparation or into the intact brain of a freely moving animal (e.g. O'Keefe and Dostrovsky, 1971; Sigurdsson et al., 2010). A similar temporal resolution is provided by calcium imaging, a functional method that utilizes chemical or genetic calcium indicators to optically probe calcium influx and hereby estimate neuronal activity. This technique can depict the calcium status of hundreds of neurons on two-dimensional microscopic images *in* or *ex vivo* (e.g. Helmchen et al., 2001; Stosiek et al., 2003). Overall, the assessment of neural activity in humans and rodents overlaps to a great extent in terms of the temporal resolution, while the spatial resolution is substantially different. On the one hand, most functional methods in rodents are restricted to small quantities of neuronal assemblies and often comprises maximum two dimensions, whereas functional units in humans include much larger quantities of several 100.000 neurons but often form a three-dimensional functional image.

In summary, there exist a substantial difference in the methods that are applied in animal and human research to quantify structural and functional abnormalities. The essential distinction is that the smallest measurable unit is much larger in human compared to rodent studies. Moreover, human data provide three-dimensional structural or functional reconstructions of the brain that allow a voxel-wise comparison without specifying brain regions in advance, whereas investigations in rodents comprise either a priori defined neural assemblies or brain slices. In addition, the *in vivo* approaches applied in humans facilitate longitudinal studies what is often prohibited by the methodology in animals research. Therefore, methods that provide three-dimensional structural or functional images need to be developed in rodents to increase the comparability of the results obtained in both fields. This could also be done at the expense of spatial resolution, but *in vivo* to enable longitudinal studies in rodents.

1.4. Manganese-enhanced magnetic resonance imaging

One way to collect three-dimensional images from the rodent brain is the adaptation of MR methods to small animals (e.g. Eckart et al., 2012). In humans, structural MRI provides sufficient soft-tissue contrast to differentiate gray and white matter of the brain, which then enables the delineation of different brain structures like the HPC (Seab et al., 1988). Appreciable contrast between gray and white matter is usually achieved by T1-weighted (T1w) images that depict the time until protons realign to the static magnetic field after excitation by a radiofrequency pulse. Unfortunately, the achievable contrast in T1w images of the mouse brain is substantially lower. The reason for this is that the brain of a mouse is 3000 times smaller than that of a human what is methodologically challenging (Herculano-Houzel et al., 2006; Azevedo et al., 2009). To achieve a comparable resolution in the mouse brain, the voxel size must be reduced accordingly, which in turn is associated with a deterioration of image quality (signal-to-noise ratio). This is often counteracted but not fully compensated by higher magnetic field strength and an increase in the number of repeated acquisitions. The latter is, however, associated with an extended scanning time, which is limited for *in vivo* studies due to the necessary anesthesia of the animal. Naïve T1w images of the mouse brain provide little contrast between cerebral compartments making it difficult to delineate brain regions (Gruenecker et al., 2010). However, this can be improved by paramagnetic contrast agents containing metal ions like gadolinium or manganese that shorten the T1 relaxation time and therefore increase image intensity (for review see Strijkers et al., 2007).

Manganese-enhanced magnetic resonance imaging (MEMRI) has gained interest in animal research because of its diverse applications. First, manganese enhances the contrast in the brain and thereby facilitates the delineation of different brain regions and even the identification of neuronal layers (Lauterbur et al., 1973; Pautler and Koretsky, 2002). This enables the three-dimensional reconstruction of the brain and semi-automatic volumetry of brain regions like the HPC *in vivo* (Gruenecker et al., 2010). Further, it has been shown that MEMRI is sensitive enough to detect even subtle volume differences and corresponds to *ex vivo* microscopy (Golub et al., 2011). Overall, this approach strongly parallels the structural methods applied in humans.

Second, MEMRI was used as a functional method to determine brain activity (Yu et al., 2005). Mainly in vitro studies have contributed to the interpretation that manganese accumulation represents a measure of neuronal activity. (i) Drapeau and Nachshen (1984) could prove, that manganese compete with calcium for the passage through calcium channels in brain derived neurons. Another experiment in cerebellar granule cells then identified *N*-methyl-D-aspartic acid (NMDA) receptors and L-type voltage dependent calcium channels (LTCCs) to essentially modulate manganese influx (figure 1.2 A; Simpson et al., 1995). NMDA receptors open during cell depolarization and simultaneous ligand binding, while activation of LTCCs depends only on the voltage of the membrane. The direct influence of NMDA receptors on MEMRI contrast has already been demonstrated *in vivo*, while the contribution of LTCCs remains unknown (Itoh et al., 2008). Therefore, MEMRI contrast might reflect neuronal activity as manganese enters the cell through activity-regulated ion channels. (ii) Another issue that is important for the application of MEMRI as a functional tool concerns the storage of manganese in the cell. There is evidence that manganese accumulates in mitochondria and thereby exerts its later described toxic effects (figure 1.2 B; Liccione and Maines, 1988). Moreover, it seems to occur also in intracellular calcium stores, yet, to a much lesser extent than calcium (Mertz et al., 1990; Fasolato et al., 1993). Half life times of manganese in the brain (5-7 days) suggest that it remains in the cells for quite a long time (Gruenecker et al., 2012), however, it is unclear how much manganese is retained and over which exact period. It is important to mention that a sustained maintenance of manganese at a place could make temporal integration possible because activity changes would then be measurable for long periods. Therefore, MEMRI could enable activity mapping over longer phases and multiple training trials. Despite the mechanistic uncertainties, quite a number of studies successfully applied functional MEMRI to map rather chronic activity regulations in mice and rats including voluntary wheel running or auditory stimulation (Yu et al., 2005, 2008; Watanabe et al., 2008; Eschenko et al., 2010a; Hoch et al., 2013). The advantage of MEMRI over other methods like fMRI is that manganese may accumulate in active brain regions of freely moving animals and only afterwards, the animal must be anesthetized for the image acquisition. In addition, the acquired T1w images provide a much better resolution compared to PET and fMRI in rodents (T1w: $125 \times 125 \times 140.3$ μm^3 vs. PET: $776 \times 776 \times 796$ μm^3 in von Reutern et al., 2013).

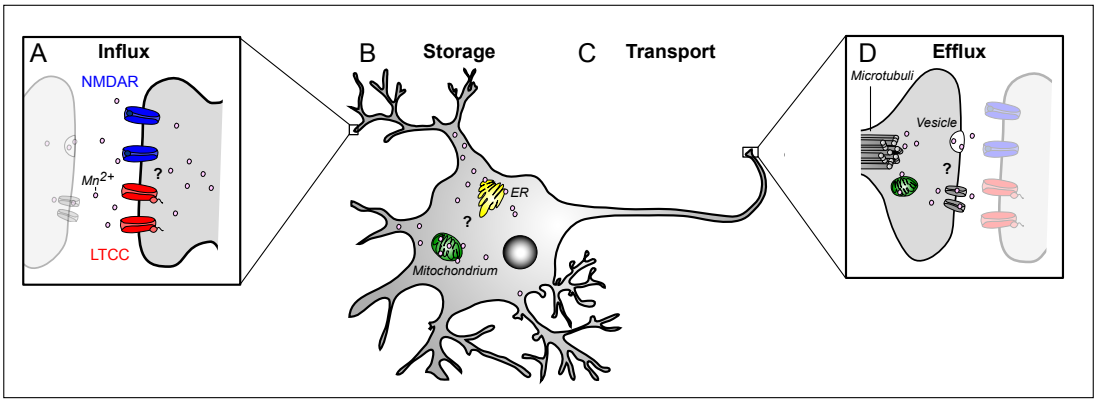

Figure 1.2.: A hypothetical model of the cellular influx, storage, transport and efflux of manganese. **(A)** Manganese ions (Mn^{2+}) enter the cell through *N*-methyl-D-aspartate receptors (NMDAR) and L-type voltage dependent calcium channels (LTCC) at the dendritic synapse, **(B)** and accumulate in the mitochondria and in intracellular calcium stores at the endoplasmic reticulum (ER). **(C)** It is transported along the axon by microtubules, **(D)** and leaves the cell at the presynaptic terminal in an activity-dependent manner where it can be taken up by the next neuron. It still remains to be shown, whether LTCCs are involved in the influx of manganese *in vivo*, how and for what time manganese is stored in the cell and whether manganese is released in vesicles or transported out by ion channels.

Third, MEMRI was used as an anterograde tract tracer to visualize brain networks (Pautler et al., 1998; Van der Linden et al., 2004). Two other major kinetic characteristics of manganese make this possible. (iii) First, manganese is transported along the axon of the neuron by the microtubules (figure 1.2 C; Sloot and Gramsbergen, 1994) and (iv) subsequently spilled out at the presynaptic terminal through depolarization (figure 1.2 D; Takeda et al., 1998). Manganese can then be taken up by the next neuron and therefore travels across synapses. Depending on the question, intracranial, intranasal or intravitreal injection of manganese was used to identify projection regions (Pautler et al., 1998, 2003). Due to the activity-dependent uptake and release of manganese, stimulation of a pathway changes the kinetics of manganese, which allows the simultaneous detection of activity aspects (Pautler et al., 2003; Yang et al., 2011). Tract tracing by MEMRI somehow parallels DTI in humans as both depict fiber tracts in whole brain images.

A major drawback of manganese as a contrast agent is that it is neurotoxic in its ionic form (Hazell, 2002; Takeda, 2003). Intoxication has been reported for miners that inhaled manganese-charged dust over a long time and later developed Parkinson-like symptoms due to the preferential accumulation of manganese in the basal ganglia (for review see Lee, 2000). Therefore, only chelated manganese is used as a contrast agent in human

medicine, which avoids toxic side effects but also looses many of its versatile applications (Federle et al., 2000). In animals, acute manganese treatment impairs HPC functions in a dose dependent manner (Eschenko et al., 2010b). One way to reduce the toxic side effects and to obtain a maximum contrast at the same time is given by repeated low-dose intraperitoneal injections of manganese (Bock et al., 2008; Gruenecker et al., 2010, 2012). An even more continuous application is achieved by implanted osmotic mini pumps that release manganese at low dosages over several days (Eschenko et al., 2010a; Sepúlveda et al., 2012; Hoch et al., 2013). Therefore, it is recommended to use either fractionated manganese application protocols or continuous low dose applications via osmotic mini pumps in order to minimize side effects.

In conclusion, the versatile applications of MEMRI make it very interesting for basic research. Moreover, it may improve translation to human research as it maps three-dimensional images of the whole brain in a relatively high spatial resolution. While MEMRI was well established *in vivo* for volumetric assessments and tract tracing, functional MEMRI is less well evaluated. One important question is, how LTCCs contribute to MEMRI contrast *in vivo* and where manganese accumulates after neural activity has changed?

1.5. Contribution of LTCCs and NMDA receptors to spatial learning and memory

Many models suggest that long-term potentiation (LTP) is the cellular mechanism, which underlies certain types of learning (Bliss and Lømo, 1973; Bliss and Collingridge, 1993). It describes a strengthening in synaptic transduction and is divided into early LTP that requires covalent protein modification and late LTP depending on protein synthesis (Frey et al., 1988; Kandel, 2001). Only late LTP is associated with long-lasting memory formation (> 3 hours) and requires calcium entry into the postsynaptic cell (Kandel, 2001). Depending on the stimulation frequency, induction of late LTP depends on NMDA receptors or critically involves LTCCs independent of NMDA (Morgan and Teyler, 1999; Bauer et al., 2002; Moosmang et al., 2005). Both, NMDA receptors and LTCCs, are sufficient

to trigger calcium dependent intracellular cascades that stimulate gene transcription and *de novo* protein synthesis via the cAMP response element-binding protein (CREB; Impey et al., 1996; Sweatt, 1999; Dolmetsch et al., 2001).

In behavioral studies, NMDA receptors in the thalamus-amygdala pathway are essential for the acquisition of a tone-shock association (Miserendino et al., 1990; Maren et al., 1996; Bauer et al., 2002). Whether LTCCs contribute only to the long-term storage of tone-shock associations or whether they also make an impact on the acquisition remains controversial (Bauer et al., 2002; Langwieser et al., 2010). Electrophysiological data, however, support the importance of an LTCC-dependent and NMDA receptor-independent LTP also for fear learning (Weisskopf et al., 1999; Langwieser et al., 2010). Unlike the acquisition, the encoding of an extinction memory to suppress a previously learned fear association requires LTCCs in the BLA, while the involvement of NMDA receptors is not entirely evidenced (Falls et al., 1992; Santini et al., 2001; Cain et al., 2002; Sotres-Bayon et al., 2007; Davis and Bauer, 2012).

A similar picture has been obtained for place memories in the Morris water maze, where NMDA receptors in the cornu ammonis 1 (CA1) of the dorsal HPC are crucially involved in its encoding (Collingridge et al., 1983; Morris et al., 1986; Bannerman et al., 1995; Tsien et al., 1996; Morris, 2013). On the other hand, LTCCs are again important for the long-term storage, but they may also be relevant for the acquisition of place memories (Moosmang et al., 2005; White et al., 2008). Problems to verify the causal involvement of LTCCs in learning and memory occur because genetic knockouts of specific LTCC isoforms are often lethal or lead to homeostatic compensation at the synaptic level (e.g. via AMPA receptors; Langwieser et al., 2010). Regarding simple response navigation, the NMDA receptor exerts no effect on the learning success. Sequential and, therefore, more complex response learning requires NMDA receptors in the HPC (Tsien et al., 1996; Rondi-Reig et al., 2001; Palencia and Ragozzino, 2004, 2005; Rondi-Reig et al., 2006). At last, NMDA receptors in the medial striatum contribute to response reversal learning, and NMDA receptor-mediated long-term depression (i.e. a long-lasting decrease in synaptic strength) in the HPC affects place reversal learning (Palencia and Ragozzino, 2004; Nicholls et al., 2008). Whether LTCCs influence response or reversal learning, has to my knowledge

not yet been explicitly investigated. Therefore, it would be worthwhile to study the impact of distinct LTCC isoforms not only on place but also on response learning and relearning.

The main LTCC isoforms in the brain are $Ca_v1.2$ and $Ca_v1.3$. $Ca_v1.2$ makes 80% of the LTCCs and is mostly situated on dendrites, while $Ca_v1.3$ is usually localized at the soma of neurons (Westenbroek et al., 1990; Hell et al., 1993; Ludwig et al., 1997; Hetzenauer et al., 2006; Sinnegger-Brauns et al., 2009). There are pharmacological and genetic approaches to interfere with the function of each LTCC channel. To identify the role of LTCC isoforms for manganese accumulation *in vivo* and later investigate the importance for spatial learning and relearning capabilities, I applied two knockout mouse strains, that either lack the $Ca_v1.2$ or $Ca_v1.3$. Since the global knockout of $Ca_v1.2$ is lethal at postnatal day 14.5 (Seisenberger et al., 2000), conventional and conditional knockout techniques were combined to achieve a complete knockout of $Ca_v1.2$ in the whole central nervous system (Langwieser et al., 2010). To this end, the loxP-flanked (floxed) exon 14 and 15 of the CACNA1C gene was eliminated in the presence of the Cre recombinase (Nagy, 2000). The Cre recombinase was expressed under the Nestin promoter, which leads to an inactivation of the $Ca_v1.2$ gene throughout the brain (Tronche et al., 1999; Langwieser et al., 2010).[1] These animals have a normal life expectancy, normal body weight and exhibit no overt abnormalities in the brain (Langwieser et al., 2010). On the other hand, a traditional global knockout of $Ca_v1.3$ does neither lead to early death of an animal nor to any overt abnormalities e.g. in the glucose metabolism. It was therefore achieved by the disruption of $Ca_v1.3$ expression through the introduction of a neomycin resistance cassette into exon 2 of the CACNA1D gene (Platzer et al., 2000). The advantage of the genetic elimination over pharmacological approaches is that it allows the clear dissociation of the channels' function and does not directly interfere with the general excitability of the neurons.

[1] The Cre-loxP system is used to achieve a tissue or cell type-specific inactivation of a gene of interest (Gu et al., 1994). Breeding of a mouse having a gene of interest flanked by loxP-sites (floxed) results in an inactivation of the gene specifically in the tissue, where the Cre recombinase is expressed. The spatial and also temporal pattern of the deletion depends on the properties of the tissue-specific promoter controlling Cre recombinase expression. Here, Nestin was used as a promoter leading to an early deletion of $Ca_v1.2$ throughout the central nervous system. A brain region-specific knockout at a later timepoint during development can be achieved by adeno-associated virus (AAV)-mediated delivery of the Cre recombinase at the site of interest in floxed mice. In that case, the date of the AAV-injection determines the time of the deletion.

It is further worthwhile to mention the crosslink of $Ca_v1.2$ to psychopathology. A polymorphism in the responsible CACNA1C gene is one of the few loci that reached repeatedly significance in genome wide association studies. It is associated with bipolar disorder, depression and schizophrenia (Ferreira et al., 2008; Green et al., 2009; Craddock and Sklar, 2013). Further, chronic elevation of calcium influx is implicated in age-related senile symptoms and Alzheimer disease (Disterhoft et al., 1994; Porter et al., 1997; Thibault et al., 2007). A substantial portion of this age-related rise was ascribed to the phosphorylation of $Ca_v1.2$ by cAMP-dependent protein kinase (PKA) in aged rats (Davare and Hell, 2003; Boric et al., 2008).

Overall, LTCCs not only modulate memory functions in the brain, but are also pathologically relevant. MEMRI might be of use to investigate LTCC action and consequently neural activity throughout the brain, however, the contribution of each LTCC isoform to the MEMRI signal must be determined. This can be best explored by the genetic ablation of $Ca_v1.2$ or $Ca_v1.3$ in the whole central nervous system. To further explore the consequences of the absence of a specific LTCC on spatial learning and relearning capabilities, memory tests are required that suits the characteristics of mice.

1.6. Aims of the thesis

The major objectives of my thesis were the following:

i. First, I aimed to establish the WCM as a suitable tool to investigate spatial learning and relearning (reversal learning and strategy switching) in mice and relate the different protocols to HPC functioning.

ii. Second, I wanted to dissect the contribution of $Ca_v1.2$ and $Ca_v1.3$ on MEMRI intensity in the mouse brain.

iii. Third, I wanted to examine, whether MEMRI is useful to reflect learning processes during training in the WCM.

iv. Fourth, the WCM should be used to further explore the contribution of LTCCs to place and response learning as well as relearning.

2. Materials and Methods

2.1. Animals

A total of 212 male mice, 2-8 month old, were single housed in standard macrolone cages type II with food and water ad libitum. With the exception of the below described knockout mice, I either employed C57BL/6N mice purchased from Charles River (Sulzfeld, Germany) or genetically identical C57BL/6M mice from our own breeding stock (C57BL/6N breeding stock established in 1996 at the Max-Planck-Institute of Biochemistry, Martinsried, Germany). The mice were maintained on a reversed 12 h light/dark cycle (lights off at 9:00) in a temperature- and humidity-controlled room. After transfer into the local animal facility, mice were allowed to get accustomed to the holding conditions for at least 10 days. All behavioral tests were conducted during the active phase of the mice.

All experiments were carried out according to the European Community Council Directive 2010/63/EEC, and effort have been made to minimize animal suffering and reduce the number of animals used. All experimental procedures were approved by the local government of Upper Bavaria (55.2.1.54-2532-41-09, 44-09 and 142-12).

2.1.1. $Ca_v1.2$ knockouts

Deletion of $Ca_v1.2$ in the brain was carried out as described in Langwieser et al. (2010). A complete knockout in the brain was obtained by using the Cre-LoxP system. Two different alleles of the CACNA1C ($Ca_v1.2$) gene were generated, i.e a recombinant allele that lost its function throughout the whole body (L1) and another allele where exon 14 and 15 of the CACNA1C gene is flanked by LoxP sites (L2; figure 2.1 A). L2 lost its function when the Cre recombinase, which was expressed selectively throughout the central nervous

system under the control of the Nestin promoter (Tronche et al., 1999), had been present. Mice that had one recombinant allele and Cre expressed under the Nestin promoter (genotype: $Ca_v1.2^{+/L1}$, $Nestin^{+/Cre}$) were mated with mice having both alleles flanked by LoxP sites (floxed; genotype: $Ca_v1.2^{L2/L2}$; figure 2.1 B). $Ca_v1.2$ knockouts (KO; genotype: $Ca_v1.2^{L1/L2}$, $Nestin^{+/Cre}$) were contrasted against their heterozygous "wild type" controls (WT; genotype: $Ca_v1.2^{+/L2}$, $Nestin^{+/Cre}$). The genetic background of the animals was C57BL/6N.

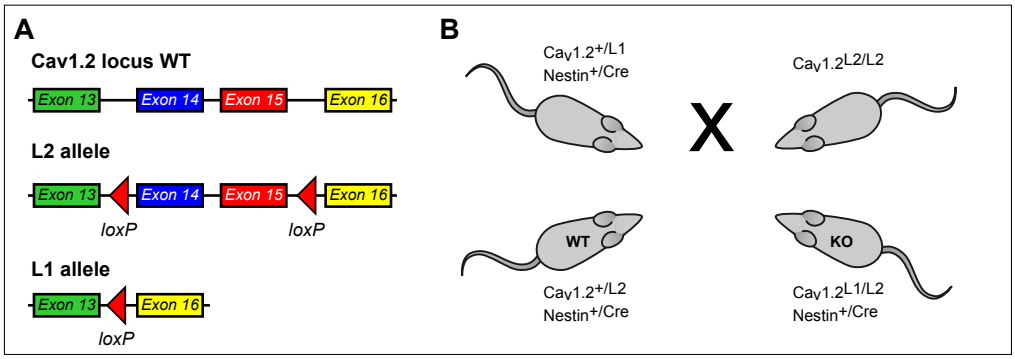

Figure 2.1.: Deletion of $Ca_v1.2$ throughout the central nervous system. **(A)** Schematic drawing of the wild type (WT) CACNA1C gene encoding $Ca_v1.2$ and the functional L2 allele having exon 14 and 15 flanked by loxP sites. In presence of the Cre recombinase, exon 14 and 15 of the L2 allele were deleted resulting in a non-functional L1 allele (modified from Langwieser et al. (2010)). **(B)** Mice that carried one L1 and one WT allele and also expressed Cre under the Nestin promoter (genotype: $Ca_v1.2^{+/L1}$, $Nestin^{+/Cre}$) were mated with mice that had two L2 alleles (genotype: $Ca_v1.2^{L2/L2}$). The breeding resulted in brain-specific $Ca_v1.2$ knockouts (KO; genotype: $Ca_v1.2^{L1/L2}$, $Nestin^{+/Cre}$) and heterozygous WT controls (genotype: $Ca_v1.2^{+/L2}$, $Nestin^{+/Cre}$).

In a second experiment, homozygous floxed mice (genotype: $Ca_v1.2^{L2/L2}$; Seisenberger et al., 2000) were injected with an adeno-associated virus (AAV) encoding either green fluorescent protein and the Cre recombinase (pAAV2.1-CMV-Cre-2A-GFP M4) or green fluorescent protein exclusively (pAAV 2.1 sc Ef1a eGFP AAV 2/2). In addition, another control group without any injection was employed. AAVs were kindly provided by Stylianos Michalakis (Faculty for Chemistry and Pharmacy, Ludwig-Maximilians-University, Munich, Germany). AAV-mediated delivery of the Cre recombinase allows a region specific knockout of $Ca_v1.2$ after injection whereas the administration of the control virus (encoding only GFP) does not influence the expression of $Ca_v1.2$.

2.1.2. $Ca_v1.3$ knockouts

CACNA1D gene (encoding $Ca_v1.3$) was knocked out as described in Platzer et al. (2000). Multiple stop codons were introduced through a neomycin resistance gene into exon 2 of the CACNA1D gene by transfection of embryonic stem cells. After homologous recombination, two positive embryonic stem cell clones were selected for blastocyst microinjection to create chimeric mice. The positive F1 progeny was mated with C57BL/6N mice and their heterozygous offspring was interbred to produce homozygous knockouts (KO; genotype: $Ca_v1.3^{-/-}$ kindly provided by Jörg Striessnig, Institute of Pharmacy, University of Innsbruck). C57BL/6N mice (Charles River, Germany) served as wild type controls (WT).

2.2. Surgery

Three independent batches of mice underwent ibotenic acid (IA) or vehicle (Veh) injection into the HPC (as perviosly described in Kleinknecht et al., 2012). IA is an excitotoxin that acts as a glutamate agonist and selectively kills cells in affected areas (Schwarcz et al., 1979). The major advantage of IA is that it spares passage fibers and creates discrete lesions without spreading to surrounding tissues (Jarrard, 1989). A keatimin/xalazine combination (50 mg/kg ketamine from Belapharm GmbH, Vechta, Germany and 40 mg/kg xylazine (Rompun) from Bayer Vital GmbH, Leverkusen, Germany) was used to anesthetize the animal; mice were fixed in a stereotactic frame (TSE-Systems, Heidelberg, Germany) and the substances were injected three times into each hemisphere of the HPC with a microinjector pump (UltraMicroPump III with Micro4 Controller, World Preciosion Instruments Inc., Saratosa, FL, USA). A volume of 0.19 μl per injection side (i. AP -1.2 mm, L ±1.2 mm, V 2.0 mm; ii. AP -2.5 mm, L ±2.5 mm, V 2.2 mm; iii. AP -3.3 mm, L ±3.1 mm, V 4.1 mm) was applied containing either 1.9 μg IA dissolved in Phosphate Buffered Saline (10 μg/μl, pH = 7.4) or pure Phosphate Buffered Saline. One injection took 2 min per coordinate and the cannula remained at the side for additional 3 min to allow for diffusion.

Further, homozygous floxed $Ca_v1.2$ mice (genotype: $Ca_v1.2$ L1/L2) underwent surgery one month before the first MRI scan. Mice were anesthetized with isoflurane (DeltaSelect, Germany), mounted to a stereotactic frame (TSE-Systems, Heidelberg, Germany) and kept under inhalation anesthesia by an isoflurane-oxygen mixture (1.5-1.7 vol% with an oxygen flow of 1-1.2 l/min). After exposure of the skull, a hole was drilled and AAVs were injected via a microinjector pump (UltraMicroPump III, World Precision Instruments Inc., Saratosa, USA). 700 nl of the respective AAV was infused into the right lateral thalamus (0.5 mm posterior, 2.1mm lateral and 4.0 mm ventral to bregma). The side of the cannula was verified by the later acquired MR images. Injections were done at a rate of 50 nl/min followed by five minutes of diffusion time, during which the cannula was left in place.

One animal was injected with manganese chloride directly into the lateral thalamus to track manganese transport in the brain. To this end, the mouse was anesthetized and positioned as described just before. After drilling, manganese chloride (50mM, pH = 7.1) was applied iontophoretically (5 μA for 15 min, 7 s on-off interval) into the lateral thalamus (0.5 mm posterior, 2.1mm lateral and 4.0 mm ventral to bregma).

In each case, surgical tolerance was achieved by local anesthesia with lidocain spray and subcutaneous injection with the analgesic Meloxicam (0.5 mg/kg in 0.2 ml saline) five minutes before surgery. Afterwards, the wound was closed with sutures and disinfected with Braunoderm®(B.Braun, Melsungen, Germany). The treatment with analgesic Meloxicam continued for three post-surgery days via the drinking water (0.5 mg/kg in 5 ml tap water).

2.3. Water-Cross Maze (WCM)

2.3.1. General procedure

The four corridors of the WCM are arranged in a cross (custom made at the MPI of Psychiatry, Munich; see figure 2.2). Each arm is 50 cm long and is confined by 30 cm deep

walls made of clear acrylic glass that allows for visual orientation via extra-maze cues in the room. As a standard nomenclature, I labeled the arms North, East, South and West. At the beginning of each testing day, the maze was filled with tap water (23 °C) 11 cm above the floor. According to the below described protocols, a 8 × 8 cm^2 platform was placed in one arms 1 cm below the water surface and the arm opposite to the starting arm was blocked by a wall made of the same clear acrylic glass. In this way, the mice were forced to turn left or right rather than swimming straight ahead. The room was dimly lit by four lights in each corner (indirect regular spectrum light emitting 14 lux at the level of the mouse). For spatial orientation, mice could rely on landmarks within the room, e.g. a sink, a cabinet, pipes at the ceiling and the walls in a non-

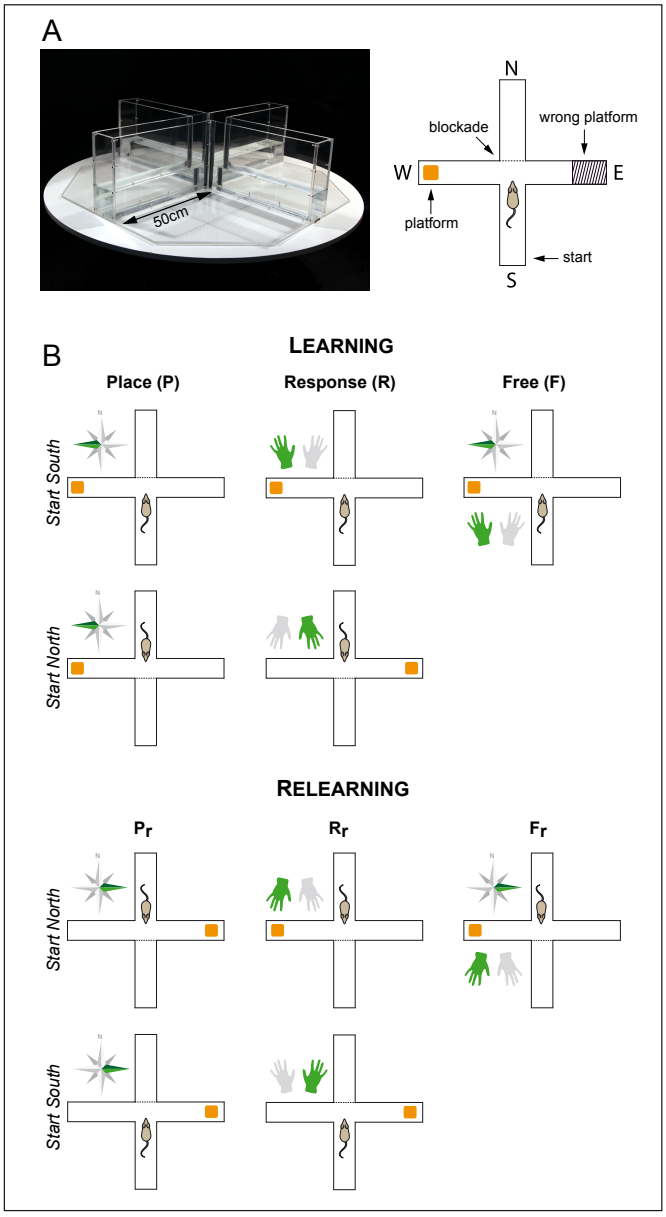

Figure 2.2.: Spatial navigation in the Water-Cross Maze (WCM). **(A)** The photo on the left depicts the actual WCM, the illustration on the right shows an exemplified constellation of the WCM having the start arm in the South and the platform arm in the West; the North arm is blocked by an acrylic glass wall and the ruled outer third of the East arm denotes the wrong platform area. **(B)** The pictogram demonstrates the constellation of the WCM for place *(P)*, response *(R)* and free *(F)* training during learning and relearning (abbreviated by a subscripted *r*; relearning is used as a generic term and includes reversal learning and strategy switching protocols). The starting position varied pseudo-randomly between North and South; the compass indicates the use of allocentric cues and the hands stand for the use of egocentric cues. While the place and the response protocol were fixed to an allocentric or egocentric strategy, respectively, the free protocol allowed for both.

specific arrangement. The room did not contain any dominant cues like a bright window or a source of acoustic signals.

For each trial, the mouse was transported from the separate holding room into the adjacent testing room; it was taken out of the cage and gently let into the water with the head facing the end of the corridor. During the trial, the experimenter stood motionless ~20 cm behind the start arm until the mouse climbed on the platform. If the animal did not find the platform within 30 s, it was guided to it. After 10 s on the platform, the mouse was removed with a shovel and put under an infrared light in the holding room to dry and warm. Only half of the cage was illuminated by the red light to obviate overheating of the animals. For each trial, the water was stirred in order to avoid olfactory cuing and the walls were wiped with soft cloth. In addition, a part of the water was replaced every three trials. Mice were tested in cohorts of 5-8 animals, which resulted in a inter-trial interval of 8-16 min per animal.

2.3.2. Learning protocols

Every animal completed six trials per day on five consecutive days for each, learning (week 1, d1-d5) and relearning (week 2, $d1_r$-$d5_r$). Between the two weeks, animals had a break of two days. The protocol was extended to eight training days, if learning had been combined with MEMRI. $Ca_v1.2$ knockouts and their controls were tested for seven days per week to exclude the possibility of a delayed learning phenotype. Mice underwent one out of three different protocols in each week: the place learning protocol (P or P_r), the response learning protocol (R or R_r) or the free learning protocol (F or F_r). Figure 2.2 schematically depicts the three learning and the three relearning protocols for both start arms (North or South). Relearning was conducted within one modality (reversal learning; e.g. P - P_r) or between modalities (strategy switching; e.g. P - R_r; relearning was used as a generic term including both, reversal learning and strategy switching). In some experiments, a probe trials was accomplished at the end of each week after the last training trial.

Place learning protocol The place learning protocol reinforced the usage of distances and angels between the surrounding extra-maze cues. This world-centered strategy made it possible to locate a constant platform position from both start arms (cf. figure 2.2). The starting corridor varied between North and South in a pseudorandom manner between the trials (e.g. d1: N-S-S-N-N-S, d2: S-N-N-S-S-N). The platform was located in the West arm during place learning (week 1) and was moved to the East arm for place relearning (week 2). An analysis of the first arm entry of 212 animals revealed no *a priori* side bias under our testing conditions (89 animals West, 93 animals East, 30 animals start arm).

Response learning protocol Upon response learning, animals had to utilize movement directions and distances in order to find the platform. The task required a body turn (response) either to the left during response learning (week 1) or to the right during response relearning (week 2) in order to locate the platform. As the starting arm was varied in pseudorandom order between South and North from trial to trial (e.g. d1: N-S-S-N-N-S, d2: S-N-N-S-S-N), the position of the platform was altered accordingly (cf. figure 2.2).

Free learning protocol The free learning protocol allowed for both, the use of extra-maze cues and body turns, to solve a trial. Here, the start arm remained always in the South for both weeks whereas the platform position was relocated after the first week from the West during learning (week 1) to the East during relearning (week 2; cf. figure 2.2).

Probe trial Animals started one trial from the North without a platform. The behavior was recorded for 30 s and analyzed offline afterwards. The northern starting position was only completely new for animals that had undergone the free learning protocol.

2.3.3. Performance parameters

The learning success was described with three basic parameters: accuracy, latency and wrong platform visits. The accuracy was further used for the calculation of three secondary parameters, i.e. the number of accurate learners, start bias and the number of biased starters. The preferred searching strategy of the mice at the end of one week was extracted from the probe trial.

Accuracy and start bias All arm entries were recorded online by the experimenter for every trial. An entry required the complete mouse body (excluding the tail) within an arm. A second entry into the same arm was considered, if the animal left the arm before. A trial was accepted as accurate and scored as 1, if the animal directly navigated to the platform and jumped on it. Otherwise the trail was scored as non-accurate (i.e. value 0). The daily *accuracy* described the percentage of accurate trials out of six. An *accurate learner* was an animal that accomplished ≥5 accurate trials per day (i.e. ≥83.3%). The number of accurate learners represents the sum of animals, that exceeded that threshold on one day as a percentage of the animals per group. The *start bias* was calculated as the absolute value of the difference between accurate trials starting in the North and accurate trials starting in the South: $|\sum(AccurateNorthTrials) - \sum(AccurateSouthTrials)|$. A score of ≥2 indicated a *biased starter* and the number of biased starters were counted for every testing day.

Latency *Latency* was described as the time, until the animal jumped on the platform, averaged over the six trials per day. In case, that the animal did not find the platform within 30 s, 31 s were accepted for calculation.

Wrong platform visits If the mouse entered the outer third of the arm opposite to the platform with the whole body excluding the tail, a *wrong platform visit* was counted. Only if the animal completely left this part again, a second wrong platform visit had been counted. The sum of all wrong platform visits was calculated per day.

Searching strategy Out of the first arm entry in the probe trial, we extracted the *searching strategy* used by the animal. If the mouse searched for the platform at the same place as it was during training, it was counted as a place learner, whereas if the animal performed the same body turn as before, it was assigned the to response learner. The total number of animals for each strategy was calculated.

Animals, that did not reach the accurate learner criterion in the first week were excluded from relearning. An exception form the experiments with ibotenic acid, since learning deficits were intended. The accuracy, latency, number of wrong platform visits and the start bias were compared between groups in a one-way analysis of variance (ANOVA) with repeated measures separately for each week. Distributions of learners vs. non-learners, biased vs. non-biased starters or place vs. response learning strategies were contrasted between groups by the χ^2-test. At last, the accuracy on d5 or $d5_r$ was opposed to the theoretical value of 100% by a one-sample t-test.

2.4. Behavioral screening

IA injected animals and their vehicle controls underwent a basic behavioral screening 3-4 weeks after surgery. Basic locomotion and exploration was tested with the open field and the holeboard test, anxiety-like behaviors in the light-dark test and hyperarousal in the startle apparatus. All equipments and experimental procedures were previously described elsewhere (Kamprath and Wotjak, 2004; Golub et al., 2009; Thoeringer et al., 2010; Sauerhöfer et al., 2012).

2.4.1. Open field and holeboard

The open field was a cubic shaped room with a white floor and walls made of transparent acrylic glass (L26 × W26 × H40 cm, TrueScan, Coulbourn Instruments, Allentown, PA, USA). For the recording of the animals' horizontal and vertical behavior, two infrared sensor rings were mounted around the transparent walls and were encircled by a second set of opaque acrylic glass walls. The holeboard test further required an elevated floor with 16 holes and another sensor ring to monitor hole exploration. The sensor rings had

a vertical distance of 1.5 cm and were connected to a computer that recorded behavior by the TrueScan software (V.99, Coulbourn Instruments). The setup was illuminated with 15 lux at the level of the mouse for the holeboard test, whereas the open field test was conducted in complete darkness.

Mice were placed from their home cages into the middle of the arena and three-dimensional movements were recorded for 15 min in the open field and 30 min in the holeboard at a sampling rate of 4 Hz. Afterwards, they returned to their home cages and the arena was cleaned thoroughly with soap and water.

The following parameters were calculated with algorithms implemented in the TrueScan software: immobility time, total distance traveled, number of rearings and duration of rearings. For the holeboard test, the number and duration of nose pokes was further looked at. Differences between IA and vehicle treated animals were tested in a two-sample t-test. To further depict the temporal development of the distance traveled in the open field, the parameter was divided into 1-min bins and the treatment was compared with a one-way ANOVA with repeated measurements.

2.4.2. Light-dark box

The light-dark box (L46 × W27 × H30 cm) was divided into a dark and a light compartment, which were separated by a 2 cm corridor. While the light compartment (⅔ of the box) was illuminated with cold light lamps (700 lux), the dark compartment was not additionally lit up (⅓ of the box, 5 lux). Three walls of the light compartment were made of white acrylic glass while the rest of the box was black. Experiments were conducted behind a light- and sound-proof curtain.

Mice were removed from their home cages and were put into a rear corner of the dark compartment. The behavior was recorded for 5 min before the animal was replaced into its home cage. The setup was cleaned thoroughly with soap and water after each trial and carefully dried.

The recording was analyzed offline from a trained observer blind to the experimental condition in terms of time and entries into the light compartment with the help of a

customized software (EVENTLOG, Robert Henderson, 1986). The time spent in the light and the entries into the light compartment were assessed and later compared between the groups in a two-sample t-test.

2.4.3. Startle response

The startle apparatus consisted of a non-restrictive acrylic glass cylinder (inner diameter 4 cm, length 8 cm) that was mounted on a platform. Below the platform, a piezoelectric element was placed to detect movements of the mouse. Eight identical startle setups were used each implemented in a sound attenuated chamber (SR-Lab, San Diego Instruments SDI, San Diego, CA, USA). Signals were amplified and later digitized and sampled at the rate of 1 kHz by a computer interface (I/O-board provided by SDI). Control stimulus and four other startle stimuli were administered, i.e. white noise bursts of 20 ms duration as control and 75, 90, 105 and 115 dB(A) intensity in a constant background noise of 50dB(A) as startle stimuli. The startle amplitude was defined as the peak voltage output within 50 ms after the stimulus onset, which was quantified by SR-Lab software. It was contrasted between IA and vehicle treated animals in an one-way ANOVA with repeated measures.

Each device was calibrated before the run in order to ensure identical output levels. Mice were put gently into the cylinder. After an acclimatization period of 5 min, the presentation of 10 control trials and 20 startle stimuli of each intensity was started in pseudorandom order. The interval between the stimuli varied pseudorandomly between 13 and 17 s. After every run, the setups were cleaned with soap and water.

2.5. Manganese-enhanced magnetic resonance imaging (MEMRI)

MEMRI was performed similarly to Gruenecker et al. (2010, 2012). Mice received intraperitoneal injections of 30mg/kg manganese chloride (MnCl2; Sigma, Germany) every 24 hours for eight consecutive days (8x30/24h). 12 to 24 hours after the last injection, MR acquisition started. To map learning induced manganese accumulation, I reduced the dose to 20mg/kg (as 30mg/kg disturbed place learning; data not shown) and started the

MR acquisition 20 min after the last swim trial (~12 h after the last injection). For some experiments, baseline MRI was assessed without prior manganese injection. For the tract tracing experiment, MRI was performed four times around every 12 hours starting 12 hours after manganese injection into the thalamus.

MR acquisition was conducted on a 7T Avance Biospec 70/30 scanner (Bruker BioSpin, Ettlingen, Germany). Mice were anaesthetized with isoflurane (DeltaSelect, Germany), fixed in a prone position on a saddle-shaped receive-only coil and were further kept under inhalation anesthesia with an isoflurane-oxygen mixture (1.5-1.7 vol% with an oxygen flow of 1.2-1.4 l/min). To record learning induced activity differences, mice were anesthetized with ketamine (50 mg/kg, Belapharm GmbH, Vechta, Germany) 10 minutes after the last swim trial and anesthesia was maintained in the scanner with a low dose of isoflurane-oxygen mixture (~0.5 vol% with an oxygen flow of 1.2-1.4 l/min) in the scanner. The head was restrained with a stereotactic devise and the frontal teeth were fixed with a surgical fiber to prevent movement artifacts. Body temperature was monitored with a rectal thermometer (Thermalert TH-5, Physitemp Instruments, USA) and kept between 34°C and 36°C using a water-based heating pad. Pulse rate was continuously monitored by a plethysmographic pulse oxymeter (Nonin 8600V, Nonin Medical Inc., USA).

T1 -weighted (T1w) brain images were acquired using a 3D gradient echo pulse sequence (TR = 50 ms, TE = 3.2 ms, matrix size = $128 \times 106 \times 106$ zero filled to $128 \times 128 \times 128$, field of view (FOV) = $16 \times 16 \times 18$ mm, number of averages = 10, resulting in a spatial resolution of $125 \times 125 \times 140.6$ μm^3). One additional T2-weighted scan was obtained but not further analyzed. The total time per measurement was ~2.5 h.

2.5.1. MRI data post-processing

After reconstruction using Paravision Software (Bruker, BioSpin, Ettlingen, Germany), images were transferred to standard ANALYSE format. Further post-processing was performed in SPM 8 (www.fil.ion.ucl.ac.uk/spm). T1w images were manually co-registered and further bias corrected in order to remove intensity gradients introduced by the ge-

ometric properties of the surface coil. For brain extraction, images were spatially normalized to a custom-made master template deriving from 216 individual images. A binary mask of the intracranial vault without large vessels (whole brain) was manually defined (MRIcro, www.sph.sc.edu/comd/rordon/mricro.html) on the master template and subsequently backtransformed to the co-registered space of each individual animal (by inverted spatial normalization). For further analysis, whole brains were extracted from the co-registered and bias-corrected T1w images.

Another binary mask defining muscles around the brain (m. masseter, m. temporalis) was drawn on the master template, backtransformed to the co-registered space and applied to the co-registered and bias-corrected images. An in-house written program in IDL (www.creaso.com) was used to determine the volume or the intensity of the extracted regions.

2.5.2. Region of interest (ROI) analysis

In a further step, the extracted whole brain images were spatially normalized to a whole brain master template (whole brains deriving from 216 individual images). Binary masks of the HPC and its subregions as well as the cortex were specified on the whole brain master template according to the anatomical atlas of the C57BL/6 mouse (Paxinos and Franklin, 2001). Masks were backdeformed into the co-registered space of each animal and the precision of the transformation was verified by the experimenter. In the case of IA and vehicle injected animals, all backdeformed masks had to be reworked manually due to the poor fitting. ROIs were then extracted from the co-registered and bias-corrected T1w images and intensity or volume was defined using the in-house written IDL program. Consequences of intracranial manganese application were specified around the thalamic injection site and in the insular cortex (sphere with a radius of 0.62 mm). Both ROIs were directly applied to the spatially normalized whole brain images to extract their intensities.

To correct for unspecific effects (e.g. gain and sensitivity effects), ROI intensities were normalized to the whole brain intensity unless whole brain differences were assumed.

This was the case for genetically modified mice, which were then referenced to the muscle intensity. Since I could neither suppose equal whole brain volumes in genetically modified animals, analyzed vaults were normalized to the whole brain volume before the percentage change from the mean of the wild type group was calculated. The remaining volume after IA injection was defined as the ratio between a specific regional volume and the mean volume of the vehicle treated mice in the same region. The coefficient of variance (COV) was determined by the standard deviation (SD) and the mean intensity of 48 brain regions ($COV = SD/mean$; 48 regions came from a custom-built MEMRI brain atlas).

The quality of the MR images and all post-processing steps were manually checked and cases were excluded if necessary. HPC volumes were compared between groups using two-sample t-tests and their linear dependence on behavioral parameters was checked by the Pearson coefficient. To consider multiple testings, Bonferroni adjusted p-values were additionally reported. ROI intensities of Ca_v knockouts and controls before and after manganese injection were examined with a one-way ANOVA with repeated measures. Scheffé's method was used for post hoc analysis, if the ANOVA revealed a significant interaction. The intensity development over time after intracerebral manganese injection was tested by the Pearson coefficient.

2.5.3. Voxel-wise comparison

As before, individual whole brain images were spatially normalized to a whole brain master template. Prior to the final analysis, brain-extracted spatially normalized images were smoothed with a Gaussian kernel of $375 \times 375 \times 421$ μm^3 at full-width half maximum. Voxel-wise comparison was implemented in SPM 5 (www.fil.ion.ucl.ac.uk/spm) since it enables the use of the SPM mouse toolbox (http://wbic.cam.ac.ak/sjs80/spmmouse.html).

First, homozygous floxed $Ca_v1.2$ mice that had been injected with Cre were compared to a control group (including sham-injected and non-injected animals) before and after manganese injection (MRI vs MEMRI). Animals were assigned to a full factorial model comprising a between factor *Group* and a within factor *Timepoint*. For correction of

unspecific intensity differences, an global intensity-by-timepoint regressor was included in the model, which adjust intensities between the groups but leaves timepoint differences unchanged. In a second experiment, MEMRI contrast was correlated with learning parameters of the WCM. To this end, animals were assigned to a multiple regression model that includes a covariate with the respective parameter (accuracy d1-8, latency d1-4, latency d5-8). Unspecific intensity differences had been taken into account by a global intensity regresssor. A final comparison contrasted $Ca_v1.2$ knockouts against controls. Groups were allocated to a two-sample t-test with a global intensity-by-group regressor to maintain basal differences.

To correct for multiple testings, a voxel-based family wise error correction was implemented at a threshold of $p < 0.005$. If this did not reveal any differences, statistical maps were sampled at a threshold of $p < 0.005$ and a cluster-based multiple test correction for family wise error with regard to non-stationary smoothness was employed (Hayasaka et al., 2004). All clusters that contained less than 100 voxels (~0.2 mm^3) were excluded. All data were plotted for a sphere round the peak voxel with a radius of minimum 0.25 mm.

2.5.4. Voxel-wise linear fitting

After manganese injection into the thalamus, one animal was scanned four times approximately every 12 hours. Extracted whole brain images were spatially normalized to a master template and smoothed with a Gaussian kernel of $625 \times 625 \times 703$ μm^3. An in-house written routine in Matlab was applied to the images, which fitted the four timepoints voxel-wise into a linear regression ($y = A + Bx$) by minimizing χ^2-error statistics. The positive slope of the regression was depicted for each voxel at an uncorrected threshold of $p < 0.005$ and clusters that comprised less than 30 voxels were excluded.

2.6. Nissl staining

After MEMRI scans were performed in IA and Vehicle injected animals, brains were prepared for histological analysis. First, they were removed, frozen in chilled 2-methylbutan on dry ice and stored at -80 °C for further processing. 30 μm thick coronal brain sections were cut in a cryostat microtome at -20 °C, collected with Superfrost®Plus slides (Thermo Scientific, Braunschweig, Germany) and later dried at least for 20 min at room temperature (~21 °C). Subsequently, slices were stained with 0.5 % cresyl violet solution (Sigma-Aldrich, Steinheim, Germany; 2 min) before they were dehydrated with different ethanol solutions (70 % and 96 %) and isopropanol (5 min). Afterwards, the tissue was protected with Roti-HistoKit (Carl-Roth, Karlsruhe, Germany) and a coverslip. Brain sections were digitized on a bright field Leica MZ APO microscope with an AxioCam MRc5 camera (Zeiss Microscopy GmbH, Göttingen, Germany) connected to a computer. 8 bit grayscale images (1548 × 1036 pixel in 3.5 × 3.5 μm^2) were acquired with AxioVision 4.7 software (Zeiss Microscopy GmbH, Göttingen, Germany).

2.7. Western blot

One month after the last imaging, homozygous floxed $Ca_v1.2$ mice were euthanized with an overdose of isoflurane and brains were removed, frozen in chilled 2-methylbutan on dry ice and stored at -80°C. After the analysis of the imaging data, brain tissues of the right thalamus and the right insular cortex were punched (cylindrical punchers with an internal diameter of 0.5 mm and a punch length of 0.5 mm) in a cryostat microtome at -20°C for subsequent western blot analysis of $Ca_v1.2$ expression. Brain slices were collected and dissection side was verified by histological analysis. One animal was excluded from the analysis, because the brain had been severely deformed during the removal.

The tissue probes were suspended in 100 μl lysis buffer per 10 mg tissue (50 mM Tris-HCl, 2% SDS, pH 7.5) and boiled for 10 min. After normalization of protein concentration in each sample (BSA equivalents measured with a NanoDrop spectrophotometer, Thermo Fischer Scientific, Germany), the homogenates were separated by 10% SDS-PAGE. The

resulting gels were transfered to PVDF membranes (Immobilion-P, Millipore, Germany) and blocked at 4°C overnight with 3% BSA and 1% Tween-20 in PBS. Then they incubated for 90 min with $Ca_v1.2$-specific antibody (kindly provided by Franz Hofmann) and α-tubulin antibody (Millipore). Further, the membranes were immersed in chemiluminescence substrate (ECL, Western Lightning Chemiluminescence, Perkin-Elmer, Germany) and digitized with a HP ScanJet scanner (40×40 μm^2). A trained investigator blind to the experimental groups quantified the bands with ImageJ (http://rsbweb.nih.gov/ij). The $Ca_v1.2$ signal was normalized to the α-tubulin signal to get the relative amount of $Ca_v1.2$. A two-sample t-test was conducted for each region.

2.8. Data presentation

Data were analyzed in SPSS 16.0 (SPSS, Chicago, IL, USA) or Statistica 5.0 (Statsoft, Tulsa, OK, USA) and plotted in GraphPad Prism 5.0 (GraphPad, San Diego, CA, USA) with the arithmetic mean and the standard error of the mean ($\bar{x} \pm S.E.M.$). Voxel-wise analysis of the MR images was performed in SPM8 or SPM5 (www.fil.ion.ucl.ac.uk/spm) while the voxel-wise linear regression was performed directly in Matlab 7.7.0 (MathWorks Inc., Natick, MA, USA). Significance has been accepted at $p \leq 0.05$, if not stated otherwise. All images were ultimately arranged in Adobe Illustrator 10.0.3 (Adobe Systems Inc., NY, USA).

3. Results

3.1. The water cross maze - a new cognitive test for mice

The first objective was to establish the WCM as a suitable test to investigate place and response learning as well as relearning in mice.

3.1.1. Reversal learning was only possible using place but not response training

First, learning and reversal capabilities were assessed for each learning protocol (i.e. place, response and free protocol) in a separate group of C57Bl/6N mice in the WCM. Five days of training were sufficient for the mice to acquire one out of the three protocols (figure 3.1 A, week 1). The animals were able to increase the accuracy when reducing the latency and the wrong platform visits. All three parameters revealed significant changes over the *Time* ($F_{(4,132)} \geq 25.54$, $p < 0.001$) but neither a *Protocol* effect ($F_{(2,33)} \leq 2.83$, $p \geq 0.073$) nor a *Time* $\times$ *Protocol* interaction ($F_{(8,132)} \leq 1.39$, $p \geq 0.204$). By the end of the first week, all mice that underwent place or free training reached the accurate learner criterion (i.e. ≥ 5 accurate trials out of 6). Yet, 3/12 animals did not catch up under the response training, which could be explained by another adequate but more complex response strategy: Instead of a direct left turn into the correct arm, the three animals swam right, turned around and swam straight into the opposite arm. The accuracy score below 17% was indicative for such an alternative strategy. At last it is worthwhile to note, that the number of accurate learner highly corresponded to the mean accuracy score (figure 3.1 A, week 1). It suggested that an increase in the mean accuracy rather presents an increase in the number of animals that successfully acquired the task (a light bulb effect) than a successive improvement over the days.

Reversal learning was conducted with all accurate learners from the first week. During the second week, the platform was relocated to the end of the opposite arm. On the first day of relearning, mice persistently searched for the platform at the previous location. This became obvious by accuracy scores far below 50%, high latency scores as well as numerous wrong platform visits (figure 3.1 A, day 1_r). While the place and the free training group successfully acquired the new platform position by the end of week 2, the response retraining led to low accuracy scores as well as high latencies and a large number of wrong platform visits (figure 3.1 A, week 2). This was statistically shown by significant main effects of the *Protocol* ($F_{(2,30)} \geq 22.09$, $p < 0.001$) and significant *Time* × *Protocol* interactions

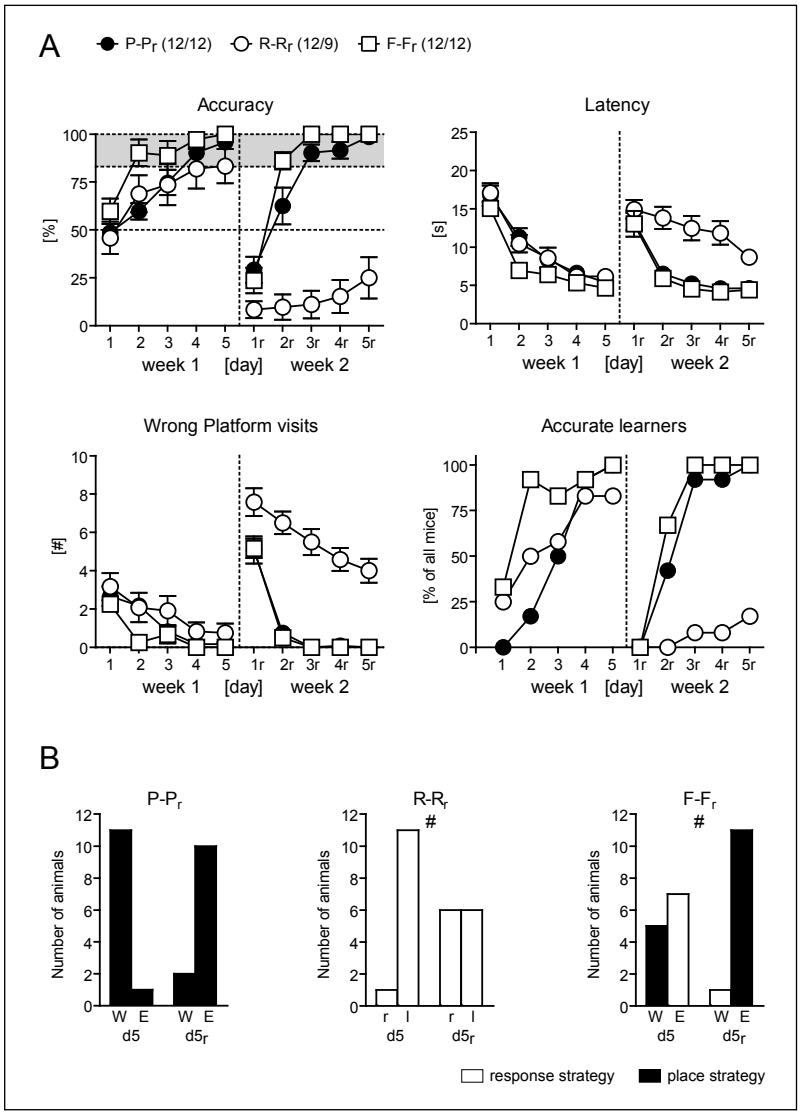

Figure 3.1.: Reversal learning in the WCM. **(A)** C57Bl/6N mice were assigned to the place (P-P_r), response (R-R_r) or free protocol (F-F_r). During learning in the first week, each protocol enabled the acquisition of the platform position indicated by high accuracies ($\geq 83\%$ designated by the gray shading) and a large number of accurate learners as well as short latencies and a low numbers of wrong platform visits at day 5. However, only the place and the free protocol facilitated reversal learning, while animals under response retraining insisted on the original platform position reflected by low accuracies, long latencies and a large number of wrong platform visits (*Protocol*: $F_{(2,30)} \geq 22.09$, $p < 0.001$; *Protocol* × *Time*: $F_{(8,120)} \geq 2.86$, $p \leq 0.006$). **(B)** At the end of each week, animals were allocated to place or response strategy users at the basis of the probe trial. The distribution varied between week 1 and 2 under response (re-)training due to their inability to reverse the previous platform position. Differential distributions were also observed under free training, which was indicative for a switch to place strategy in the second week ($\chi^2 = 6.75, p = 0.009$; modified from Kleinknecht et al. (2012)).

for accuracy, latency and wrong platform visits ($F_{(8,120)} \geq 2.86$, $p \leq 0.006$). Especially the numerous wrong platform visits of the response training group underscored the inability to reverse the previously acquired platform position. By the end of the second week, the response protocol enabled only 2/9 mice to reach the accurate learner criterion while all animals from the other groups succeeded.

At the end of each week, probe trials were conducted to extract information about the searching strategy (figure 3.1 B). Not surprisingly, most animals that underwent place protocol entered the arm, which contained the platform during training. Differences in the distributions occurred under response protocol resembling the inability to reverse the previously learned platform position ($\chi^2 = 5.04, p = 0.024$). Most instructive was the probe trial after free (re-)learning, as the animals were allocated to the new starting position for the first time after five days of training. While nearly half of the mice had chosen a place (5/12) or a response strategy (7/12) after the first week, almost all of them adopted a place strategy after the second week (11/12; $\chi^2 = 6.75, p = 0.009$).

Taken together, C57Bl/6N mice readily acquired the task within the first week of training irrespective of the learning protocol. Reversal learning, however, appeared to be only feasible if animals could rely on a place strategy. This was supported by the inability of mice to relearn a platform position under response training. Further, animals that underwent free protocol preferred the place strategy for reversal learning on the expense of a response strategy.

3.1.2. Place training allowed relearning independent of the original learning strategy

Second, strategy switching capabilities of C57Bl6/N mice were investigated to rule out, whether it was the original response strategy of the first or the response training in the second week that had prevented relearning. For that purpose, new groups of animals were trained that switched from place protocol in the first week to response in the second or vice versa (strategy switching: P - R_r, R - P_r; figure 3.2 A). As a control and replication sample,

one group underwent place training in the first and the reversal in the second week (P - P_r). All three groups easily acquired the task till the end of the first week (*Time*: $F_{(4,64)} \geq 36.78$, $p < 0.001$ for accuracy, latency and wrong platform visits; for the sake of simplicity, the following figures dispense with latency, wrong platform visits and accurate learners). In the second week, only the group that changed from place to response protocol was not able to reach a high accuracy level while the others were. This was reflected by a trend for a *Protocol* effect ($F_{(2,16)} = 3.24$, $p = 0.066$) and a significant *Time* × *Protocol* interaction ($F_{(8,64)} = 8.14$, $p < 0.001$). The latency and the number of wrong platform visits underscored the perseverance, with which the animals adhered to the original learning rule (*Protocol*: $F_{(2,16)} \geq 4.21$, $p \leq 0.034$; *Time* × *Protocol*: $F_{(8,64)} \geq 3.47$, $p \leq 0.002$). Only 2/7 animals that switched from place to response protocol reached the accurate learner criterion by the last day of retraining. This was contrary to 5/6 mice, which underwent response training in the first and place training in the second week ($\chi^2 = 3.89, p = 0.048$).

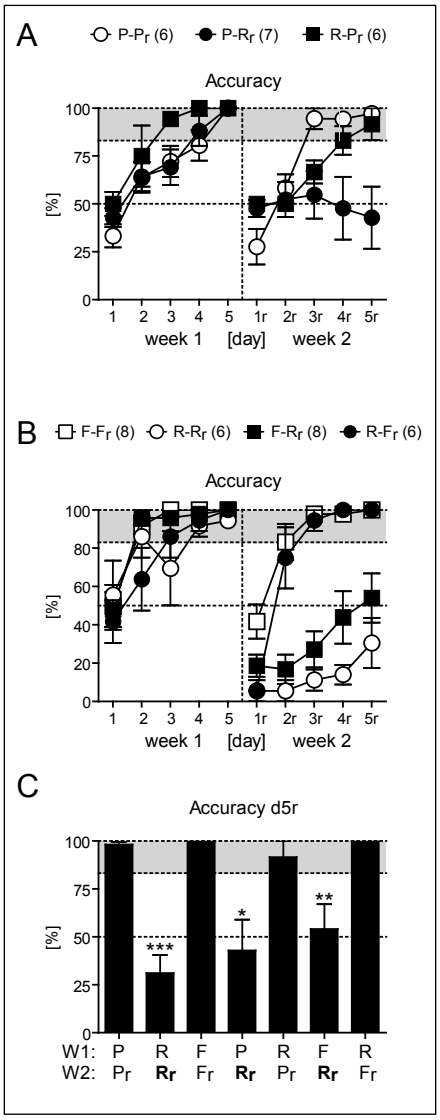

Figure 3.2.: Strategy switching in the WCM. **(A)** Mice that switched from place to response training (P-R_r) were unable to reach a high accuracy level by the end of week 2 when the other two groups attained that (P-P_r, R-P_r; *Protocol*: $F_{(2,16)} = 3.24, p = 0.066$; *Protocol* × *Time*: $F_{(8,64)} = 8.14, p < 0.001$). **(B)** A switch from free to response training in the second week (F-R_r) prevented relearning while the protocol in the reverse order (R-F_r) made relearning possible. (*Protocol*: $F_{(3,24)} = 83.35, p < 0.001$; *Protocol* × *Time*: $F_{(12,96)} = 5.28, p < 0.001$). **(C)** The figure summarizes the accuracy scores of all seven protocol constellations on $d5_r$. Relearning was impossible under response training in the second week ($t \geq 3.52, p \leq 0.012$ in the one sample t-test; $p \leq 0.05(*), p \leq 0.01(**), p \leq 0.001(***)$; adopted from Kleinknecht et al. (2012)).

Within the next experiment, new groups of mice were tested to contrast response and free protocol during learning and relearning. To this end, two experimental groups were employed having either the free protocol in first and the response protocol in second week or the other way round (F - R_r, R - F_r; figure 3.2 B). They were compared to animals that either underwent response reversal training or free reversal training (response reversal: R - R_r, free reversal: F - F_r). All groups became highly accurate by the end of the first week independent of the protocol, however, both groups that underwent response training in the second week were unable to relearn while the free protocol made relearning possible (*Protocol*: $F_{(3,24)} \geq 24.63$, $p < 0.001$). Instead, animals under response retraining kept swimming to the previous platform position. Free retraining enabled all animals to reach the accurate learner criterion while only 3/8 mice successfully acquired the task under response retraining ($\chi^2 = 5.83, p = 0.015$).

Still unclear was, whether ongoing response training or one week of intermittent free training would help the animals to relearn. Two groups out of the preceding experiment, namely the group that had response training in both weeks and the group, which had response in the first and free training in the second week, went on with response training for an additional week (R - R_r - R_r, R - F_r - R_r). In face of successful relearning under free training in the second week, it is remarkable that both groups failed to relearn under response protocol even in the third week (data not shown). Merely one animals out of each group reached the accurate learner criterion. These results again demonstrated that not only ongoing response training did not lead to accuracy improvements, but also that a successful training in-between does not help to acquire a new response.

A summary of all results obtained so far is given in figure 3.2 C. The relearning capabilities of C57Bl/6N mice were severely impaired under response protocol ($t \geq 3.52, p \leq 0.012$). This could be observed independent of the original learning rule. In contrast, the place training made relearning possible for the mice and was further preferred for relearning under free protocol as indicated by the probe trials. Further, I could exclude, that relearning under the response protocol is possible if the animals train twice as much.

3.2. Volumetric MEMRI depicted relearning capabilities in HPC lesioned mice

As the HPC is known for its role in place learning, and relearning had been dependent on the place protocol, the causal involvement of the HPC for place learning and relearning was investigated in the WCM.

3.2.1. HPC lesion impaired place learning and relearning capabilities

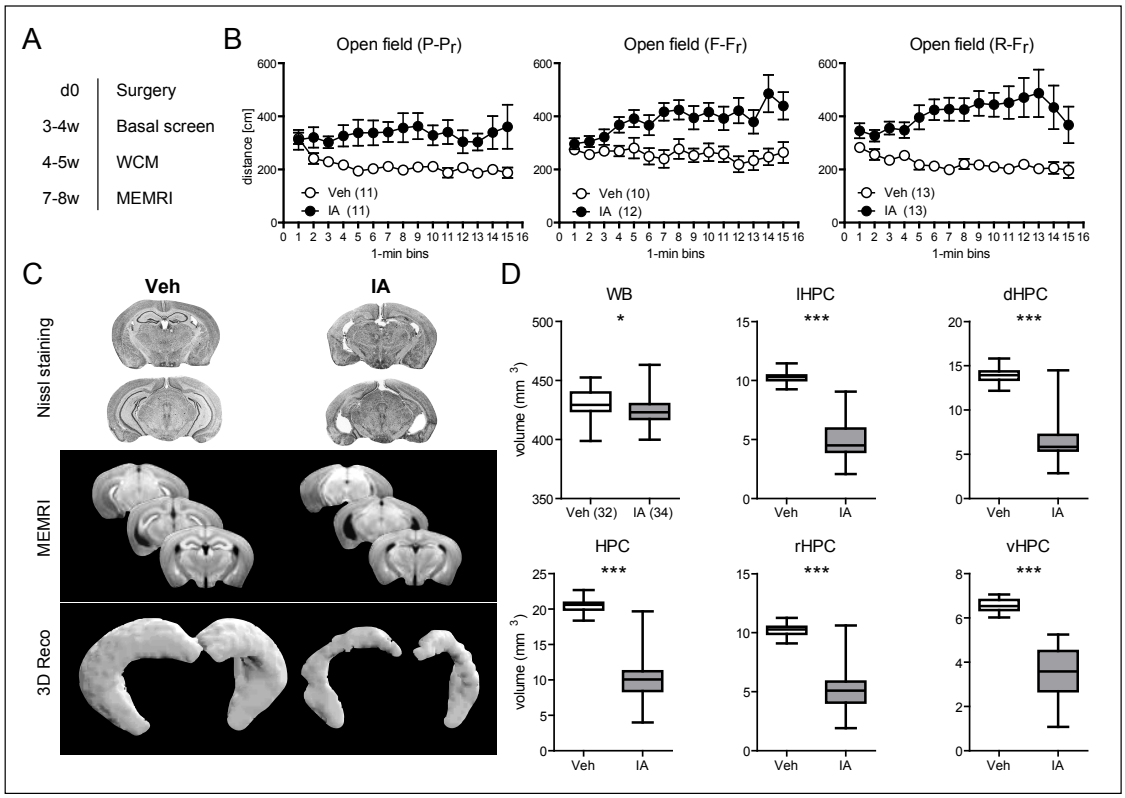

Figure 3.3.: Consequences of ibotenic acid (IA) lesions. **(A)** HPC lesion experiments were scheduled as shown (day (d), week (w)). **(B)** The distance traveled in the open field is depicted in one minute bins separately for three independent batches (P-P_r, F-F_r, R-F_r). IA injected animals developed a hyperactive phenotype, which was characterized by a stable or even increasing activity after starting at the same level as Veh injected mice (Treatment: $F \geq 5.48, p \leq 0.029$; Treatment $\times$ Time: $F \geq 2.09, p \leq 0.012$). **(C)** HPC volume was evaluated by volumetric MEMRI. Representative Nissl stained slices, mean MEMRI images and representative 3D reconstructions of the HPC (3D Reco) are shown for IA and Veh treated animals. **(D)** The volumes of the whole brain (WB) and the HPC as well as its different portions (left (lHPC), right (rHPC), dorsal (dHPC) and ventral HPC (vHPC)) were quantified. IA injection induced a HPC shrinkage of ~50% ($t_{64} = 20.15, p < 0.001, p_{Bonf.} < 0.001$), which was accompanied by a marginal whole brain shrinkage ($t_{64} = 13.60, p = 0.017, p_{Bonf.} = 0.102$). The magnitude of the volume reduction was somewhat similar in the different subregions of the HPC ($t_{64} \geq 16.55, p < 0.001, p_{Bonf.} < 0.001$; $p \leq 0.05(*), p \leq 0.001(***)$; adopted from Kleinknecht et al. (2012)).

To investigate the role of the HPC for learning and relearning in the WCM, we employed three independent cohorts of C57Bl/6N mice. Bilateral lesions in the complete HPC were precipitated with ibotenic acid (IA) and compared to sham-injected controls (Veh). A behavioral screening of the mice was conducted three to four weeks after the surgery, which included testings for locomotion, exploration, anxiety-like behavior and startle response (figure 3.3 A). Table 3.1 provides an overview of the tests and the corresponding parameters. Significant differences occurred in the open field and the holeboard. IA mice showed less immobility time, they traveled longer distances and rearing lasted shorter ($t \geq 4.31, p < 0.001$), yet, the number of rearings remained at the same level. These differences were consistently found for both tests. In order to describe that hyperactivity phenotype in more detail, the temporal development of the traveled distance in the open field was depicted separately for each cohort (figure 3.3 B). It revealed a remarkably similar phenotype between the three batches, where both groups began at the same level but IA animals remained or even increased in activity over time (sensitization; *Treatment*: $F \geq 5.48$, $p \leq 0.029$, *Treatment* × *Time*: $F \geq 2.09$, $p \leq 0.012$).

Test	Parameter	Sham	HPC lesion	Statistics
Open field	**Immobility time**	383 ± 10 s	287 ± 11 s	$t_{(69)} = 6.333$, **p < 0.001**
	Distance	3463 ± 133 cm	5887 ± 430 cm	$t_{(69)} = 5.068$, **p < 0.001**
	Rearing (number)	252 ± 9	258 ± 10	$t_{(69)} = 0.488, p = 0.627$
	Rearing (duration)	327 ± 13 s	250 ± 12 s	$t_{(69)} = 4.306$, **p < 0.001**
Holeboard	**Immobility time**	533 ± 12 s	354 ± 18 s	$t_{(64)} = 7.836$, **p < 0.001**
	Distance	3586 ± 93 cm	7492 ± 649 cm	$t_{(64)} = 5.446$, **p < 0.001**
	Rearing (number)	246 ± 10	246 ± 13	$t_{(64)} = 0.011, p = 0.992$
	Rearing (duration)	362 ± 20 s	239 ± 16 s	$t_{(64)} = 4.876$, **p < 0.001**
	Nose pokes (number)	33 ± 3	32 ± 2	$t_{(64)} = 0.374, p = 0.709$
	Nose pokes (duration)	21 ± 2 s	17 ± 1 s	$t_{(64)} = 1.715, p = 0.091$
Light-dark	time in the light	31 ± 2 %	35 ± 2 %	$t_{(69)} = 1.180, p = 0.242$
	Light entries	42 ± 1 %	42 ± 1 %	$t_{(69)} = 0.149, p < 0.882$
Startle	Background	17 ± 1 mV	17 ± 1 mV	Two-Way ANOVA:
	75 dB	34 ± 4 mV	33 ± 2 mV	- Treatment
	90 dB	58 ± 11 mV	57 ± 8 mV	$F_{(4,280)} = 0.733, p = 0.990$
	105 dB	264 ± 29 mV	277 ± 27 mV	- Intensity × Treatment
	115 dB	393 ± 28 mV	392 ± 34 mV	$F_{(1,70)} = 0.012, p = 0.915$

Table 3.1.: Behavioral screening after IA injection. Data represent the mean ± SEM for 33 Veh and 38 IA lesioned mice from all three batches (P - P_r, F - F_r, R - F_r). Bold p-values indicate statistically significant parameters (modified from Kleinknecht et al. (2012)).

HPC lesioning was confirmed by volumetric MEMRI at the end of the experiment seven to eight weeks after surgery (figure 3.3 A, C). IA induced a strong volume reduction of

~50% in the total HPC (figure 3.3 D; $t_{(64)} = 20.15, p < 0.001, p_{Bonf.} < 0.001$) while the volume reduction of the whole brain averaged < 2%, which remained only significant on the uncorrected level ($t_{(64)} = 13.60, p = 0.017, p_{Bonf.} = 0.102$). Further, the volume reduction was equally distributed over the different portions of the HPC (46 - 54%; $t_{(64)} \geq 16.55, p < 0.001, p_{Bonf.} < 0.001$).

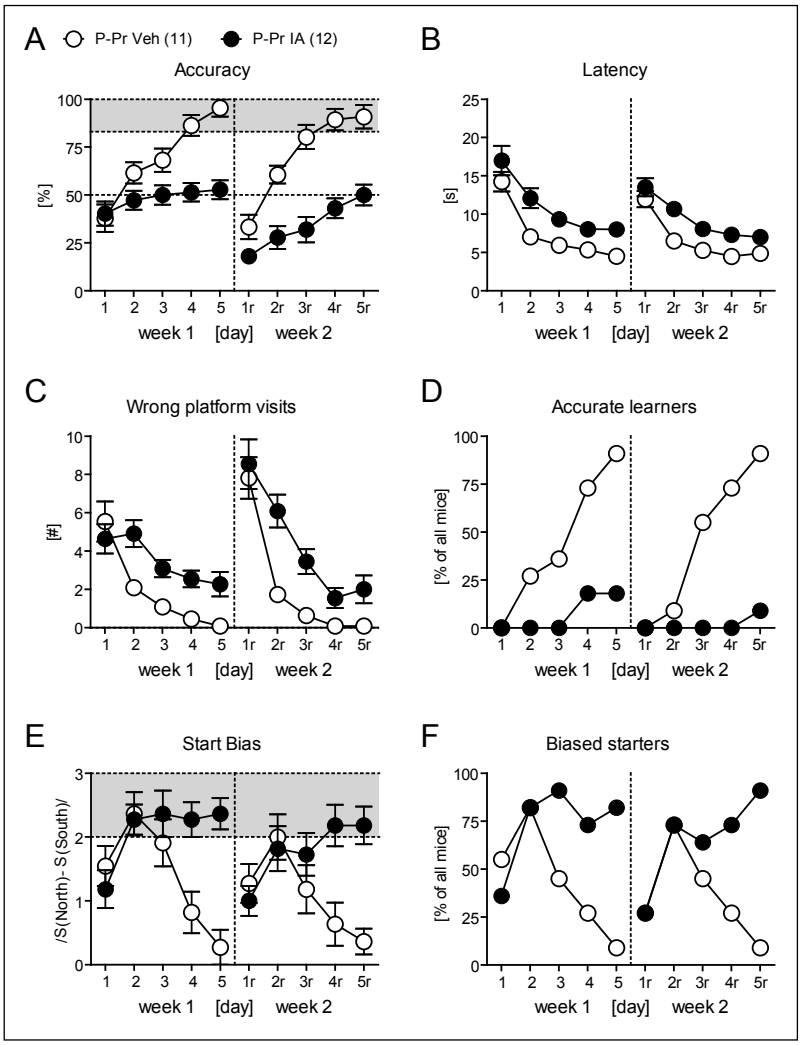

Figure 3.4.: IA induced place learning deficits. **(A, D)** IA lesioning prevented place learning as well as place relearning, which was indicated by accuracy scores approaching 50% (Treatment: $F_{(1,21)} \geq 14.32$, $p < 0.001$; Treatment × Time: $F_{(4,84)} \geq 5.17$, $p < 0.001$). Merely 2/12 and 1/12 IA injected mice exceeded the accurate learner criterion at the end of week 1 and 2, respectively. **(B, C)** Beside the general retardation in IA mice ($F_{(1,21)} \geq 6.61, p \leq 0.008$), they were still able to reduce the latency and the number of wrong platform visits over the course of training (*Time*: $F_{(4,84)} \geq 17.94, p < 0.001$). **(E, F)** As the latency and the number of wrong platform visits contradicted performance by chance, the start bias was computed (biased performance is indicated by values ≥ 2 and the gray shading). It uncovered an alternative response strategy that explained these improvements (details are described in the text; modified from Kleinknecht et al. (2012)).

With the help of IA treated mice, we first demonstrated that place learning in the WCM had been HPC-dependent. Therefore, the first cohort of IA and Veh treated animals underwent place training in the first and place reversal in the second week, starting four to five weeks after surgery (P - P_r; figure 3.3 A, 3.4). IA mice were neither able to achieve high accuracies during learning nor during relearning (figure 3.4 A; Treatment: $F_{(1,21)} \geq 14.32$, $p < 0.001$; Treatment ×

Time: $F_{(4,84)} \geq 5.17$, $p < 0.001$). The accuracy scores rather approach 50%, indicating performance by chance. This is also reflected in the number of accurate learner, which counted merely 2/12 in the first and 1/12 in the second week in the IA group compared to 10/11 and 11/11 in the Veh animals ($\chi^2 \geq 12.68, p < 0.001$). However, a closer inspection revealed, that IA mice were able to reduce their latency within both weeks (*Time*: $F_{(4,84)} \geq 38.57, p < 0.001$; *Treatment* × *Time*: $F_{(4,84)} \leq 0.87, p \geq 0.480$), even so on a different level (*Treatment*: $F_{(1,21)} \geq 6.61, p \leq 0.018$). The same could be observed for the number of wrong platform visits, which declined over time on a different level between the two groups (*Treatment*: $F_{(1,21)} \geq 13.37, p = 0.001$; *Time*: $F_{(4,84)} \geq 17.94, p < 0.001$; *Treatment* × *Time*: $F_{(4,84)} = 4.03, p = 0.005$ only in the first week). A possible explanation for that seemingly contradicting results was given by the following observation: IA animals apparently always made the same body turn wherever they started. If they turned into the correct arm, they directly approached the platform. However, if they turned into the wrong arm, they performed a u-turn before the end of the corridor and then swam straight to the platform position. This adapted response strategy meant that they were 100% accurate from one starting position and 0% from the other. Since the accuracy parameter was not sensitive to detect this behavior, I calculated the start bias to quantify that observation (figure 3.4 E). The rise in the start bias from d1 to d2 in both groups indicated the use of a response strategy at the beginning of the first week (*Treatment*: $F_{(1,21)} = 4.54, p = 0.045$; *Time*: $F_{(4,84)} = 5.18, p = 0.001$; *Treatment* × *Time*: $F_{(4,84)} = 5.96, p < 0.001$). While the start bias of Veh animals declined from the third day on, the IA mice remained at a high level indicating that the Veh group got rid of the initial response whereas the IA mice stayed with the response strategy. In addition, the number of biased starters strongly paralleled the side bias score as ≥ 82% of the IA animals fulfilled the criterion of a biased starter by the end of the week (figure 3.4 F; $\chi^2 \geq 12.68, p < 0.001$ on d5 or $d5_r$).

3.2.2. HPC lesion impaired free relearning capabilities

In a second cohort, the learning and relearning capabilities under free training were contrasted between IA and Veh injected mice. Despite a slight delay in the acquisition, IA mice could fully acquire the task during the first week as indicated by the accuracy score

≥ 83% (figure 3.5 A; *Treatment*: $F_{(1,21)} \geq 5.24, p \leq 0.032$ for accuracy, latency and wrong platform visits). The majority of IA treated animals (11/13) were able to reach the accurate learner criterion while all Veh mice (10/10) succeeded after the first week. The analysis of the second week revealed that IA mice were unable to acquire the exact platform position under free training (*Treatment*: $F_{(1,21)} \geq 7.88, p \leq 0.011$ for accuracy, latency and wrong platform visit). However, it is worth to mention, that again IA animals were able to reduce the latency and the number of wrong platform visits in the second week like IA animals had done under place protocol (*Time*: $F_{(4,84)} = 5.18, p = 0.001$; *Treatment* × *Time*: $F_{(4,84)} = 5.96, p < 0.001$). At the end, only 5/13 IA injected mice accurately relearned the task compared to 10/10 Veh controls ($\chi^2 = 9.43, p = 0.002$).

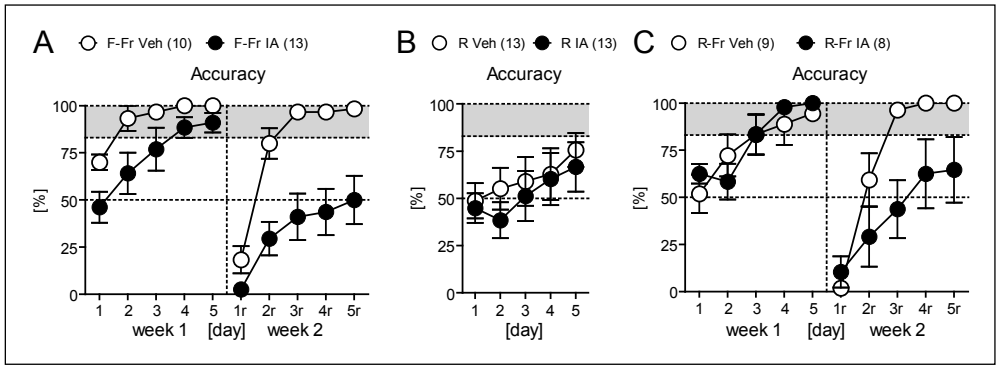

Figure 3.5.: IA induced relearning deficits. **(A)** Free training was evaluated for learning and relearning in IA and Veh treated mice. The low accuracy of IA mice on $d5_r$ pointed to a severe impairment of their relearning capabilities (*Treatment*: $F_{(1,21)} = 20.02, p < 0.001$). Merely 5/13 animals reached the accurate learner criterion (data not shown). **(B)** IA and Veh treated mice acquired the trained response similarly well in the first week, yet, a considerable number of animals did not surpass the 83% accuracy within each group (4 Veh and 5 IA mice). **(C)** Only animals, which accurately learned the task in the first week, went on with free training in the second week. IA mice were not able to reach a high accuracy level (*Treatment*: $F_{(1,15)} = 5.66, p = 0.030$). Yet, 5/9 IA animals successfully completed the free retraining (data not shown; modified from Kleinknecht et al. (2012)).

To determine the consequences of HPC lesions on response learning and to replicate the relearning deficit under free protocol, a third cohort of animals underwent response training during the first and free training during the second week. IA mice acquired the response equally well as Veh treated controls by the end of the first week (figure 3.5 B; *Treatment*: $F_{(1,24)} \leq 0.92, p \geq 0.346$; *Treatment* × *Time*: $F_{(4,96)} \leq 0.87, p \geq 0.485$), yet, a considerable number of animals of both treatment groups did not exceed the accurate learner criterion (4 Veh and 5 IA mice). The accuracy ≤17% indicated the use of the previously described

alternative response strategy in these animals and therefore justified their exclusion (figure 3.5 C). Still, there was neither a significant *Treatment* effect nor a *Treatment* × *Time* interaction during response training in the first week (*Treatment*: $F_{(1,15)} \leq 0.63, p \geq 0.441$; *Treatment* × *Time*: $F_{(4,60)} \leq 1.25, p \geq 0.229$). During free relearning, IA mice exhibited low accuracies, high latencies and large numbers of wrong platform visits (*Treatment*: $F_{(1,15)} \geq 5.25, p \leq 0.036$). As described before, IA treated animals were still able to reduce their latency and the number of wrong platform visits during free retraining in the second week (*Treatment*: $F_{(4,60)} \geq 47.65, p < 0.001$). 9/9 Veh controls exceeded the accurate learner criterion after relearning but 5/8 IA mice succeeded as well. Due to the heterogeneity in the behavioral consequences of IA treatment, I decided to set the extension of IA lesion into relation to the relearning capabilities.

3.2.3. Volume reduction in the left ventral HPC reflected relearning capabilities

The relearning capabilities under free training in IA mice were remarkably scattered. A closer inspection revealed, that nearly half of the mice from the F-F_r IA and R-F_r IA groups successfully relearned the task until the end of the second week, while the other half failed completely (figure 3.6 A). To further analyze the relation between learning capabilities and remaining HPC volume (as assessed by MEMRI; cf. figure 3.3), animals were classified as learner (L) and non-learner (NL) at the end of the second week based on the accurate learner criterion. Learner had more remaining HPC tissue compared to non-learner (figure 3.6 B; $t_{(13)} = 2.39, p = 0.032$). The largest differences were found in the left ventral portion of the HPC ($t_{(13)} = 3.52, p = 0.003$) followed by the left HPC in total ($t_{(13)} = 3.02, p = 0.009$). Other analyzed portions exhibited no significant differences. Only the left ventral HPC remained significant after multiple test correction ($p_{Bonf.} = 0.027$).

To further disentangle the contribution of the different portions of the HPC on the behavior, the remaining volume was correlated with learning parameters of the WCM as well as parameters resembling basic exploration in the open field and holeboard test (figure 3.6 C). The mean accuracy of free retraining (mean accuracy of $d1_r$ - $d5_r$) most highly correlated with the remaining tissue of the left ventral HPC ($r = 0.63, p = 0.011$) followed by the left

HPC ($r = 0.59, p = 0.021$) and the HPC in total ($r = 0.54, p = 0.036$). The analysis revealed neither a significant correlation with other portions nor between HPC volume and the mean latency ($d1_r$ - $d5_r$). At last, the analysis revealed significant correlations between the rearing time in the open field or the holeboard and the dorsal and more specifically the left dorsal portion of the remaining HPC volume ($r \geq 0.37, p \leq 0.047$). Despite the fact that non of the correlations survived multiple test correction, the consistency of the data made it newsworthy reporting it.

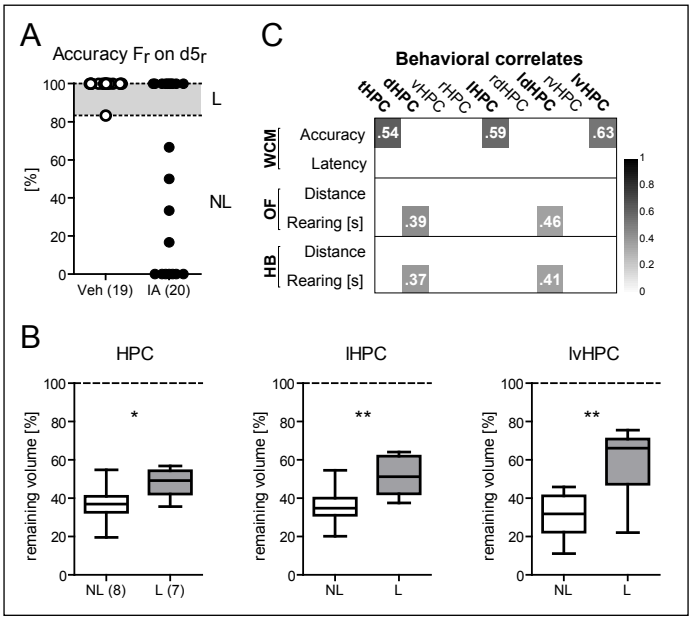

Figure 3.6.: Volume of the left ventral HPC reflected relearning capabilities. **(A)** Most of the IA mice either showed 100% or 0% accuracy at the end of free retraining. **(B)** Therefore, the subsequent analysis contrasted the remaining volume of the different portions in the HPC between learner (L) and non-learner (NL). Compared to L, NL exhibited a decrease in the total HPC volume ($t_{(13)} = 2.39, p = 0.032$). The most reduced volume was observed in the left ventral HPC (lvHPC; $t_{(13)} = 3.52, p = 0.003, p_{Bonf.} = 0.027$) followed by the overall left HPC (lHPC; $t_{(13)} = 3.02, p = 0.009, p_{Bonf.} = 0.081$). **(C)** The correlation analysis confirmed the previous finding, that the mean accuracy of IA mice under free retraining correlated most strongly with the volume of the lvHPC ($r = 0.63, p = 0.011$) followed by the lHPC ($r = 0.59, p = 0.021$) and the total HPC($r = 0.54, p = 0.036$). On the other hand, the rearing time of IA mice in the open field and the holeboard test significantly correlated with the left dorsal HPC (ldHPC) and the overall dorsal portion (dHPC; $r \geq 0.37, p \leq 0.047$). None of the correlations withstood a multiple test correction ($p \leq 0.05(*), p \leq 0.01(**)$; modified from Kleinknecht et al. (2012)).

Taken together, IA lesions in the HPC induced a place learning deficit. Further, impairments during relearning occurred not only under place but also under free retraining. Problems during relearning were independent of the protocol in the first week. The large differences in relearning success under free retraining could be mainly attributed to the remaining volume of the left ventral HPC. Notably, the dorsal HPC and in particular the left dorsal portion seems to contribute to basic exploration in the open field.

3.3. $Ca_v1.2$ is essential for manganese-dependent contrast increase in the brain

I have shown that the HPC is essential for place learning in the WCM. In a next step, I wanted to employ MEMRI as a functional tool to map brain activity *in vivo*. To do this, the basics of manganese accumulation changing the contrast in MR images need to be better described. Therefore, the contribution of $Ca_v1.2$ and $Ca_v1.3$ on MEMRI intensity in the brain was examined using respective knockout (KO) mice.

3.3.1. $Ca_v1.2$, but not $Ca_v1.3$, affected manganese-dependent contrast increase in the brain

$Ca_v1.2$ and $Ca_v1.3$ KOs underwent baseline MRI followed by a one-week recovery period before 8 × 30mg/kg MEMRI protocol was applied (figure 3.7 A). The comparison of the whole brain intensities between $Ca_v1.2$ KOs and their wild type controls (WT) revealed that both main effects and the interaction became significant (figure 3.7 B, C; *Group*: $F_{(1,11)} = 6.01, p = 0.032$; *Timepoint*: $F_{(1,11)} = 34.75, p < 0.001$; *Group* × *Timepoint*: $F_{(1,11)} = 5.39, p = 0.041$). Scheffé's post hoc test showed differences between KOs and WTs after manganese injection ($p = 0.014$) and a significant increase between MRI and MEMRI intensity in WT mice ($p = 0.001$). However, the KOs' intensity did not significantly rise after manganese injection ($p = 0.133$). A second readout for manganese accumulation is the coefficient of variance (COV) representing the contrast increase in the brain. Since all effects of the ANOVA became significant (*Group*: $F_{(1,11)} = 8.25, p = 0.015$; *Timepoint*: $F_{(1,11)} = 264.99, p < 0.001$; *Group* × *Timepoint*: $F_{(1,11)} = 17.24, p = 0.001$), post hoc Scheffé tests were conducted. They revealed increasing variances along with manganese application in both, WT and KO animals ($p < 0.001$). Still, the COV was significantly lower in KO mice after manganese injection ($p < 0.001$). Two brain regions that were also included into the COV-analysis were depicted to illustrate intensity fluctuations in inner brain regions. Again, all three effects of the ANOVA were proven to be significant for the HPC as well as the Cortex (*Group*: $F_{(1,11)} \geq 6.53, p \leq 0.026$; *Timepoint*: $F_{(1,11)} \geq 35.89, p < 0.001$; *Group* × *Timepoint*: $F_{(1,11)} \geq 5.37, p \leq 0.041$). Post hoc tests revealed a lower MEMRI contrast in

KOs compared to WTs ($p \leq 0.013$) as well as a statistically significant contrast increase between MRI and MEMRI in WT animals ($p \leq 0.001$) but not KOs. Only the HPC showed a trend for an increased MEMRI signal compared to baseline MRI in KO mice ($p = 0.053$).

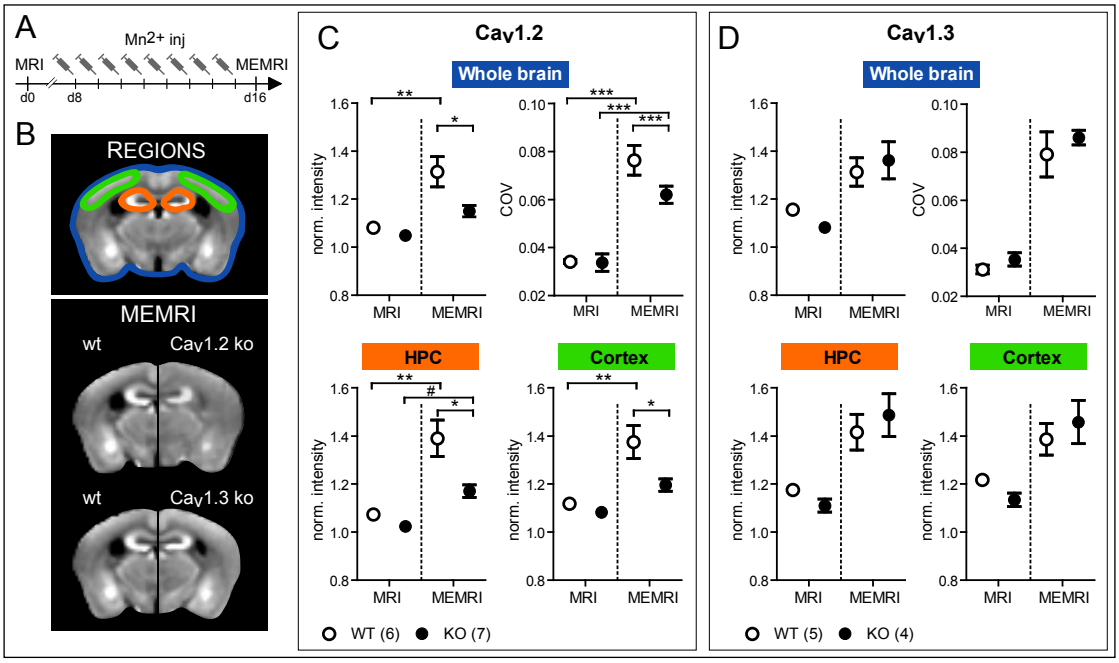

Figure 3.7.: $Ca_v1.2$ but not $Ca_v1.3$ affected manganese-dependent contrast increase. **(A)** Baseline MRI was performed one week before MEMRI procedure started comprising eight manganese injections followed by the MR acquisition (injection (inj), day (d)). **(B)** At the top, analyzed brain regions are shown. The lower panel depicts mean MEMRI images of calcium channel knockouts ($Ca_v1.2$ and $Ca_v1.3$ KO) and its wild type controls (WT). Accumulation differences between $Ca_v1.2$ KOs and WT controls became visible. **(C)** $Ca_v1.2$ KOs showed a less strong intensity and contrast increase after manganese treatment in the whole brain (*Group*: $F_{(1,11)} \geq 6.01, p \leq 0.032$; *Timepoint*: $F_{(1,11)} \geq 34.75, p < 0.001$; *Group* × *Timepoint*: $F_{(1,11)} \geq 5.39, p \leq 0.041$; coefficent of variance (COV)). This could also be translated to different brain regions, as exemplified by the HPC and the cortex (*Group*: $F_{(1,11)} \geq 6.53, p \leq 0.026$; *Timepoint*: $F_{(1,11)} \geq 35.89, p < 0.001$; *Group* × *Timepoint*: $F_{(1,11)} \geq 5.37, p \leq 0.041$). **(D)** $Ca_v1.3$ KOs did not exhibit differences in manganese-dependent intensity or contrast increase in any of the regions (*Group*: $F_{(1,7)} = 0.54, p = 0.485$; *Group* × *Timepoint*: $F_{(1,7)} \leq 2.46, p \geq 0.160$).

The impact of $Ca_v1.3$ on MEMRI contrast was investigated comparing conventional knockouts (KO; lack $Ca_v1.3$ expression throughout the entire body) with C57Bl/6N "wild type" (WT) controls. Intensities of both groups increased in the whole brain, the HPC and the cortex due to manganese injections (figure 3.7 D; *Timepoint*: $F_{(1,7)} \geq 14.81, p \leq 0.001$). However, analyses neither revealed a group difference nor an interaction (*Group*: $F_{(1,7)} \leq 0.08, p \geq 0.775$; *Group* × *Timepoint*: $F_{(1,7)} \leq 2.46, p \geq 0.160$). The same applied for the COV, where neither the group effect nor the interaction reached significance

(*Group*: $F_{(1,7)} = 0.54, p = 0.485$; *Timepoint*: $F_{(1,7)} = 58.71, p < 0.001$; *Group* × *Timepoint*: $F_{(1,7)} = 0.01, p = 0.958$).

On avarage, $Ca_v1.2$ KOs exhibited merely 50% of the intensity increase seen in WT mice. In contrast, the intensities of the $Ca_v1.3$ KOs ascended similarly to controls.

3.3.2. Region specific knockout of $Ca_v1.2$ affected MEMRI contrast in a projection region

Since the $Ca_v1.2$ gene had already been inactivated in KOs early in live, developmental causes for the lack of manganese accumulation could not be excluded. For this reason, an adeno-associated virus was injected into the lateral thalamus of homozygous floxed $Ca_v1.2$ mice at the age of three month. The viral construct encoded for the Cre recombinase precipitated the knockout of $Ca_v1.2$ at the injection site (figure 3.8 A). MRI and MEMRI was conducted as described before one month after surgery. Floxed $Ca_v1.2$ mice of the control group (Ctrl) were injected either with an AAV encoding GFP (n = 4) or remained uninjected (both groups were collapsed to increase the power of the analysis). To my surprise, the voxel-wise comparison of Cre and Ctrl animals revealed an *Group* × *Timepoint* interaction in the insular cortex (i.e. far away from the injection site), but not the thalamus, which remained significant after cluster-based family wise error correction (figure 3.8 B; $K_{voxel} = 397, F = 19.45, p_{corrected} = 0.048$). Post hoc analysis with a directional t-test revealed an increased intensity at baseline MRI (i.e. prior to manganese treatment) only in the lateral thalamus ($K_{voxel} = 461, T = 6.69, p_{corrected} = 0.026$). After manganese application, only the single cluster in the insular cortex survived family wise error correction in the t-test ($K_{voxel} = 687, T = 4.29, p_{corrected} = 0.050$). These results demonstrate reduced manganese-related intensity in the insular cortex but not at the site of virus injection, i.e. in the lateral thalamus.

To exclude the possibility of an anterograde transport of the virus, the amount of $Ca_v1.2$ channels was quantified in the lateral thalamus and the insular cortex by western blot analysis (figure 3.8 A, C). While the expression of $Ca_v1.2$ in the lateral thalamus was reduced after Cre injection ($t_{(12)} = 6.70, p < 0.001$), it remained at the same level in the

insular cortex ($t_{(12)} = 1.47, p = 0.166$).

The most parsimonious explanation for these seemingly paradox findings would be a preferential accumulation of manganese in projection terminals of neurons (Sloot and Gramsbergen, 1994). According to this scenario, a reduction in $Ca_v1.2$ expression at dendritic or somatic synapses would result in reduced manganese signal at the axon terminals. To test this assumption, I investigated the transport of manganese from the lateral thalamus to the insular cortex. For that purpose, manganese was injected into the lateral thalamus of one animal and MEMRI scans were recorded four times approximately every 12 hours after injection (figure 3.8 D). The intensity of the lateral thalamus and the insular cortex was calculated in a sphere around each peak voxel which then entered regression analysis. While the intensity at the injection site decreased over time ($r^2 = 0.837, slope = -0.203, p = 0.042$), the contrast in the insular cortex increased slightly, but sig-

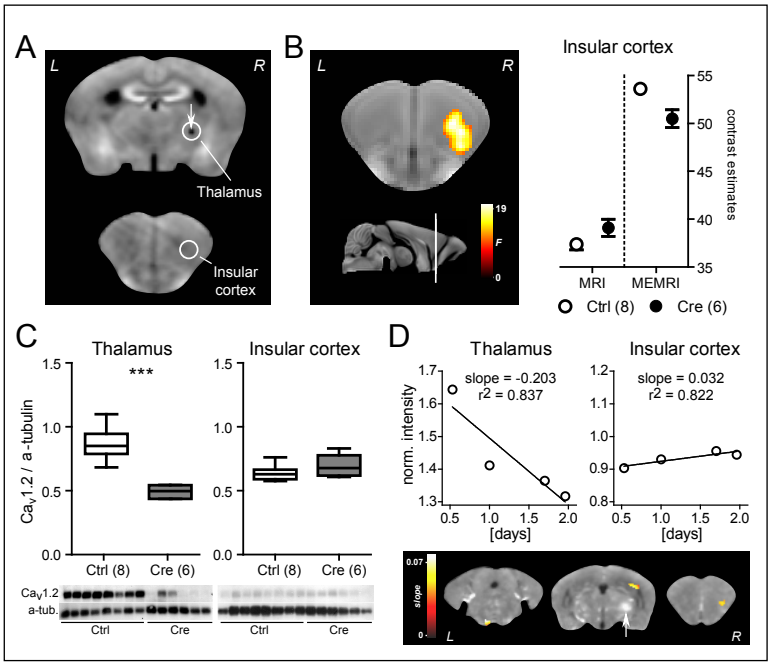

Figure 3.8.: Region specific knockout of $Ca_v1.2$ affected the contrast in a projection region. **(A, B)** $Ca_v1.2$ gene had been inactivated in the lateral thalamus (indicated by the arrow) of adult floxed $Ca_v1.2$ mice by injection of an AAV encoding for the Cre recombinase. MR images were acquired one month after surgery as described before. The voxel-wise comparison between Cre injected mice (Cre) and controls (Ctrl) revealed one significant interacting cluster in the insular cortex, which survived correction (*Group* × *Timepoint*: $F = 19.45, p_{corrected} = 0.048$), indicating a less strong intensity increase after manganese injection. **(C)** Expression levels of $Ca_v1.2$ were examined post mortem by western blot analysis. There was a down regulation of $Ca_v1.2$ in the thalamus ($t_{(12)} = 6.70, p < 0.001$), while the insular cortex appeared to be unaffected (punching sites are indicated by the white circles in A). **(D)** To assess manganese transport, manganese was infused into the lateral thalamus and repeated MR images were acquired at approximately 12 hours interval. Whereas the intensity in the thalamus dropped down between 12 and 48 hours after injection, it increased slightly in the insular cortex (ROI analysis). The slope was also depicted voxel-wise at an uncorrected threshold of p < 0.005. This analysis confirmed the intensity increase in the insular cortex but also in the HPC and the ventral pons with a maximum slope of 0.07.

nificant ($r^2 = 0.822, slope = 0.031, p = 0.046$). This became also visible in the voxel-wise regression analysis. Significant contrast increases that exceeded the uncorrected threshold of $p < 0.005$ were observed in the insular cortex but also in the HPC and the ventral pons. As in the ROI analysis, the slope was rather small with 0.07 at its maximum. These data are congruent with a shift in manganese accumulation away from the uptake site (dendrites or soma) to the projection areas (i.e. the axon terminals).

In summary, these data confirm that manganese accumulation is primarily, but not exclusively, mediated by $Ca_v1.2$, which was independent of developmental influences. In addition, they suggested that contrast changes are biased towards projection areas.

3.4. MEMRI intensity correlated with place learning

Since calcium signaling is an important mechanism for learning/memory acquisition, I questioned whether MEMRI could reflect the learning process in the WCM. To this end, C57Bl/6M mice underwent place training on eight consecutive days, receiving eight manganese injections each approximately 12 hours before training (figure 3.9 A). 10 minutes after the last swim trial, mice were anesthetized with ketamine and transported to the MR scanner to start MEMRI acquisition. 18/20 mice readily acquired the task as indicated by accuracy scores above 83% by day four of training (figure 3.9 B). These mice were included into the further analysis. As a first attempt, I took the mean accuracy scores over all eight days and correlated them voxel-wise with the image intensity of all accurate learner. After cluster-based family wise error correction with regard to non-stationary smoothness, the left BLA and the left ventral HPC showed a significant correlation with the accuracy score (figure 3.9 C). While the left BLA was negatively correlated ($K_{voxel} = 164, F = 34.72, p_{corrected} = 0.026$), the cluster in the left ventral HPC showed a positive correlation ($K_{voxel} = 109, F = 62.34, p_{corrected} = 0.035$).

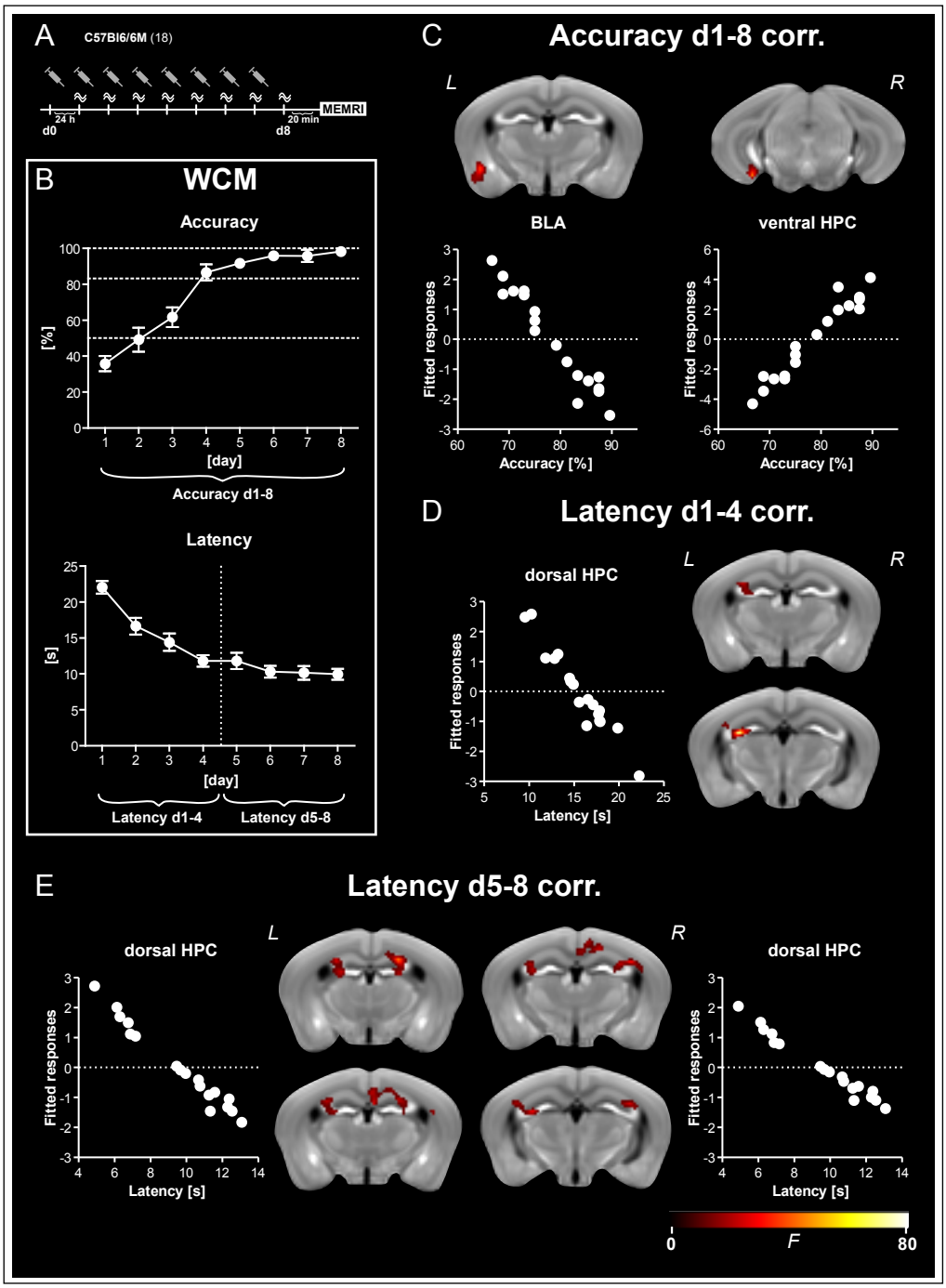

Figure 3.9.: MEMRI intensity correlated with place learning. **(A)** Manganese was injected eight times 12 hours (h) before place training. MR acquisition started 20 minutes after the last training trial. **(B)** Animals readily learned to locate the platform by day 4 of place training indicated by high accuracies above 83%. **(C)** The voxel-wise correlation between the image intensity and the mean accuracy revealed one negatively correlated cluster in the left basolateral amygdala (BLA) and one positively correlated cluster in the left ventral HPC ($F \geq 34.72, p_{corrected} \leq 0.035$) stretching further posterior into the substantia nigra (not shown). **(D)** As the latency is more scattered until the end of training, I separated the mean latency during early (d1-4) from the mean latency during late place memory acquisition (d5-8). The correlation analysis between the MR intensity and the mean latency of d1-4 revealed a significant negative correlation in the CA3 region of the left dorsal HPC ($F = 77.15, p_{corrected} = 0.003$). **(E)** The same cluster correlated negatively with the mean latency of d5-8 ($F = 27.56, p_{corrected} = 0.006$). Additionally, a cluster in the right dorsal HPC reached significance that comprised not only the CA3 but also the CA1 region and the retrosplenial cortex ($F = 43.42, p_{corrected} = 0.002$).

Since the accuracy score displayed minimal standard deviations from day 5 on, the latency was much more suitable to differentiate between early (day 1-4; figure 3.9 D) and late acquisition (day 5-8; figure 3.9 E). The following lines describe all significant clusters found after family wise error correction with regard to non-stationary smoothness. First, mean latencies of day 1-4 were correlated with MEMRI intensity. Only one cluster within the cornu ammonis 3 (CA3) of the left dorsal HPC survived multiple test correction, which was negatively correlated with the behavior ($K_{voxel} = 209, F = 77.15, p_{corrected} = 0.003$). If I took the mean latency over all days, only the same cluster appeared to be significant after multiple test correction ($K_{voxel} = 302, F = 67.82, p_{corrected} = 0.001$). The second analysis, which included the mean latency from day 5-8, revealed clusters in both hemispheres of the dorsal HPC showing a negative correlation ($K_{voxel} \geq 233, F \geq 27.56, p_{corrected} \leq 0.006$). It is important to mention that the cluster in the right HPC also extended to the CA1 region and further to the retrosplenial cortex.

Taken together, accuracy and latency could be related to regional differences in manganese accumulation.

3.5. $Ca_v1.2$ was involved, but not essential for place learning

It was shown that $Ca_v1.2$ affected MEMRI intensity (cf. figure 3.7 and 3.8) and MEMRI intensity correlated with place learning (cf. figure 3.9). Therefore, the contribution of $Ca_v1.2$ to place and response learning as well as relearning was investigated.

To first identify the most affected brain regions in a basal state, MEMRI intensities of 13 animals having $Ca_v1.2$ eliminated throughout the brain and 13 controls (including the MEMRI scans from figure 3.7) were compared in a voxel-wise manner (figure 3.10 A). The analysis revealed lower intensities in the KOs within the medial prefrontal cortex (mPFC), the bed nucleus of the stria terminalis (BNST), the globus pallidus (GP), the retrosplenial cortex (RSC) and the CA1 of the dorsal HPC. Unilateral signal reductions were seen in the right amygdaloid complex (Amy) and the right CA3 as well as the left inferior culliculus (IC) ($t \geq 8.02, p_{corrected} \leq 0.005$). The inverted contrast (KOs > WTs) revealed no significant differences. Besides the intensity, the volume of the ventral

HPC was evaluated at baseline (figure 3.10 B). $Ca_v1.2$ KOs had a smaller ventral HPC (vHPC; $t_{(24)} = 2.69, p = 0.012, p_{Bonf.} = 0.038$), which was rather due to the right (rvHPC; $t_{(24)} = 2.31, p = 0.029, p_{Bonf.} = 0.088$) than to the left part ($t_{(24)} = 1.15, p = 0.261$). The reduction was ~5% in each case.

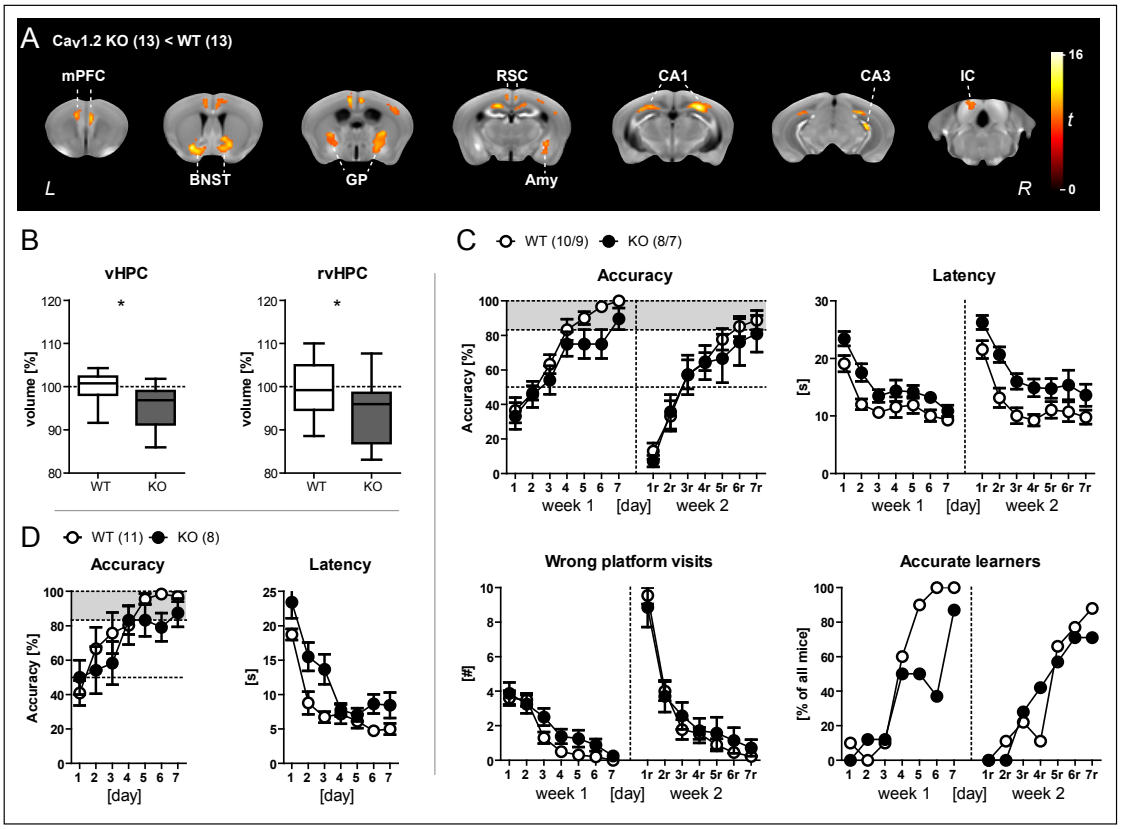

Figure 3.10.: $Ca_v1.2$ was involved, but not essential for place learning. **(A)** $Ca_v1.2$ KOs showed a basal bilateral intensity reduction in the medial prefrontal cortex (mPFC), bed nucleus of the stria terminalis (BNST), globus pallidus (GP), retrosplenial cortex (RSC) and the CA1 region of the dorsal HPC. Unilateral signal reductions were measured in the right amygdala (Amy), the right CA3 region and the left inferior colliculus (IC; $t \geq 8.02, p_{corrected} \leq 0.005$). **(B)** The volumetric analysis of the HPC revealed lower volumes at a basal state in the ventral portion (vHPC; $t_{(24)} = 2.69, p = 0.012, p_{Bonf.} = 0.038$) and the right ventral part (rvHPC; $t_{(24)} = 2.31, p = 0.029, p_{Bonf.} = 0.088$) of ~5%. **(C)** Due to the functional and morphological abnormalities in $Ca_v1.2$ KOs, one might expect place learning and relearning deficits. $Ca_v1.2$ KOs were significantly slower during both weeks of place training (*Genotype*: $F \geq 22.60, p \leq 0.011$ for the latency), yet, the accuracy and the number of wrong platform visits indicated a very subtle deficit if any (*Genotype*: $F_{(1,16)} \geq 3.81, p \leq 0.068$). Only 3/8 $Ca_v1.2$ KOs acquired the task by day 6, however, most of them reached the accurate learner criterion by day 7 (7/8). **(D)** $Ca_v1.2$ KOs were similarly delayed during response training (*Genotype*: $F_{(1,17)} = 9.19, p = 0.007$ for latency), however, the accuracy revealed no significant differences.

The functional and morphological abnormalities in $Ca_v1.2$ KOs suggested deficits in place learning and relearning. To test this, a new batch of $Ca_v1.2$ KOs and WT controls underwent place training and retraining (figure 3.10 C). KOs exhibited increased escape latencies in both weeks (*Genotype*: $F \geq 22.60, p \leq 0.011$). Accuracy and the wrong platform

visits, in contrast, only showed a trend for the *Genotype* effect in the first week ($F_{(1,16)} \geq 3.81, p \leq 0.068$), which was absent during the second week ($F_{(1,14)} \leq 0.25, p \geq 0.62$). The number of accurate learners in the first week indicated that only half of the KOs successfully learned the task until day 6 (3/8 compared to 10/10 WTs; $\chi^2 = 8.65, p = 0.003$), yet, most reached the criterion by day 7 (7/8). The number of accurate animals did not differ during relearning.

At last, further groups were trained with the response protocol for one week (figure 3.10 D; for the sake of simplicity, only accuracy and latency are shown). Despite a significant *Genotype* effect and a *Genotype* × *Time* interaction for the latency parameter (*Genotype*: $F_{(1,17)} = 9.19, p = 0.007$; *Genotype* × *Time*: $F_{(6,102)} = 2.54, p = 0.023$), no statistically significant *Genotype* or interaction effects were observed for the other parameters (*Genotype*: $F_{(1,17)} \leq 0.79, p \geq 0.384$; *Genotype* × *Time*: $F_{(6,102)} = 1.11, p = 0.363$).

Taken together, $Ca_v1.2$ KOs exhibited functional and morphological abnormalities that suggested place learning and relearning deficits. However, they developed only a slight delay during place learning where half of the animals became accurate only by day 7. On the other hand, response learning was not changed.

4. Discussion

Here I established a new cognitive test for mice that allowed to distinguish between place and response navigation strategies. I could demonstrate that C57Bl/6N mice were only able to relearn under place, but not response training, which was completely independent of the original learning strategy in the first week. HPC lesions caused severe volume reductions and made place learning impossible. Further, they disrupted successful relearning of the platform position, which was mainly associated with the volume reduction in the left ventral HPC. Next, I dissected the influence of $Ca_v1.2$ and $Ca_v1.3$ on manganese-related contrast enhancement to validate MEMRI as an functional imaging tool. Manganese accumulation was primarily, but not exclusively, mediated by $Ca_v1.2$. In addition, a reduction in $Ca_v1.2$ expression selectively caused a diminished MEMRI contrast in the projection area far away from the affected region. In a next step, animals were treated with manganese during place learning to map brain activity *in vivo*. The correlation analysis throughout the brain revealed a negative relation between the contrast in the dorsal HPC and the latency. On the other hand, the accuracy was associated with the left ventral HPC and the left BLA, each in an opposite direction. $Ca_v1.2$ knockout mice exhibited a reduced MEMRI contrast in some learning-associated regions, however, it entailed only a slight retardation but not an impairment in place learning.

4.1. Advantages of the WCM

The WCM enables the clear dissection or the combination of place and response strategies by using the appropriate protocol (originally proposed by Tolman et al., 1946). This also permits the separation of reversal learning and strategy switching, two abilities that are ascribed to the central executive. Compared to the Morris water maze, the narrow corridors of the WCM reduce the degrees of freedom and thereby the possibilities of using

unwanted strategies (Wolfer and Lipp, 2000). Nonetheless, some animals still improve in latency and wrong platform visits under place protocol by adopting an unintended response strategy. Accuracy scores around 50% are indicative for this behavior that can be quantified more precisely by the start bias (cf. figure 3.4). Therefore, this alternative response can be easily recognized using the standard parameters and does not require retrospective and complex analyses as in the Morris water maze (Wolfer and Lipp, 2000; Ruediger et al., 2012). Another advantage of the spatial restriction is the reduced time an animal spends in average in the water (i.e. 25 s on the first day down to 5 s at the end of the training). It decreases the risk for hypothermia and may also contribute to a lower stress level in the animals (Iivonen et al., 2003). As high stress favors response at the expense of place strategies, the equalized use of place and response strategies indicated by the probe trial after one week of free training reflects the well-adjusted stress load in the WCM (cf. figure 3.1 B; Packard and Wingard, 2004; Schwabe et al., 2010). Finally, the mice were able to maintain their motivation over periods up to 14 days what became apparent by the robust performance even of animals that were accurate very early during training (cf. figure 3.10). This advantage of water as a source of motivation adds to the argument that the otherwise required food deprivation represents a considerable stressor on its own (Cabib et al., 2000). Overall, the WCM combines the robustness of the Morris water maze with the simple analysis and clear differentiation of strategies in the plus-maze task. Especially the effective prevention of many alternative strategies makes the WCM particularly suitable for mice.

4.2. The flexible adaptation of spatial memories requires place strategies

All three training protocols (i.e. place, response and free training) enabled the accurate navigation to the platform position within five days. Although statistically not significant, the free training had an advantage of two days considering the mean accuracy exceeding 83% (figure 3.1 A). This indicates that free learning is slightly more efficient probably because it allows to use both strategies. While all animals became accurate during five days under place or free training, a few animals were unable to successfully acquire a response. This matches early observation that response learning is more difficult than

place learning for rats (Tolman et al., 1946; Packard, 2009). The non-accurate mice, however, performed far below chance level (i.e. accuracy score < 17%) suggesting the acquisition of another less adequate strategy. On closer inspection, these mice learned a more complex response strategy, i.e. swimming right, turning around before the end of the corridor and swimming straight to the platform instead of turning initially left. One reason could be that the animals received continuous reward for their behavior once they have tried it in this way. Important details about the place learning process are provided by the side bias (cf. figure 3.4). It increases between day 1 and day 2 before it declines to the end of place training in sham-operated C57Bl/6N mice. Since a high start bias indicates the use of a response strategy, this progress speaks for the acquisition of a response before the animals switch to the place strategy. It also matches similar finding under place training in the Morris water maze, where animals start with random swimming followed by response based searching strategies before they acquire a place memory (Wolfer and Lipp, 2000; Garthe et al., 2009; Ruediger et al., 2012). At last, all three protocols of the WCM have in common that the curve of the accuracy parallels the accurate learner profile (e.g. figure 3.1). This speaks in favor of a sudden insight rather than a successive trial and error learning that occurs in each mouse. Insights are usually associated with episodic memories in humans and therefore support the episodic-like character of the place memory (Morris, 2001). An explanation, why response learner also exhibit this phenotype, might be that the required response is a very simple by nature and therefore does not necessitate shaping.

In contrast to the acquisition, the capabilities of mice to revert a previously approached stimulus (reversal learning) was clearly different between the protocols. While place and free training enabled reversal learning within five days, response retraining resulted in low accuracies, long latencies and a large number of wrong platform visits (cf. figure 3.1 A) even after extension of the training for another five days. In particular, accuracy values well below 50% and the high number of wrong platform visits until the end of response retraining indicate a rigid adherence to the original navigation strategy and support the inflexibility of response memories (Ragozzino, 2007). Similar results were obtained in rats, which were incapable to succeed reversal training upon response protocol

in the same environment even after the double number of trials (McDonald et al., 2001). However, other studies report that rats are generally able but delayed in response reversal compared to place reversal training (Oliveira et al., 1997; Ragozzino et al., 1999). One explanation for my results might be that it is much easier for mice to expand (i.e. turning left and swim to the end of the corridor as in the first week of training, then turn around and swim straight to the platform at the end of the opposite arm) than to overcome the original strategy in order to locate the new platform position. As both possibilities are continuously reinforced, I cannot exclude that response reversal is possible in mice, if the reinforcement of the expanded response strategy would be prevented (e.g. by making the platform unaccessible upon wrong choices). Nonetheless, C57Bl/6N mice persistently adhere to the original response strategy until the end of response retraining, which was neither seen in other protocols nor in the rat literature. Overall, it could indicate that the original response memory is remarkably rigid, however, it could also be that the response protocol in the second week prohibits successful relearning.

Therefore, the capability of mice to switch between strategies (strategy switching) was examined. It became clear that animals under response retraining failed to relearn, no matter, which strategy they acquired before (cf. figure 3.2). This contradicts the results obtained by Ragozzino et al. (1999), where rats successfully relearned under response protocol after they acquired a place memory. However, these animals needed twice as many trials to reach criterion like rats did under response reversal. Further, the here presented data reject the hypothesis that the original response memory is responsible for the rigidity under response reversal. In fact, the place strategy appears to be essential for spatial relearning.

As a consequence, animals under free protocol in the second week should employ place instead of response strategies to reach criterion. The probe trials, which were indicative for the exerted strategy during each week, support this hypothesis (figure 3.1 B). At the end of the first week of free training, half of the animals used a place and the other half a response strategy, while almost all animals employed a place strategy at the end of free retraining. Studies in rats also obtained equal distributions between the strategies in a free protocol adapted for the Morris water maze, yet, the used strategies under free relearning

was not investigated (McDonald and White, 1994; Sutherland et al., 1997). Overall, these data provide evidence that relearning depends on place strategies in C57BL/6N mice. This suggests that, in addition to frontal regions, the HPC plays an essential role for the relearning. To verify this, the consequences of HPC lesions on learning and relearning capabilities were examined in the following experiments.

4.3. Place learning and relearning depends on the HPC

Lesioning of the HPC prohibits place learning as previously shown in numerous classical rat studies (figure 3.4; O'Keefe et al., 1975; Packard et al., 1989; McDonald and White, 1994). On the other hand, HPC-lesioned mice get accurate by response training and acquire compensatory response strategies during place training reflected by a constantly high start bias (figure 3.4 E, F). This is consistent with studies in rats, where response learning can occur independent of the hippocampus or even improves after HPC lesioning (Packard and McGaugh, 1996; McDonald et al., 2002; Stringer et al., 2005). Since response learning remains unaffected under identical conditions in HPC-lesioned mice, it is highly unlikely that the place learning deficits originate from motivational or motoric impairments. Further, it is implausible that the hyperactive phenotype observed in the open field after HPC lesioning has any impact on the performance in the WCM. The reason is that differences did not appear within the first minute, which is the relevant period for the WCM. Another interesting observation is that HPC-lesioned animals were able to reduce the number of wrong platform visits while the accuracy remained at chance level (~50%). This seemingly contradicting result might be due to the fact that the mice are still able to distinguish the corridors when they enter it. If mice always perform the same response at the center of the maze, it results in 50% accuracy, but if they enter the wrong arm and turn around well before the end, they still can reduce the perseverance errors. Similar is observed in HPC-lesioned mice that fail to discriminate two arms in an radial arm maze but still acquire a go/no-go rule if only one arm is presented (Etchamendy et al., 2003; Mingaud et al., 2007). At last, HPC lesions had no effect on the performance during free training most likely because these animals adopted a response strategy to succeed. Overall, the results suggest that HPC-lesioned mice are only able to acquire a response

but not a place memory, which is clearly due to mnemonic deficits. Since place learning is essential for relearning, lesions in the HPC should impede also relearning under free retraining. To test this, response and free learner were subjected to free protocol in the second week. In both cases, mice with HPC lesions exhibited clear relearning deficits, however, mice under response training in the first week had a high variability between the individual performances in the second week (figure 3.5). Slightly different results were obtained in HPC-lesioned rats, which were impaired but not unable to relearn upon response protocol (Oliveira et al., 1997). In sum, place but not response learning requires an intact HPC and relearning is essentially affected by HPC lesions as it depends on place strategies.

4.4. The left ventral HPC best reflects relearning capabilities

Large differences in the performance of HPC-lesioned mice under free retraining prompted to put the learning parameters in relation to the severity of the lesions. First, IA-injection reduced the total HPC volume by ~50% on average (figure 3.3 C, D), which was well correlated with the mean accuracy score over five days of free retraining indicating greater learning difficulties when less HPC tissue remains. However, the clear bimodality in the performance on $d5_r$ assumes that mice require a minimal residue of the HPC to relearn (figure 3.6 A). When contrasting the HPC size of learner and non-learner during free retraining, it became clear that a remaining volume of 47.7 ± 2.7% was sufficient for relearning, while 36.9 ± 3.4% was not enough. Kassem et al. (2012) estimated that neurons, their dendrites and axons represent ~66% of the HPC volume suggesting neuronal cell loss as a supposable underlying mechanism for the reported threshold. The existence of such a limiting residue has also been reported by Moser et al. (1995), where lesions in the dorsal HPC leaving 40% - 60% of the total HPC intact disturbed the acquisition of a place memory in the Morris water maze. In contrast, lesions in the ventral HPC did not affect place learning at all. This functional dissection of the HPC structure initiated a detailed volumetric analysis of the different portions of the HPC and their relation to the relearning performance.

On average, the IA-induced volume reduction was about 50% in the dorsal or ventral as well as in the left or right portion of the HPC. The highest correlate of the accuracy was the volume in the left ventral HPC, however, not significant after multiple test correction. On the other hand, the stratification into learner and non-learner based on the accuracy on $d5_r$ resulted in significant lower remaining volumes in the left ventral portion of the HPC in non-learner compared to learner (figure 3.6 B). This effect even withstood the multiple test correction of Bonferroni and therefore best reflects relearning deficits here in this study. Beside the well described role of the ventral HPC in emotional memories (Kjelstrup et al., 2002; Rudy and Matus-Amat, 2005; Fanselow and Dong, 2010), a recent publication by Ruediger et al. (2012) investigated the importance of the ventral murine HPC during place learning in the Morris water maze. The authors demonstrate that electrolytic lesions in the ventral HPC selectively deteriorate the performance in the middle of the learning progress (day 2-7) while dorsal HPC lesions disrupt the performance at the end of training (day 7-11). As the ventral HPC is not only strongly connected to the dorsal part but also to striatal regions, the authors argue that it subserves strategy selection by relating emotional information, in that case a reinforcement, to the context (Fanselow and Dong, 2010; Pennartz et al., 2011; Ruediger et al., 2012). Since most animals in my study either surpass 83% accuracy by using a place strategy or drop below 17% indicating a complete failure, the inability to select the place strategy during relearning is a reasonable explanation for the correlation with a ventral portion of the HPC. However, selective lesioning of the ventral HPC combined with prolonged training over at least seven days would be necessary to prove that it is essential for relearning.

Moreover, volume differences between learner and non-learner arise not only in the left ventral portion of the HPC, but also the entire left HPC revealed a trend in the same direction after multiple test correction. This emphasizes the importance of especially the left hemisphere to reach high accuracy levels during relearning. In humans, the brain activation in the left HPC predicts the use of response strategies in a virtual star maze, whereas the right HPC is associated with place learning (Iglói et al., 2010). Since animals are still able to acquire a response in the first week that they may continue to use in the second week, this hemispheric differentiation might explain the emphasis on the left

hemisphere. However, hemispheric differences are difficult to investigate as the function can always be taken over by the intact side.

At last, the dorsal HPC and especially the left dorsal portion correlated moderately with the rearing duration in the open field, however, on an uncorrected level. Nevertheless, these results were replicated in the holeboard test, which emphasizes their importance. Rearing is an exploratory behavior describing four-legged animals standing only on their hind legs raising their forelimbs of the ground, which naturally occurs in completely or partially new environments. It has been shown, that HPC lesions prevent the increase in rearing in a novel surrounding and place cells in the dorsal HPC might also contribute to it (Moses et al., 2002; Frank et al., 2004; Lever et al., 2006). Therefore, these correlations support the importance of the dorsal HPC for exploration in completely or partially new environments.

Overall, a remaining HPC volume of more than 40% is sufficient to relearn successfully in the WCM. Further, the left ventral HPC best reflects relearning capabilities in C57Bl/6N mice. The supposable deteriorated function of the left ventral portion might be a selection of a place strategy, which is required for successful place learning and relearning. *In vivo* imaging of brain activity during training might help to get a better understanding of the HPC involvement in place learning. In order to employ MEMRI as an *in vivo* functional imaging tool in mice, the basics of manganese accumulation in the brain first need to be better described. Therefore, the contribution of $Ca_v1.2$ and $Ca_v1.3$ on MEMRI intensity in the brain is examined in a next step.

4.5. $Ca_v1.2$ affects at least 50% of the manganese-dependent contrast increase *in vivo*

Based on *ex vivo* studies, it has been often assumed that MEMRI contrast depends on LTCCs (Simpson et al., 1995; Pautler and Koretsky, 2002). With the help of modern knockout techniques, I was able to demonstrate that $Ca_v1.2$, the prevailing LTCC in brain, makes a major contribution to manganese-dependent contrast increase *in vivo*, which can be dissected from $Ca_v1.3$ that had no significant effect on the image intensities

(figure 3.7). Considering the whole brain intensity, merely 50% of the manganese-induced contrast increase was detectable in $Ca_v1.2$ knockouts compared to wild type controls. Having in mind the homeostatic change in calcium permeable α-amino-3-hydroxy-5-methyl-4-isoxazolepropionic acid (AMPA) receptor expression that maintains normal neuronal functioning in $Ca_v1.2$ knockouts, manganese accumulation seems to be rather specific to $Ca_v1.2$ channels (Langwieser et al., 2010). Another primary modulator of MEMRI intensity is the NMDA receptor, however, this was investigated by means of pharmacological inhibition or activation, which might additionally alter the neuronal activity of the neurons per se and therefore the activity of other voltage-dependent calcium channels like $Ca_v1.2$ (Itoh et al., 2008). Nevertheless, Itoh et al. also observed a 50% reduction in intensity by NMDA receptor inactivation, which indicate that both together, $Ca_v1.2$ and NMDA receptors, control the majority of manganese accumulation in the brain. A conceivable reason that only $Ca_v1.2$ but not $Ca_v1.3$ affect the image intensity could be simply the quantity of each channel. The $Ca_v1.2$ makes ~80% of the LTCCs in the brain, while the $Ca_v1.3$ accounts for less than 15% (Hetzenauer et al., 2006; Sinnegger-Brauns et al., 2009). This would then indicate that MEMRI is not sensitive to the possible minor contribution of $Ca_v1.3$ on the signal intensity. A further explanation could be the location of $Ca_v1.2$ at the dendritic site (Westenbroek et al., 1990; Hell et al., 1993; Ludwig et al., 1997). If manganese is released at the presynapse in an activity-dependent manner (Takeda et al., 1998), it would be highest concentrated at the proximity of the synaptic cleft and not close to the soma, where $Ca_v1.3$ is dominantly situated (Hell et al., 1993; Ludwig et al., 1997).

One disadvantage of the here applied knockout technique is, that the early inactivation could cause unknown developmental alteration e.g. in the permeability of the blood brain barrier. In order to exclude that possibility, a $Ca_v1.2$ knockout in the right lateral thalamus was achieved by injection of a virus coding for the Cre recombinase in adult mice having the $Ca_v1.2$ gene flanked by loxP sides. The voxel-wise comparison of Cre and control animals revealed a significant *Group* × *Timepoint* interaction after multiple test correction in the right insular cortex but not at the injection site (figure 3.8 B). It indicates a lower manganese-dependent contrast increase in the insular cortex, which cannot be attributed

to tissue damage resulting from the injection procedure due to its long distance from the injection site. Further, western blot analysis confirmed the actual down-regulation of $Ca_v1.2$ expression at the injection site whereas the expression in the insular cortex remained unaffected (figure 3.8 C). According to Sloot and Gramsbergen (1994), these results can be best explained by a preferential accumulation of manganese at the projection terminals of the neurons. This assumption is supported by the analysis of manganese transport, which revealed an intensity increase in the insular cortex after manganese injection into the lateral thalamus (figure 3.8 D). Despite the wide spreading of manganese at the injection site and the many nuclei of the thalamus with the various projection areas, voxel-wise regression analysis identified only three brain regions including the insular cortex that display a significant increase in the image intensity. This demonstrates the rather specific transport of manganese from the lateral thalamus to the insular cortex and overall indicates a shift in manganese accumulation away from the uptake site to the projection areas. These findings are consistent with the often described characteristic of manganese that it is transported along the axon of neurons by microtubules to the projection terminals, where it is released in an activity-dependent manner (Sloot and Gramsbergen, 1994; Pautler et al., 2003; Yang et al., 2011). Overall, these experiments speak against developmental alterations that cause changes in manganese-accumulation in $Ca_v1.2$ knockouts and suggest changes in contrast happening at the site of the projection terminals.

In summary, manganese accumulation in the brain is primarily, but not exclusively, mediated by $Ca_v1.2$, which, to the best of my knowledge, has not yet been demonstrated *in vivo*. Moreover, it is very likely that the NMDA receptors also contribute to manganese influx into neurons. Both receptor types are regulated in an voltage-dependent manner, suggesting that the manganese-dependent contrast increase is to a large extent a direct indicator of neuronal activity. Finally, it is very likely that activity induced contrast differences are biased towards projection areas of a region (i.e. at the site of the axon terminals) rather than appearing at the uptake site (i.e. at the site of the dendrites or the soma).

4.6. MEMRI depicts brain activity during place learning *in vivo*

I have argued before, that manganese accumulation depends on neural activity. In order to prove that MEMRI can depict brain activity during place learning *in vivo*, I combined place training with manganese injections before image acquisition started 20 minutes after the last swim trial (figure 3.9). The manganese dose was reduced to prevent any neurotoxic effects in the HPC. C57Bl/6M mice exceeded the critical accuracy of 83% on day four of place training, which is similar to the learning curve of untreated mice (cf. figure 3.1). This adds to previous findings that fractionated manganese application reduces toxic side effects in the HPC compared to a single injection protocol (Eschenko et al., 2010b; Gruenecker et al., 2012). I could demonstrate, that manganese accumulation in the left ventral HPC, particularly its most ventral pole as part of the subiculum, was positively correlated with the mean accuracy over eight days of place training, while the contrast in the BLA was negatively correlated. When incorporating the previous finding that contrast differences might occur at a projection site, these results indicate more active afferents into the ventral HPC during successful acquisition. These incoming signals might then be forwarded within the ventral HPC to the subiculum as the main output region of the HPC, which would explain the accumulation at that specific site. It further denotes that there are less active afferents into the BLA. The bidirectional connection between the ventral HPC and the BLA suggests a reciprocal innervation, however, other areas like medial prefrontal regions could mediate this effect (Fanselow and Dong, 2010; Prasad and Chudasama, 2013). The positive correlation in the ventral HPC is in line with the detrimental effects of ventral HPC-lesions on place learning performance in the Morris water maze (Ruediger et al., 2012). Moreover, it supports the before described involvement of the left ventral HPC in relearning since relearning depends on place strategies. In addition, the BLA is part of a network that modulate contextual fear (Herry et al., 2008; Sotres-Bayon et al., 2012), which might become active under stress induction that worsens specifically place learning performance in mice (Schwabe et al., 2010). Conversely, successful learning might reduce the stress level and therefore afferent signals into the BLA. If the ventral HPC relates emotional to contextual information as suggested by Ruediger et al. (2012), it might gain control over the BLA via medial

prefrontal regions like it is known for extinction processes after fear conditioning (Sotres-Bayon et al., 2012). On the other hand, projections from the BLA to the ventral HPC directly interfere with anxiety-related behavior in mice (Felix-Ortiz et al., 2013). This projection might resemble a feedback mechanism controlling ventral HPC action during place learning. Taken together, the antagonistic involvement of the BLA and the ventral HPC in place learning might resemble the integration of emotional valences into cognitive processes. Future research is necessary to prove, that selective up or down regulation of the activity in the BLA impacts place learning.

Next, the mean latency of the first and second half of training was correlated with the MEMRI intensity. Based on the accuracy, the latency was dissected into an early (d1-4) and an late acquisition phase (d5-8; figure 3.9). This was possible because the latency in contrast to the accuracy is sufficiently dispersed in the second half of training. Interestingly, the mean latency of the first half correlated only with a cluster in the left CA3 region of the dorsal HPC after multiple test correction while the mean latency of the second half was additionally associated with a cluster in the dorsal right HPC comprising less the CA3 but more the CA1 region and stretches into the restrosplenial cortex. Considering especially the grid cells in the entorhinal cortex that may contribute to the formation of place cells in the HPC (O'Keefe and Dostrovsky, 1971; Hafting et al., 2005), active neurons in the entorhinal cortex probably project directly (via the temporoammonic pathway) or indirectly (via the perforant path and the mossy fibers) to the CA3 region, which may lead to manganese accumulation at this location. A recent publication could demonstrate that theta-frequency stimulation at the entorhinal input to the HPC generates neuronal activity, which propagates through the CA3 into the CA1 where it induces NMDA receptor-dependent LTP (Stepan et al., 2012). On the other hand, other stimulation frequencies are not further propagated, but are filtered at axonal synapses terminating in the CA3. Accordingly, the correlation in the left CA3 region may indicate not further propagated signals from the entorhinal cortex, however, the right CA3 eventually passed the signal to the CA1 what might have led to place memory formation. This also matches my previous observation, that the first four days of place training are associated with response based searching indicated by the start bias that continues to

decrease until day five of place training. Similar results have been reported for the Morris water maze, where place learning occurs not before day five of training (Ruediger et al., 2012). Finally, virtual reality studies in humans provide evidence, that the two HPC hemispheres are responsible for complementary representations during virtual navigation, which enables the parallel acquisition of spatial knowledge (Iglói et al., 2009, 2010). Whereas activation of the left HPC during free navigation predicted the use of response strategies, the right HPC was associated with place searching. Since the first half of place training in the WCM was dominated by response based strategies, the corresponding association in the left HPC fits the human findings. On the other hand, the right HPC was only related to the second half of training that represents place searching. In sum, the correlation in the left and right HPC during the second half of training is congruent with the scenario of the parallel processing of egocentric and allocentric cues to locate the platform.

Overall, the accuracy is linked to a fear associated network comprising the BLA and the ventral HPC as it may reflect the learning success in a rather categorical way. On the other hand, the latency stands for continuous learning improvements in the WCM and therefore depicts response or place learning success in the left or right HPC, respectively. At last, especially the right HPC might be associated with LTP in the CA1 region underlying place memory formation. Whether the manganese accumulation in the right HPC depends on NMDA receptors or LTCCs is unknown. Therefore, place and response learning capabilities of $Ca_v1.2$ knockouts were tested in a next step.

4.7. $Ca_v1.2$ is involved in, but not essential for place learning

To better understand the contribution of $Ca_v1.2$ to learning and relearning processes, knockouts lacking $Ca_v1.2$ throughout the central nervous system were opposed to their littermate controls having one functional $Ca_v1.2$ allele and therefore $Ca_v1.2$ expression left in the brain (Langwieser et al., 2010). It is important to mention that both lines express the Cre recombinase throughout the central nervous system (under the control of the Nestin promoter), which can thus be excluded as a cause of variation. Further, it is unlikely that

peripheral expression changes due to a shortened $Ca_v1.2$ allele in the entire body of the knockouts as heterozygous knockout and wild type animals exhibit comparable RNA levels in the embryonic heart (Seisenberger et al., 2000). Therefore, phenotype differences can be primarily attributed to differences of $Ca_v1.2$ expression in the central nervous system.

To study first the functional and morphological properties of the knockouts, differences in MEMRI contrast were examined and ventral HPC volumes were determined. Knockouts exhibit peak intensity reductions in a number of regions from which the CA1 and the amygdala overlap with the correlation obtained during place learning (figure 3.10 A). Given the important role of $Ca_v1.2$ for late LTP in the CA1 region *in vitro* (Moosmang et al., 2005) and the negative correlation between MEMRI intensity of the CA1 and the latency, the reduced contrast in the CA1 region of $Ca_v1.2$ knockouts would indicate performance deficits during place learning in the WCM. On the other hand, the lower intensity in the amygdala might be beneficial for place learning since it was associated with higher accuracy values. However, the previous correlation analysis highlighted the right BLA, which does not exactly match the differences in the left central amygdala obtained here. Despite that both nuclei belong to the amygdaloid complex, they represent different functional units. The BLA on the one hand is involved in fear memory storage, while the central nucleus resembles the most important output relay of the complex and is therefore associated with the expression of fear (Maren, 1999; Sigurdsson et al., 2007). Beyond the CA1 and the amygdala, the reduced contrast in the medial prefrontal and the restrosplenial cortex of $Ca_v1.2$ knockouts not only matches the before described correlation with the latency in the right HPC stretching to the retrosplenial cortex, but also links to the discussion about a possible role of the medial prefrontal cortex in mediating BLA and ventral HPC activity. For that reason, it endorse the hypothesis that $Ca_v1.2$ knockouts could be affected in place learning. Nevertheless, one need to keep in mind that completely different afferents might account for manganese accumulation within a same region. Further, the baseline accumulation obtained here does not necessarily predict the manganese accumulation during training in the WCM. Apart from the intensity, especially the ventral HPC had smaller vaults by ~5% in the knockouts compared to control animals

(figure 3.10 B). This might indicate not only a relearning impairment due to the observed correlation between the accuracy and the left ventral HPC, but also impairments during initial place learning as relearning was shown to depend on place strategies. Overall, the structural and functional analysis of $Ca_v1.2$ knockouts indicates place learning deficits in the WCM, which also should affect the relearning.

Despite the functional and morphological evidence, $Ca_v1.2$ knockouts did neither exhibit a severe deficit in place learning, nor in response learning or in reversal learning as indicated by the accuracies (figure 3.10 C, D). Irrespective of a general delay seen in the latency in all tasks, knockout mice display a specific retardation only during place learning on day five and six of training. At first glance, this would seem to contradict previous findings, where $Ca_v1.2$ knockouts exhibited longer latencies and less accuracy in choosing the right platform in the Morris water maze (Moosmang et al., 2005). However, these mice were trainied only for five days with 10 trials a day, what precludes learning later during training as it is shown here. Yet, the same authors subjected the animals to another spatial maze, a labyrinth maze made of transparent tubes, where a performance deficit became apparent exclusively in the middle of the training course. Further, White et al. (2008) observed no deteriorations in $Ca_v1.2$ knockouts during place training in the Morris water maze, but describes disruptions in the remote memory. According to Ruediger et al. (2012), place learning starts at day 5 in the Morris water maze. Therefore, this rather specific deterioration during the cause of place training might resemble initial place learning difficulties possibly because of the impaired late LTP in the CA1 region of the HPC (Moosmang et al., 2005). The reason, why $Ca_v1.2$ knockout mice can still handle the situation, might be that they compensate the knockout by AMPA receptor expression (Langwieser et al., 2010). This fundamental alteration might have enabled the knockouts to form a fear memory, whereas pharmacological inhibition blocked proper fear acquisition.

In conclusion, $Ca_v1.2$ is involved in place learning, however, an early knockout of the channel cannot prevent place memory formation maybe because animals compensate the loss via AMPA receptors. In the end, only a knockout of $Ca_v1.2$ precipitated shortly before place training could ultimately prove that the channel is essential and not only involved in place memory acquisition.

5. Conclusion and Outlook

First, I evaluated the suitability of the WCM as a spatial memory test for mice. I was able to demonstrate that particularly the spatial confinement to narrow corridors prevents the acquisition of unwanted strategies that are often adopted by mice in open mazes. Conceptually, the WCM allows to distinguish place from response navigation strategies and consequently also reversal learning from strategy switching. For future research, it might be very interesting to also evaluate working memory protocols in the WCM like matching-to-sample or non-matching-to-sample tasks (e.g. Sigurdsson et al., 2010; Han et al., 2012). The systematic analysis of spatial learning and relearning capabilities in C57Bl/6N mice revealed that relearning is enabled only by place but not by response strategies. This is independent of the original learning strategy acquired in the first week of training. It suggests that not only place learning but also relearning is predicated on the HPC structure. In the WCM, lesioning of the HPC not only prevents place learning in mice, but it also impairs relearning, at least, if less than 40% of the total HPC volume remains. A supposable underlying mechanism for this threshold might be neuronal cell loss, which should be investigated in the future. Detailed analyses of the different portions in the HPC further revealed, that the left ventral part best reflects relearning capabilities of lesioned animals, however, whether it is essential remains to be shown by selective removal in the future.

Second, I investigated the contribution of $Ca_v1.2$ and $Ca_v1.3$ to MEMRI intensity. I was able to demonstrate for the first time that $Ca_v1.2$, the prevailing LTCC in the central nervous system, affects at least 50% of the manganese dependent contrast increase *in vivo*. On the other hand, $Ca_v1.3$ caused no significant alterations in MEMRI intensity. Together with NMDA receptors, $Ca_v1.2$ therefore regulates voltage dependent manganese influx into neurons, what rises the possibility that MEMRI can be used as an activity marker in

living mice. In addition, the data indicate that activity induced intensity differences are biased towards axon terminals, which is in line with the often described characteristic of manganese that it is transported along the axon by microtubules. Nevertheless, it still remains unclear, how the MEMRI contrast changes or displaces as a function of up or down regulations in neural activity.

Next, I combined place training with manganese injections to map brain activity during place learning. To the best of my knowledge, I could demonstrate for the first time a spatial memory trace *in vivo* in mice. On the one hand, the accuracy is related to a fear associated network comprising the BLA and the ventral HPC. On the other hand, the latency correlates with the dorsal HPC, where the left CA3 region might resemble response navigation and the right CA1 regions place memory formation. This also speaks in favor of a parallel processing of egocentric and allocentric information during place navigation. Together, the associated brain regions indicate the integration of emotional contents into cognitive processes. Overall, MEMRI enabled the hypothesis-free analysis of brain activity during a learning task and therefore the identification of previously non-supposed brain regions. In the future, selective activity modulations in the identified regions might provide new insights into the mechanisms involved in place learning.

At last, the learning and relearning capabilities of $Ca_v1.2$ knockout mice were investigated. Despite reduced MEMRI intensities in place learning associated regions and diminished volumes of the ventral HPC, knockout mice successfully acquired a place as well as a response memory and they were able to relearn under place training in the second week. However, knockouts exhibit a significant retardation specifically during place learning, which might be due to an impaired late LTP in the CA1 region of the HPC (Moosmang et al., 2005). Overall, compensatory effects could account for the largely intact learning capabilities of the knockout animals, which should be avoided in future studies by precipitating the knockout shortly before training.

All in all, I successfully applied volumetric MEMRI (vMEMRI) to identify hippocampal size and established functional MEMRI (*f*MEMRI) as a powerful tool to determine brain activity *in vivo*. This allowed me to define for the first time networks throughout the brain associated with place learning in freely moving mice.

Bibliography

Ashburner, J. and Friston, K. J. (2000). Voxel-based morphometry - the methods. *Neuroimage*, 11(6):805–821.

Azevedo, F. A., Carvalho, L. R., Grinberg, L. T., Farfel, J. M., Ferretti, R. E., Leite, R. E., Lent, R., and Herculano-Houzel, S. (2009). Equal numbers of neuronal and nonneuronal cells make the human brain an isometrically scaled-up primate brain. *J Comp Neurol*, 513(5):532–541.

Baddeley (2000). The episodic buffer: a new component of working memory? *Trends Cogn Sci*, 4(11):417–423.

Baddeley, A. and Hitch, G. (1974). *Recent advances in learning and motivation*, chapter Working memory, pages 47–90. New York: Academic Press.

Bannerman, D. M., Good, M. A., Butcher, S. P., Ramsay, M., and Morris, R. G. (1995). Distinct components of spatial learning revealed by prior training and nmda receptor blockade. *Nature*, 378(6553):182–186.

Barch, D. M. and Ceaser, A. (2012). Cognition in schizophrenia: core psychological and neural mechanisms. *Trends Cogn Sci*, 16(1):27–34.

Barnes, C. A. (1979). Memory deficits associated with senescence: a neurophysiological and behavioral study in the rat. *J Comp Physiol Psychol*, 93(1):74–104.

Barnes, T. D., Kubota, Y., Hu, D., Jin, D. Z., and Graybiel, A. M. (2005). Activity of striatal neurons reflects dynamic encoding and recoding of procedural memories. *Nature*, 437(7062):1158–1161.

Basser, P. J., Mattiello, J., and LeBihan, D. (1994). MR diffusion tensor spectroscopy and imaging. *Biophys J*, 66(1):259–267.

Bauer, E. P., Schafe, G. E., and LeDoux, J. E. (2002). NMDA receptors and L-type voltage-gated calcium channels contribute to long-term potentiation and different components of fear memory formation in the lateral amygdala. *J Neurosci*, 22(12):5239–5249.

Benhamou, S. and Poucet, B. (1995). A comparative analysis of spatial memory processes. *Behavioural Processes*, 35(1):113–126.

Bissonette, G. B., Martins, G. J., Franz, T. M., Harper, E. S., Schoenbaum, G., and Powell, E. M. (2008). Double dissociation of the effects of medial and orbital prefrontal cortical lesions on attentional and affective shifts in mice. *J Neurosci*, 28(44):11124–11130.

Bliss, T. V. and Collingridge, G. L. (1993). A synaptic model of memory: long-term potentiation in the hippocampus. *Nature*, 361(6407):31–39.

Bliss, T. V. and Lømo, T. (1973). Long-lasting potentiation of synaptic transmission in the dentate area of the anaesthetized rabbit following stimulation of the perforant path. *J Physiol*, 232(2):331–356.

Bock, N. A., Paiva, F. F., and Silva, A. C. (2008). Fractionated manganese-enhanced MRI. *NMR Biomed*, 21(5):473–478.

Boric, K., Muñoz, P., Gallagher, M., and Kirkwood, A. (2008). Potential adaptive function for altered long-term potentiation mechanisms in aging hippocampus. *J Neurosci*, 28(32):8034–8039.

Branchi, I. and Ricceri, L. (2004). Refining learning and memory assessment in laboratory rodents. An ethological perspective: Biostatical and ethological approaches for the promotion of welfare of laboratory animals and quality of experimental data. *Annali dell'Istituto superiore di sanità*, 40(2):231–236.

Cabib, S., Orsini, C., Moal, M. L., and Piazza, P. V. (2000). Abolition and reversal of strain differences in behavioral responses to drugs of abuse after a brief experience. *Science*, 289(5478):463–465.

Cain, C. K., Blouin, A. M., and Barad, M. (2002). L-type voltage-gated calcium channels are required for extinction, but not for acquisition or expression, of conditional fear in mice. *J Neurosci*, 22(20):9113–9121.

Chamberlain, S. R., Blackwell, A. D., Fineberg, N. A., Robbins, T. W., and Sahakian, B. J. (2005). The neuropsychology of obsessive compulsive disorder: The importance of failures in cognitive and behavioural inhibition as candidate endophenotypic markers. *Neurosci Biobehav Rev*, 29(3):399–419.

Chapman, R. M. and Bragdon, H. R. (1964). Evoked responses to numerical and non-numerical visual stimuli while problem solving. *Nature*, 203:1155–1157.

Ciocchi, S., Herry, C., Grenier, F., Wolff, S. B., Letzkus, J. J., Vlachos, I., Ehrlich, I., Sprengel, R., Deisseroth, K., Stadler, M. B., et al. (2010). Encoding of conditioned fear in central amygdala inhibitory circuits. *Nature*, 468(7321):277–282.

Collingridge, G., Kehl, S., and McLennan, H. T. (1983). Excitatory amino acids in synaptic transmission in the schaffer collateral-commissural pathway of the rat hippocampus. *J Physiol*, 334(1):33–46.

Craddock, N. and Sklar, P. (2013). Genetics of bipolar disorder. *Lancet*, 381(9878):1654–1662.

Davare, M. A. and Hell, J. W. (2003). Increased phosphorylation of the neuronal L-type Ca^{2+} channel $Ca_v1.2$ during aging. *Proc Natl Acad Sci U S A*, 100(26):16018–16023.

Davis, S. E. and Bauer, E. P. (2012). L-type voltage-gated calcium channels in the basolateral amygdala are necessary for fear extinction. *J Neurosci*, 32(39):13582–13586.

Dias, R., Robbins, T. W., and Roberts, A. C. (1996). Dissociation in prefrontal cortex of affective and attentional shifts. *Nature*, 380(6569):69–72.

Disterhoft, J. F., Moyer, J. R., and Thompson, L. T. (1994). The calcium rationale in aging and Alzheimer's disease. *Ann N Y Acad Sci*, 747(1):382–406.

Dolmetsch, R. E., Pajvani, U., Fife, K., Spotts, J. M., and Greenberg, M. E. (2001). Signaling to the nucleus by an L-type calcium channel-calmodulin complex through the MAP kinase pathway. *Science*, 294(5541):333–339.

Doyon, J., Gaudreau, D., Laforce, R., Castonguay, M., Bédard, P. J., Bédard, F., and Bouchard, J. P. (1997). Role of the striatum, cerebellum, and frontal lobes in the learning of a visuomotor sequence. *Brain Cogn*, 34(2):218–245.

Drapeau, P. and Nachshen, D. A. (1984). Manganese fluxes and manganese-dependent neurotransmitter release in presynaptic nerve endings isolated from rat brain. *J Physiol*, 348:493–510.

Eckart, M. T., Huelse-Matia, M. C., and Schwarting, R. K. W. (2012). Dorsal hippocampal lesions boost performance in the rat sequential reaction time task. *Hippocampus*, 22(5):1202–1214.

Eichenbaum, H., Stewart, C., and Morris, R. G. (1990). Hippocampal representation in place learning. *J Neurosci*, 10(11):3531–3542.

Eschenko, O., Canals, S., Simanova, I., Beyerlein, M., Murayama, Y., and Logothetis, N. K. (2010a). Mapping of functional brain activity in freely behaving rats during voluntary running using manganese-enhanced MRI: implication for longitudinal studies. *Neuroimage*, 49(3):2544–2555.

Eschenko, O., Canals, S., Simanova, I., and Logothetis, N. K. (2010b). Behavioral, electrophysiological and histopathological consequences of systemic manganese administration in MEMRI. *Magn Reson Imaging*, 49:2544–2555.

Essman, W. and Jarvik, M. (1961). A water-escape test for mice. *Psychol Rep*, 8(1):58–58.

Etchamendy, N., Desmedt, A., Cortes-Torrea, C., Marighetto, A., and Jaffard, R. (2003). Hippocampal lesions and discrimination performance of mice in the radial maze: sparing or impairment depending on the representational demands of the task. *Hippocampus*, 13(2):197–211.

Falls, W., Miserendino, M., and Davis, M. (1992). Extinction of fear-potentiated startle: blockade by infusion of an NMDA antagonist into the amygdala. *J Neurosci*, 12(3):854–863.

Fanselow, M. S. and Dong, H.-W. (2010). Are the dorsal and ventral hippocampus functionally distinct structures? *Neuron*, 65(1):7–19.

Fasolato, C., Hoth, M., and Penner, R. (1993). Multiple mechanisms of manganese-induced quenching of fura-2 fluorescence in rat mast cells. *Pflügers Archiv*, 423(3-4):225–231.

Federle, M., Chezmar, J., Rubin, D. L., Weinreb, J., Freeny, P., Schmiedl, U. P., Brown, J. J., Borrello, J. A., Lee, J. K., and Semelka, R. C. (2000). Efficacy and safety of mangafodipir trisodium (MnDPDP) injection for hepatic MRI in adults: results of the US multicenter phase III clinical trials. efficacy of early imaging. *J Magn Reson Imaging*, 12(5):689–701.

Felix-Ortiz, A. C., Beyeler, A., Seo, C., Leppla, C. A., Wildes, C. P., and Tye, K. M. (2013). BLA to vHPC inputs modulate anxiety-related behaviors. *Neuron*, 79(4):658–664.

Ferreira, M. A., O'Donovan, M. C., Meng, Y. A., Jones, I. R., Ruderfer, D. M., Jones, L., Fan, J., Kirov, G., Perlis, R. H., and Green, E. K. (2008). Collaborative genome-wide association analysis supports a role for ANK3 and CACNA1C in bipolar disorder. *Nat Genet*, 40(9):1056–1058.

Fisk, J. E. and Sharp, C. A. (2004). Age-related impairment in executive functioning: updating, inhibition, shifting, and access. *J Clin Exp Neuropsychol*, 26(7):874–890.

Fox, N. C., Warrington, E. K., Freeborough, P. A., Hartikainen, P., Kennedy, A. M., Stevens, J. M., and Rossor, M. N. (1996). Presymptomatic hippocampal atrophy in Alzheimer's disease. a longitudinal MRI study. *Brain*, 119:2001–2007.

Frank, L. M., Stanley, G. B., and Brown, E. N. (2004). Hippocampal plasticity across multiple days of exposure to novel environments. *J Neurosci*, 24(35):7681–7689.

Frey, U., Krug, M., Reymann, K. G., and Matthies, H. (1988). Anisomycin, an inhibitor of protein synthesis, blocks late phases of LTP phenomena in the hippocampal CA1 region in vitro. *Brain Res*, 452(1):57–65.

Frick, K. M., Stillner, E. T., and Berger-Sweeney, J. (2000). Mice are not little rats: species differences in a one-day water maze task. *Neuroreport*, 11(16):3461–3465.

Garthe, A., Behr, J., and Kempermann, G. (2009). Adult-generated hippocampal neurons allow the flexible use of spatially precise learning strategies. *PLoS One*, 4(5):e5464.

Golub, Y., Kaltwasser, S. F., Mauch, C. P., Herrmann, L., Schmidt, U., Holsboer, F., Czisch, M., and Wotjak, C. T. (2011). Reduced hippocampus volume in the mouse model of posttraumatic stress disorder. *J Psychiatr Res*, 45(5):650–659.

Golub, Y., Mauch, C. P., Dahlhoff, M., and Wotjak, C. T. (2009). Consequences of extinction training on associative and non-associative fear in a mouse model of posttraumatic stress disorder (PTSD). *Behav Brain Res*, 205(2):544–549.

Gould, N., Holmes, M., Fantie, B., Luckenbaugh, D., Pine, D., Gould, T., Burgess, N., Manji, H., and Zarate, C. (2007). Performance on a virtual reality spatial memory navigation task in depressed patients. *Am J Psychiatry*, 164(3):516–519.

Green, E., Grozeva, D., Jones, I., Jones, L., Kirov, G., Caesar, S., Gordon-Smith, K., Fraser, C., Forty, L., and Russell, E. (2009). The bipolar disorder risk allele at CACNA1C also confers risk of recurrent major depression and of schizophrenia. *Mol Psychiatry*, 15(10):1016–1022.

Gruenecker, B., Kaltwasser, S., Peterse, Y., Saemann, P., Schmidt, M., Wotjak, C., and Czisch, M. (2010). Fractionated manganese injections: effects on MRI contrast enhancement and physiological measures in C57BL/6 mice. *NMR Biomed*, 23(8):913–921.

Gruenecker, B., Kaltwasser, S. F., Zappe, A. C., Bedenk, B. T., Bicker, Y., Spoormaker, V. I., Wotjak, C. T., and Czisch, M. (2012). Regional specificity of manganese accumulation and clearance in the mouse brain: implications for manganese-enhanced MRI. *NMR Biomed*, 26(5):542–556.

Gu, H., Marth, J. D., Orban, P. C., Mossmann, H., and Rajewsky, K. (1994). Deletion of a DNA polymerase beta gene segment in T cells using cell type-specific gene targeting. *Science*, 265(5168):103–106.

Gundersen, H. and Jensen, E. (1987). The efficiency of systematic sampling in stereology and its prediction. *J Microsc*, 147(3):229–263.

Guzowski, J. F., McNaughton, B. L., Barnes, C. A., and Worley, P. F. (1999). Environment-specific expression of the immediate-early gene Arc in hippocampal neuronal ensembles. *Nat Neurosci*, 2(12):1120–1124.

Guzowski, J. F., Timlin, J. A., Roysam, B., McNaughton, B. L., Worley, P. F., and Barnes, C. A. (2005). Mapping behaviorally relevant neural circuits with immediate-early gene expression. *Curr Opin Neurobiol*, 15(5):599–606.

Hafting, T., Fyhn, M., Molden, S., Moser, M.-B., and Moser, E. I. (2005). Microstructure of a spatial map in the entorhinal cortex. *Nature*, 436(7052):801–806.

Han, J., Kesner, P., Metna-Laurent, M., Duan, T., Xu, L., Georges, F., Koehl, M., Abrous, D. N., Mendizabal-Zubiaga, J., Grandes, P., Liu, Q., Bai, G., Wang, W., Xiong, L., Ren, W., Marsicano, G., and Zhang, X. (2012). Acute cannabinoids impair working memory through astroglial CB1 receptor modulation of hippocampal LTD. *Cell*, 148(5):1039–1050.

Harris, M. A., Wiener, J. M., and Wolbers, T. (2012). Aging specifically impairs switching to an allocentric navigational strategy. *Front Aging Neurosci*, 4:29.

Harro, J., Kanarik, M., Matrov, D., and Panksepp, J. (2011). Mapping patterns of depression-related brain regions with cytochrome oxidase histochemistry: relevance of animal affective systems to human disorders, with a focus on resilience to adverse events. *Neurosci Biobehav Rev*, 35(9):1876–1889.

Hassabis, D., Chu, C., Rees, G., Weiskopf, N., Molyneux, P. D., and Maguire, E. A. (2009). Decoding neuronal ensembles in the human hippocampus. *Curr Biol*, 19(7):546–554.

Hayasaka, S., Phan, K. L., Liberzon, I., Worsley, K. J., and Nichols, T. E. (2004). Nonstationary cluster-size inference with random field and permutation methods. *Neuroimage*, 22(2):676–687.

Hazell, A. S. (2002). Astrocytes and manganese neurotoxicity. *Neurochem Int*, 41(4):271–277.

Hell, J. W., Westenbroek, R. E., Warner, C., Ahlijanian, M. K., Prystay, W., Gilbert, M. M., Snutch, T. P., and Catterall, W. A. (1993). Identification and differential subcellular localization of the neuronal class C and class D L-type calcium channel $\alpha 1$ subunits. *J Cell Biol*, 123(4):949–962.

Helmchen, F., Fee, M. S., Tank, D. W., and Denk, W. (2001). A miniature head-mounted two-photon microscope: high-resolution brain imaging in freely moving animals. *Neuron*, 31(6):903–912.

Herculano-Houzel, S., Mota, B., and Lent, R. (2006). Cellular scaling rules for rodent brains. *Proc Natl Acad Sci U S A*, 103(32):12138–12143.

Herry, C., Ciocchi, S., Senn, V., Demmou, L., Müller, C., and Lüthi, A. (2008). Switching on and off fear by distinct neuronal circuits. *Nature*, 454(7204):600–606.

Hetzenauer, A., Sinnegger-Brauns, M., Striessnig, J., and Singewald, N. (2006). Brain activation pattern induced by stimulation of L-type Ca^{2+}-channels: Contribution of $Ca_v1.3$ and $Ca_v1.2$ isoforms. *Neuroscience*, 139(3):1005–1015.

Hicks, L. H. (1964). Effects of overtraining on acquisition and reversal of place and response learning. *Psychol Rep*, 15(2):459–462.

Hoch, T., Kreitz, S., Gaffling, S., Pischetsrieder, M., and Hess, A. (2013). Manganese-enhanced magnetic resonance imaging for mapping of whole brain activity patterns associated with the intake of snack food in ad libitum fed rats. *PLoS One*, 8(2):e55354.

Iglói, K., Doeller, C. F., Berthoz, A., Rondi-Reig, L., and Burgess, N. (2010). Lateralized human hippocampal activity predicts navigation based on sequence or place memory. *Proc Natl Acad Sci U S A*, 107(32):14466–14471.

Iglói, K., Zaoui, M., Berthoz, A., and Rondi-Reig, L. (2009). Sequential egocentric strategy is acquired as early as allocentric strategy: Parallel acquisition of these two navigation strategies. *Hippocampus*, 19(12):1199–1211.

Iivonen, H., Nurminen, L., Harri, M., Tanila, H., and Puoliväli, J. (2003). Hypothermia in mice tested in morris water maze. *Behav Brain Res*, 141(2):207–213.

Impey, S., Mark, M., Villacres, E. C., Poser, S., Chavkin, C., and Storm, D. R. (1996). Induction of Cre-mediated gene expression by stimuli that generate long-lasting LTP in area CA1 of the hippocampus. *Neuron*, 16(5):973–982.

Itoh, K., Sakata, M., Watanabe, M., Aikawa, Y., and Fujii, H. (2008). The entry of manganese ions into the brain is accelerated by the activation of N-methyl-D-aspartate receptors. *Neuroscience*, 154(2):732–740.

Jarrard, L. E. (1989). On the use of ibotenic acid to lesion selectively different components of the hippocampal formation. *J Neurosci Methods*, 29(3):251–259.

Jernigan, T. L., Archibald, S. L., Berhow, M. T., Sowell, E. R., Foster, D. S., and Hesselink, J. R. (1991). Cerebral structure on MRI, part I: Localization of age-related changes. *Biol Psychiatry*, 29(1):55–67.

Kamprath, K. and Wotjak, C. T. (2004). Nonassociative learning processes determine expression and extinction of conditioned fear in mice. *Learn Mem*, 11(6):770–786.

Kandel, E. R. (2001). The molecular biology of memory storage: a dialogue between genes and synapses. *Science*, 294(5544):1030–1038.

Kandel, E. R., Kupfermann, I., and Iversen, S. (2000). *Principles of neural science*, chapter Learning and memory, pages 1227–1246. McGraw-Hill, New York.

Kassem, M. S., Lagopoulos, J., Stait-Gardner, T., Price, W. S., Chohan, T. W., Arnold, J. C., Hatton, S. N., and Bennett, M. R. (2012). Stress-induced grey matter loss determined by MRI is primarily due to loss of dendrites and their synapses. *Mol Neurobiol*, 47(2):645–661.

Kjelstrup, K. G., Tuvnes, F. A., Steffenach, H.-A., Murison, R., Moser, E. I., and Moser, M.-B. (2002). Reduced fear expression after lesions of the ventral hippocampus. *Proc Natl Acad Sci U S A*, 99(16):10825–10830.

Kleinknecht, K. R., Bedenk, B. T., Kaltwasser, S. F., Grünecker, B., Yen, Y.-C., Czisch, M., and Wotjak, C. T. (2012). Hippocampus-dependent place learning enables spatial flexibility in C57BL6/N mice. *Front Behav Neurosci*, 6:87.

Knowlton, B. J., Mangels, J. A., and Squire, L. R. (1996). A neostriatal habit learning system in humans. *Science*, 273(5280):1399–1402.

Kupfer, D. J., Frank, E., and Phillips, M. L. (2012). Major depressive disorder: new clinical, neurobiological, and treatment perspectives. *Lancet*, 379(9820):1045–1055.

Lammertsma, A. A. (2001). PET/SPECT: functional imaging beyond flow. *Vision Res*, 41(10):1277–1281.

Langwieser, N., Christel, C. J., Kleppisch, T., Hofmann, F., Wotjak, C. T., and Moosmang, S. (2010). Homeostatic switch in hebbian plasticity and fear learning after sustained loss of $Ca_v1.2$ calcium channels. *J Neurosci*, 30(25):8367–8375.

Lauterbur, P. C. et al. (1973). Image formation by induced local interactions: examples employing nuclear magnetic resonance. *Nature*, 242(5394):190–191.

Lavenex, P., Lavenex, P. B., Bennett, J. L., and Amaral, D. G. (2009). Postmortem changes in the neuroanatomical characteristics of the primate brain: hippocampal formation. *J Comp Neurol*, 512(1):27–51.

Lee, J.-W. (2000). Manganese intoxication. *Arch Neurol*, 57(4):597.

Lesh, T. A., Niendam, T. A., Minzenberg, M. J., and Carter, C. S. (2011). Cognitive control deficits in schizophrenia: mechanisms and meaning. *Neuropsychopharmacology*, 36(1):316–338.

Lever, C., Burton, S., and O'Keefe, J. (2006). Rearing on hind legs, environmental novelty, and the hippocampal formation. *Rev Neurosci*, 17(1-2):111–133.

Liccione, J. J. and Maines, M. D. (1988). Selective vulnerability of glutathione metabolism and cellular defense mechanisms in rat striatum to manganese. *J Pharmacol Exp Ther*, 247(1):156–161.

Logothetis, N. K., Pauls, J., Augath, M., Trinath, T., and Oeltermann, A. (2001). Neurophysiological investigation of the basis of the fMRI signal. *Nature*, 412(6843):150–157.

Ludwig, A., Flockerzi, V., and Hofmann, F. (1997). Regional expression and cellular localization of the $\alpha 1$ and β subunit of high voltage-activated calcium channels in rat brain. *J Neurosci*, 17(4):1339–1349.

Maguire, E. A., Burgess, N., Donnett, J. G., Frackowiak, R. S., Frith, C. D., and O'Keefe, J. (1998). Knowing where and getting there: a human navigation network. *Science*, 280(5365):921–924.

Maren, S. (1999). Long-term potentiation in the amygdala: a mechanism for emotional learning and memory. *Trends Neurosci*, 22(12):561–567.

Maren, S., Aharonov, G., Stote, D. L., and Fanselow, M. S. (1996). N-methyl-d-aspartate receptors in the basolateral amygdala are required for both acquisition and expression of conditional fear in rats. *Behav Neurosci*, 110(6):1365.

McDonald, R. J., King, A. L., and Hong, N. S. (2001). Context-specific interference on reversal learning of a stimulus-response habit. *Behav Brain Res*, 121(1-2):149–165.

McDonald, R. J., Ko, C. H., and Hong, N. S. (2002). Attenuation of context-specific inhibition on reversal learning of a stimulus-response task in rats with neurotoxic hippocampal damage. *Behav Brain Res*, 136(1):113–126.

McDonald, R. J. and White, N. M. (1994). Parallel information processing in the water maze: evidence for independent memory systems involving dorsal striatum and hippocampus. *Behav Neural Biol*, 61(3):260–270.

McGaugh, J. L. (2000). Memory–a century of consolidation. *Science*, 287(5451):248–251.

Meese, W., Kluge, W., Grumme, T., and Hopfenmüller, W. (1980). CT evaluation of the CSF spaces of healthy persons. *Neuroradiology*, 19(3):131–136.

Mertz, L. M., Baum, B. J., and Ambudkar, I. (1990). Refill status of the agonist-sensitive Ca^{2+} pool regulates Mn^{2+} influx into parotid acini. *J Biol Chem*, 265(25):15010–15014.

Milad, M. R. and Rauch, S. L. (2012). Obsessive-compulsive disorder: beyond segregated cortico-striatal pathways. *Trends Cogn Sci*, 16(1):43–51.

Miller, G. A. (1956). The magical number seven plus or minus two: some limits on our capacity for processing information. *Psychol Rev*, 63(2):81–97.

Mingaud, F., Moine, C. L., Etchamendy, N., Mormède, C., Jaffard, R., and Marighetto, A. (2007). The hippocampus plays a critical role at encoding discontiguous events for subsequent declarative memory expression in mice. *Hippocampus*, 17(4):264–270.

Miserendino, M. J., Sananes, C. B., Melia, K. R., and Davis, M. (1990). Blocking of acquisition but not expression of conditioned fear-potentiated startle by NMDA antagonists in the amygdala. *Nature*, 345:716–718.

Mitra, R., Jadhav, S., McEwen, B. S., Vyas, A., and Chattarji, S. (2005). Stress duration modulates the spatiotemporal patterns of spine formation in the basolateral amygdala. *Proc Natl Acad Sci U S A*, 102(26):9371–9376.

Miyake, A., Friedman, N. P., Emerson, M. J., Witzki, A. H., Howerter, A., and Wager, T. D. (2000). The unity and diversity of executive functions and their contributions to complex "frontal lobe" tasks: a latent variable analysis. *Cogn Psychol*, 41(1):49–100.

Moffat, S. D., Hampson, E., and Hatzipantelis, M. (1998). Navigation in a "virtual" maze: Sex differences and correlation with psychometric measures of spatial ability in humans. *Evolution and Human Behavior*, 19(2):73–87.

Moosmang, S., Haider, N., Klugbauer, N., Adelsberger, H., Langwieser, N., Müller, J., Stiess, M., Marais, E., Schulla, V., Lacinova, L., Goebbels, S., Nave, K.-A., Storm, D. R., Hofmann, F., and Kleppisch, T. (2005). Role of hippocampal $Ca_v1.2$ Ca^{2+} channels in NMDA receptor-independent synaptic plasticity and spatial memory. *J Neurosci*, 25(43):9883–9892.

Morgan, S. and Teyler, T. (1999). VDCCs and NMDARs underlie two forms of LTP in CA1 hippocampus in vivo. *J Neurophysiol*, 82(2):736–740.

Morris, R. (1984). Developments of a water-maze procedure for studying spatial learning in the rat. *J Neurosci Methods*, 11(1):47–60.

Morris, R. G. (2001). Episodic-like memory in animals: psychological criteria, neural mechanisms and the value of episodic-like tasks to investigate animal models of neurodegenerative disease. *Philos Trans R Soc Lond B Biol Sci*, 356(1413):1453–1465.

Morris, R. G., Anderson, E., Lynch, G. S., and Baudry, M. (1986). Selective impairment of learning and blockade of long-term potentiation by an N-methyl-D-aspartate receptor antagonist, AP5. *Nature*, 319(6056):774–776.

Morris, R. G., Garrud, P., Rawlins, J. N., and O'Keefe, J. (1982). Place navigation impaired in rats with hippocampal lesions. *Nature*, 297(5868):681–683.

Morris, R. G. M. (2013). Nmda receptors and memory encoding. *Neuropharmacology*.

Moser, M. B., Moser, E. I., Forrest, E., Andersen, P., and Morris, R. G. (1995). Spatial learning with a minislab in the dorsal hippocampus. *Proc Natl Acad Sci U S A*, 92(21):9697–9701.

Moses, S. N., Sutherland, R. J., and McDonald, R. J. (2002). Differential involvement of amygdala and hippocampus in responding to novel objects and contexts. *Brain Res Bull*, 58(5):517–527.

Nagy, A. (2000). Cre recombinase: the universal reagent for genome tailoring. *Genesis*, 26(2):99–109.

Nedelska, Z., Andel, R., Laczó, J., Vlcek, K., Horinek, D., Lisy, J., Sheardova, K., Bureš, J., and Hort, J. (2012). Spatial navigation impairment is proportional to right hippocampal volume. *Proc Natl Acad Sci U S A*, 109(7):2590–2594.

Nicholls, R. E., Alarcon, J. M., Malleret, G., Carroll, R. C., Grody, M., Vronskaya, S., and Kandel, E. R. (2008). Transgenic mice lacking NMDAR-dependent LTD exhibit deficits in behavioral flexibility. *Neuron*, 58(1):104–117.

O'Keefe, J. and Dostrovsky, J. (1971). The hippocampus as a spatial map: Preliminary evidence from unit activity in the freely-moving rat. *Brain Res*, 34(1):171–175.

O'Keefe, J., Nadel, L., Keightley, S., and Kill, D. (1975). Fornix lesions selectively abolish place learning in the rat. *Exp Neurol*, 48(1):152–166.

Oliveira, M. G., Bueno, O. F., Pomarico, A. C., and Gugliano, E. B. (1997). Strategies used by hippocampal- and caudate-putamen-lesioned rats in a learning task. *Neurobiol Learn Mem*, 68(1):32–41.

Olton, D. and Samuelson, R. (1976). Remembrance of places passed: Spatial memory in rats. *J Exp Psychol Anim Behav Process*, 2(2):97–116.

Ormerod, B. K. and Beninger, R. J. (2002). Water maze versus radial maze: differential performance of rats in a spatial delayed match-to-position task and response to scopolamine. *Behav Brain Res*, 128(2):139–152.

Packard, M. G. (2009). Exhumed from thought: basal ganglia and response learning in the plus-maze. *Behav Brain Res*, 199(1):24–31.

Packard, M. G., Hirsh, R., and White, N. M. (1989). Differential effects of fornix and caudate nucleus lesions on two radial maze tasks: evidence for multiple memory systems. *J Neurosci*, 9(5):1465–1472.

Packard, M. G. and McGaugh, J. L. (1992). Double dissociation of fornix and caudate nucleus lesions on acquisition of two water maze tasks: further evidence for multiple memory systems. *Behav Neurosci*, 106(3):439–446.

Packard, M. G. and McGaugh, J. L. (1996). Inactivation of hippocampus or caudate nucleus with lidocaine differentially affects expression of place and response learning. *Neurobiol Learn Mem*, 65(1):65–72.

Packard, M. G. and Wingard, J. C. (2004). Amygdala and "emotional" modulation of the relative use of multiple memory systems. *Neurobiol Learn Mem*, 82(3):243–252.

Palencia, C. A. and Ragozzino, M. E. (2004). The influence of NMDA receptors in the dorsomedial striatum on response reversal learning. *Neurobiol Learn Mem*, 82(2):81–89.

Palencia, C. A. and Ragozzino, M. E. (2005). The contribution of NMDA receptors in the dorsolateral striatum to egocentric response learning. *Behav Neurosci*, 119(4):953.

Pautler, R. G. and Koretsky, A. P. (2002). Tracing odor-induced activation in the olfactory bulbs of mice using manganese-enhanced magnetic resonance imaging. *Neuroimage*, 16(2):441–448.

Pautler, R. G., Mongeau, R., and Jacobs, R. E. (2003). In vivo trans-synaptic tract tracing from the murine striatum and amygdala utilizing manganese enhanced MRI (MEMRI). *Magn Reson Med*, 50(1):33–39.

Pautler, R. G., Silva, A. C., and Koretsky, A. P. (1998). In vivo neuronal tract tracing using manganese-enhanced magnetic resonance imaging. *Magn Reson Med*, 40(5):740–748.

Paxinos, G. and Franklin, K. (2001). *The mouse brain in stereotaxic coordinates*. Academic Press, San Diego.

Pennartz, C. M. A., Ito, R., Verschure, P. F. M. J., Battaglia, F. P., and Robbins, T. W. (2011). The hippocampal-striatal axis in learning, prediction and goal-directed behavior. *Trends Neurosci*, 34(10):548–559.

Peppiatt, C. M., Howarth, C., Mobbs, P., and Attwell, D. (2006). Bidirectional control of CNS capillary diameter by pericytes. *Nature*, 443(7112):700–704.

Platzer, J., Engel, J., Schrott-Fischer, A., Stephan, K., Bova, S., Chen, H., Zheng, H., and Striessnig, J. (2000). Congenital deafness and sinoatrial node dysfunction in mice lacking class D L-type Ca^{2+} channels. *Cell*, 102(1):89–97.

Porter, N. M., Thibault, O., Thibault, V., Chen, K.-C., and Landfield, P. W. (1997). Calcium channel density and hippocampal cell death with age in long-term culture. *J Neurosci*, 17(14):5629–5639.

Prasad, J. A. and Chudasama, Y. (2013). Viral tracing identifies parallel disynaptic pathways to the hippocampus. *J Neurosci*, 33(19):8494–8503.

Ragozzino, M. E. (2007). The contribution of the medial prefrontal cortex, orbitofrontal cortex, and dorsomedial striatum to behavioral flexibility. *Ann N Y Acad Sci*, 1121:355–375.

Ragozzino, M. E. and Choi, D. (2004). Dynamic changes in acetylcholine output in the medial striatum during place reversal learning. *Learning & Memory*, 11(1):70–77.

Ragozzino, M. E., Detrick, S., and Kesner, R. P. (1999). Involvement of the prelimbic-infralimbic areas of the rodent prefrontal cortex in behavioral flexibility for place and response learning. *J Neurosci*, 19(11):4585–4594.

Ragozzino, M. E., Ragozzino, K. E., Mizumori, S. J., and Kesner, R. P. (2002). Role of the dorsomedial striatum in behavioral flexibility for response and visual cue discrimination learning. *Behav Neurosci*, 116(1):105.

Ritchie, B., Aeschliman, B., and Peirce, P. (1950). Studies in spatial learning: VIII. Place performance and the acquisition of place dispositions. *J Comp Physiol Psychol*, 43(2):73.

Robbins, T. W. (1996). Dissociating executive functions of the prefrontal cortex. *Philos Trans R Soc Lond B Biol Sci*, 351(1346):1463–70.

Rondi-Reig, L., Libbey, M., Eichenbaum, H., and Tonegawa, S. (2001). CA1-specific N-methyl-D-aspartate receptor knockout mice are deficient in solving a nonspatial transverse patterning task. *Proc Natl Acad Sci U S A*, 98(6):3543–3548.

Rondi-Reig, L., Petit, G. H., Tobin, C., Tonegawa, S., Mariani, J., and Berthoz, A. (2006). Impaired sequential egocentric and allocentric memories in forebrain-specific-NMDA

receptor knock-out mice during a new task dissociating strategies of navigation. *J Neurosci*, 26(15):4071–4081.

Rudy, J. W. and Matus-Amat, P. (2005). The ventral hippocampus supports a memory representation of context and contextual fear conditioning: implications for a unitary function of the hippocampus. *Behav Neurosci*, 119(1):154–163.

Ruediger, S., Spirig, D., Donato, F., and Caroni, P. (2012). Goal-oriented searching mediated by ventral hippocampus early in trial-and-error learning. *Nat Neurosci*, 15(11):1563–71.

Sakata, J. T., Crews, D., and Gonzalez-Lima, F. (2005). Behavioral correlates of differences in neural metabolic capacity. *Brain Res Rev*, 48(1):1–15.

Santini, E., Muller, R. U., and Quirk, G. J. (2001). Consolidation of extinction learning involves transfer from nmda-independent to nmda-dependent memory. *J Neurosci*, 21(22):9009–9017.

Sauerhöfer, E., Pamplona, F. A., Bedenk, B., Moll, G. H., Dawirs, R. R., von Hörsten, S., Wotjak, C. T., and Golub, Y. (2012). Generalization of contextual fear depends on associative rather than non-associative memory components. *Behav Brain Res*, 233(2):483–493.

Schenk, F. (1987). Comparison of spatial learning in woodmice (apodemus sylvaticus) and hooded rats (rattus norvegicus). *J Comp Psychol*, 101(2):150–158.

Schwabe, L., Schächinger, H., de Kloet, E. R., and Oitzl, M. S. (2010). Stress impairs spatial but not early stimulus-response learning. *Behav Brain Res*, 213(1):50–55.

Schwarcz, R., Hökfelt, T., Fuxe, K., Jonsson, G., Goldstein, M., and Terenius, L. (1979). Ibotenic acid-induced neuronal degeneration: a morphological and neurochemical study. *Exp Brain Res*, 37(2):199–216.

Scoville, W. B. and Milner, B. (1957). Loss of recent memory after bilateral hippocampal lesions. *J Neurol Neurosurg Psychiatry*, 20(1):11–21.

Seab, J., Jagust, W., Wong, S., Roos, M., Reed, B., and Budinger, T. (1988). Quantitative NMR measurements of hippocampal atrophy in Alzheimer's disease. *Magn Reson Med*, 8(2):200–208.

Seisenberger, C., Specht, V., Welling, A., Platzer, J., Pfeifer, A., Kühbandner, S., Striessnig, J., Klugbauer, N., Feil, R., and Hofmann, F. (2000). Functional embryonic cardiomyocytes after disruption of the L-type α1C ($Ca_v1.2$) calcium channel gene in the mouse. *J Biol Chem*, 275(50):39193–39199.

Sepúlveda, M., Dresselaers, T., Vangheluwe, P., Everaerts, W., Himmelreich, U., Mata, A., and Wuytack, F. (2012). Evaluation of manganese uptake and toxicity in mouse brain during continuous MnCl2 administration using osmotic pumps. *Contrast media & molecular imaging*, 7(4):426–434.

Sigurdsson, T., Doyère, V., Cain, C. K., and LeDoux, J. E. (2007). Long-term potentiation in the amygdala: a cellular mechanism of fear learning and memory. *Neuropharmacology*, 52(1):215–227.

Sigurdsson, T., Stark, K. L., Karayiorgou, M., Gogos, J. A., and Gordon, J. A. (2010). Impaired hippocampal–prefrontal synchrony in a genetic mouse model of schizophrenia. *Nature*, 464(7289):763–767.

Simpson, P., Challiss, R., and Nahorski, S. (1995). Divalent cation entry in cultured rat cerebellar granule cells measured using Mn^{2+} quench of fura 2 fluorescence. *Eur J Neurosci*, 7(5):831–840.

Singewald, N. (2007). Altered brain activity processing in high-anxiety rodents revealed by challenge paradigms and functional mapping. *Neurosci Biobehav Rev*, 31(1):18–40.

Sinnegger-Brauns, M. J., Huber, I. G., Koschak, A., Wild, C., Obermair, G. J., Einzinger, U., Hoda, J.-C., Sartori, S. B., and Striessnig, J. (2009). Expression and 1,4-dihydropyridine-binding properties of brain L-type calcium channel isoforms. *Mol Pharmacol*, 75(2):407–414.

Sloot, W. N. and Gramsbergen, J. B. (1994). Axonal transport of manganese and its relevance to selective neurotoxicity in the rat basal ganglia. *Brain Res*, 657(1-2):124–132.

Snyder, H. R. (2012). Major depressive disorder is associated with broad impairments on neuropsychological measures of executive function: A meta-analysis and review. *Psychol Bull*, 139(1):81–132.

Sotres-Bayon, F., Bush, D. E., and LeDoux, J. E. (2007). Acquisition of fear extinction requires activation of NR2B-containing NMDA receptors in the lateral amygdala. *Neuropsychopharmacology*, 32(9):1929–1940.

Sotres-Bayon, F., Sierra-Mercado, D., Pardilla-Delgado, E., and Quirk, G. J. (2012). Gating of fear in prelimbic cortex by hippocampal and amygdala inputs. *Neuron*, 76(4):804–812.

Spieker, E. A., Astur, R. S., West, J. T., Griego, J. A., and Rowland, L. M. (2012). Spatial memory deficits in a virtual reality eight-arm radial maze in schizophrenia. *Schizophr Res*, 135(1):84–89.

Spiers, H. J., Maguire, E. A., and Burgess, N. (2001). Hippocampal amnesia. *Neurocase*, 7(5):357–382.

Squire, L. R. (1992). Memory and the hippocampus: a synthesis from findings with rats, monkeys, and humans. *Psychol Rev*, 99(2):195–231.

Stepan, J., Dine, J., Fenzl, T., Polta, S. A., von Wolff, G., Wotjak, C. T., and Eder, M. (2012). Entorhinal theta-frequency input to the dentate gyrus trisynaptically evokes hippocampal CA1 LTP. *Front Neural Circuits*, 6:64.

Stosiek, C., Garaschuk, O., Holthoff, K., and Konnerth, A. (2003). In vivo two-photon calcium imaging of neuronal networks. *Proc Natl Acad Sci U S A*, 100(12):7319–7324.

Strijkers, G. J., Mulder, M., Willem, J., van Tilborg, F., Geralda, A., and Nicolay, K. (2007). MRI contrast agents: current status and future perspectives. *Anticancer Agents Med Chem*, 7(3):291–305.

Stringer, K. G., Martin, G. M., and Skinner, D. M. (2005). The effects of hippocampal lesions on response, direction, and place learning in rats. *Behav Neurosci*, 119(4):946–952.

Sutherland, R. J., McDonald, R. J., and Savage, D. D. (1997). Prenatal exposure to moderate levels of ethanol can have long-lasting effects on hippocampal synaptic plasticity in adult offspring. *Hippocampus*, 7(2):232–238.

Sweatt, J. D. (1999). Toward a molecular explanation for long-term potentiation. *Learn Mem*, 6(5):399–416.

Takeda, A. (2003). Manganese action in brain function. *Brain Res Rev*, 41(1):79–87.

Takeda, A., Ishiwatari, S., and Okada, S. (1998). In vivo stimulation-induced release of manganese in rat amygdala. *Brain Res*, 811(1):147–151.

Thibault, O., Gant, J. C., and Landfield, P. W. (2007). Expansion of the calcium hypothesis of brain aging and Alzheimer's disease: minding the store. *Aging Cell*, 6(3):307–317.

Thoeringer, C. K., Pfeiffer, U. J., Rammes, G., Pamplona, F. A., Moosmang, S., and Wotjak, C. T. (2010). Early life environment determines the development of adult phobic-like fear responses in BALB/cAnN mice. *Genes Brain Behav*, 9(8):947–957.

Thompson, R. F. and Kim, J. J. (1996). Memory systems in the brain and localization of a memory. *Proc Natl Acad Sci U S A*, 93(24):13438–13444.

Tolman, E., Ritchie, B., and Kalish, D. (1946). Studies in spatial learning. II. place learning versus response learning. *J Exp Psychol*, 36(1):221–229.

Tronche, F., Kellendonk, C., Kretz, O., Gass, P., Anlag, K., Orban, P. C., Bock, R., Klein, R., and Schütz, G. (1999). Disruption of the glucocorticoid receptor gene in the nervous system results in reduced anxiety. *Nat Genet*, 23(1):99–103.

Tsien, J. Z., Huerta, P. T., and Tonegawa, S. (1996). The essential role of hippocampal CA1 NMDA receptor–dependent synaptic plasticity in spatial memory. *Cell*, 87(7):1327–1338.

Tulving, E. (1972). *Organization of memory*, chapter Episodic and semantic memory, pages 381–403. Academic Press, New York.

Tulving, E. and Schacter, D. L. (1990). Priming and human memory systems. *Science*, 247(4940):301–306.

Van der Linden, A., Van Meir, V., Tindemans, I., Verhoye, M., and Balthazart, J. (2004). Applications of manganese-enhanced magnetic resonance imaging (MEMRI) to image brain plasticity in song birds. *NMR Biomed*, 17(8):602–612.

von Reutern, B., Gruenecker, B., Yousefi, B. H., Henriksen, G., Czisch, M., and Drzezga, A. (2013). Voxel-based analysis of amyloid-burden measured with [11C] PiB PET in a

double transgenic mouse model of Alzheimer's disease. *Mol Imaging Biol*, Epub ahead of print.

Watanabe, T., Frahm, J., and Michaelis, T. (2008). Manganese-enhanced MRI of the mouse auditory pathway. *Magn Reson Med*, 60(1):210–212.

Weisskopf, M. G., Bauer, E. P., and LeDoux, J. E. (1999). L-type voltage-gated calcium channels mediate NMDA-independent associative long-term potentiation at thalamic input synapses to the amygdala. *J Neurosci*, 19(23):10512–10519.

Weniger, G. and Irle, E. (2008). Allocentric memory impaired and egocentric memory intact as assessed by virtual reality in recent-onset schizophrenia. *Schizophr Res*, 101(1):201–209.

Westenbroek, R. E., Ahlijanian, M. K., and Catterall, W. A. (1990). Clustering of L-type Ca^{2+} channels at the base of major dendrites in hippocampal pyramidal neurons. *Nature*, 347(6290):281–284.

Whishaw, I. Q. and Tomie, J. (1996). Of mice and mazes: similarities between mice and rats on dry land but not water mazes. *Physiol Behav*, 60(5):1191–1197.

White, J. A., McKinney, B. C., John, M. C., Powers, P. A., Kamp, T. J., and Murphy, G. G. (2008). Conditional forebrain deletion of the L-type calcium channel Cav1. 2 disrupts remote spatial memories in mice. *Learn Mem*, 15(1):1–5.

Wolfer, D. P. and Lipp, H. P. (2000). Dissecting the behaviour of transgenic mice: is it the mutation, the genetic background, or the environment? *Exp Physiol*, 85(6):627–634.

Wong-Riley, M. T. (1989). Cytochrome oxidase: an endogenous metabolic marker for neuronal activity. *Trends Neurosci*, 12(3):94–101.

Yang, P.-F., Chen, D.-Y., Hu, J. W., Chen, J.-H., and Yen, C.-T. (2011). Functional tracing of medial nociceptive pathways using activity-dependent manganese-enhanced MRI. *Pain*, 152(1):194–203.

Yu, X., Wadghiri, Y. Z., Sanes, D. H., and Turnbull, D. H. (2005). In vivo auditory brain mapping in mice with Mn-enhanced MRI. *Nat Neurosci*, 8(7):961–968.

Yu, X., Zou, J., Babb, J. S., Johnson, G., Sanes, D. H., and Turnbull, D. H. (2008). Statistical mapping of sound-evoked activity in the mouse auditory midbrain using Mn-enhanced MRI. *Neuroimage*, 39(1):223–230.

A. Own publications

Parts of this thesis have already been published in peer review journals. I contributed during my three years of doctoral research to the following publications:

Kleinknecht, K. R.*, Bedenk, B. T.*, Kaltwasser, S. F., Gruenecker, B., Yen, Y.-C., Czisch, M., and Wotjak, C. T. (2012). Hippocampus-dependent place learning enables spatial flexibility in C57BL6N mice. *Front Behav Neurosci*, 6:87. * contributed equally

Gruenecker, B., Kaltwasser, S. F., Zappe, A. C., Bedenk, B. T., Bicker, Y., Spoormaker, V. I., Wotjak, C. T., and Czisch, M. (2012). Regional specificity of manganese accumulation and clearance in the mouse brain: implications for manganese-enhanced MRI. *NMR Biomed*, 26(5):542-56.

Sauerhoefer, E., Pamplona, F. A., Bedenk, B., Moll, G. H., Dawirs, R. R., von Hoersten, S., Wotjak, C. T., and Golub, Y. (2012). Generalization of contextual fear depends on associative rather than non-associative memory components. *Behav Brain Res*, 233(2):483-493.

Part of the data presented in this thesis have already been published in Kleinknecht et al. (2012). For that reason, it is reprinted in full below.


not shown in the online version


not shown in the online version


not shown in the online version


not shown in the online version


not shown in the online version


not shown in the online version


not shown in the online version


not shown in the online version


not shown in the online version


not shown in the online version


not shown in the online version


not shown in the online version


not shown in the online version


not shown in the online version


not shown in the online version


not shown in the online version


not shown in the online version

B. Contributions

Benedikt T. Bedenk essentially contributed to the design of all studies, partially analyzed and conceptualized the WCM experiments depicted in figure 3.1, 3.2, 3.4 and 3.5, carried out the analysis of the basal screening depicted in figure 3.3 B and table 3.1, performed and analyzed all MR measurements without the manually definition of the ROIs reported in figure 3.3 and conducted and statistically analyzed the WCM experiments reported in figure 3.9 and 3.10.

Carsten T. Wotjak supervised all experiments and contributed to the design and the interpretation of all data.

Michael Czisch supervised the MR scanning and the analysis of the MR data.

Karl R. Kleinknecht conducted and partially analyzed the WCM experiments of figure 3.1, 3.2, 3.4 and 3.5 and accomplished the basal screening experiments of table 3.1 and figure 3.3 B.

Sebastian F. Kaltwasser assisted with the MR measurements and conducted the manual definition of the ROIs for figure 3.3 and 3.6.

Barbara Grünecker assisted with the MR measurements and voxel-wise analysis of the MEMRI data depicted in figure 3.9.

Andreas Genewsky injected manganese iontophoretically into the thalamus, which is depicted in figure 3.8.

Angela Jurik provided all the $Ca_v1.2$ knockout mice.

Andrea Reßle carried out the western blot analysis of $Ca_v1.2$.

Anna Mederer conducted the ibotenic acid and vehicle injections into the HPC.

Armin Mann gave technical support with the MR system.

Caitlin Riebe helped with the illustrations.

C. Acknowledgments

I would like to thank all contributers for their individual efforts.

First, I would like to thank my mentor and supervisor PD. Dr. Carsten T. Wotjak, who encouraged me to reconquer a former field of psychology. I feel it as a privilege that I could discuss with you so much. Thank you for your time.

I want to thank Dr. Michael Czisch, who always brought me back to the ground. Thank you especially for the breaks in front of the door.

Further, I would like to thank Dr. Markus Wöhr, who was not only there when I started science, but will also be there at the tentative end.

My special thanks go to my officemates Dr. Barbara Grünecker and Dr. Sebastian F. Kaltwasser, who became real friends. It was a great time with you.

Many thanks also go to the whole research group of Carsten T. Wotjak and Michael Czisch, who have helped me whenever they could.

Thanks also go to my parents, who always took care of me and supported me on my way.

Last but not least, I want to thank my girlfriend Teresa and my son Nepomuk, who have always picked me up from work when it became late. I hope it will not become late today.

D. Curriculum vitae

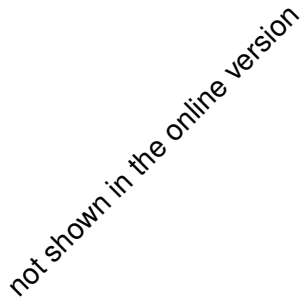


not shown in the online version

E. Erklärung

Ich versichere, dass ich meine Dissertation

Mapping brain activity *in vivo* during spatial learning in mice

selbstständig, ohne unerlaubte Hilfe angefertigt und mich dabei keiner anderen als der von mir ausdrücklich angegebenen Quellen und Hilfen bedient habe.

Diese Dissertation wurde in der jetzigen oder einer ähnlichen Form noch bei keiner anderen Hochschule eingereicht und hat noch keinen sonstigen Prüfungszwecken gedient.

_____ _____

Ort, Datum Unterschrift